UNIVERSITY OF CALIFORNIA, SAN DIEGO

AMPA Receptor Complexes: Mechanisms of Assembly and Modulation

A dissertation submitted in partial satisfaction of the requirements for the degree Doctor of Philosophy

in

Neurosciences

by

Natalie Frances Shanks

Committee in charge:

Professor Terunaga Nakagawa, Chair
Professor Yishi Jin, Co-Chair
Professor Mauricio Montal
Professor Gentry Patrick
Professor Franck Polleux

2013

The Dissertation of Natalie Frances Shanks is approved, and it is acceptable in quality and form for publication on microfilm and electronically:

_____

_____

_____

_____
Co-Chair

_____
Chair

University of California, San Diego

2013

DEDICATION

I would like to dedicate this dissertation to my parents: Thank you for the lifetime of love, encouragement and support. I I am here today because of the invaluable opportunites that you provided me. I love you so much!

EPIGRAPH

“Learn from yesterday, live for today, hope for tomorrow. The important thing is to not stop questioning.” –Albert Einstein

TABLE OF CONTENTS

LIST OF TABLES

Chapter III

LIST OF FIGURES

Chapter IV

Chapter V

LIST OF ABBREVATIONS

AMPA-R - α-amino-3-hydroxy-5-methyl-4-isoxazolepropionic acid receptor

KA-R – kainate receptor

NMDA-R - N-methyl-D-aspartic acid receptor

iGluR – ionotropic glutamate receptor

CoIP – coimmunoprecipitation

DOX - doxycycline

ACKNOWLEDGEMENTS

I would like to sincerely thank my advisor, Terunaga Nakagawa for his guidance throughout this entire process. He is personally is responsible for much of my training, and has been an integral part of my development as a scientist. I would also like to thank my committee for their time and the scientific guidance they have provided. Much of the work in this dissertation has been collaborative and would not have been possible without the scientific the contributions of other people. Jeff Savas has been a particularly helpful collaborator. Finally, I need to acknowledge my family and friends for their continued support and understanding. They have certainly made this experience more enjoyable.

Chapter II, in full, is a reproduction of the material as it appears in Journal of Neuroscience 2010. Shanks, Natalie F.; Maruo, Tomohiko; Farina, Anthony N.; Ellisman, Mark H.; Nakagawa, Terunaga, the Society for Neuroscience, 2012. The dissertation author was the primary contributor to the investigation and writing of the manuscript. Permission of all authors has been obtained.

Chapter III, in full, is a reproduction of the material as it appears in Cell Reports 2012. Shanks, Natalie F.; Savas, Jeffrey N.; Maruo, Tomohiko; Cais, Ondrej; Hirao, Atsushi; Oe, Souichi; Ghosh, Anirvan; Noda, Yasuko; Greger, Ingo H.; Yates. John R. III; Nakagawa, Terunaga, Elsevier 2012. The

dissertation author was among the primary investigators and authors of the manuscript. Permission has been obtained from all authors.

Chapter IV, in full, is currently being prepared for submission.

VITAE

2001-2006 Bachelor of Science in Biology
Bachelor of Arts in Psychology
University of California San Diego

2006-2008 University of California San Diego
Research Associate II

2008-2013 Doctor of Philosophy, Neurosciences
University of California, San Diego

Publications

Shanks, N.F., Maruo, T., Farina, A.N., Ellisman, M.H., Nakagawa, T. Contribution of the global subunit structure and stargazin on the maturation of AMPA receptors. *J Neurosci.* (2010). 30:2728-40.

Shanks, N.F., Savas, J.N., Maruo, T., Cais, O., Hirao, A., Oe, S., Ghosh, A., Noda, Y., Greger, I.H., Yates, J.R., and Nakagawa, T. Differences of AMPA and kainate receptor interactomes facilitate identification of AMPA receptor auxiliary subunit, GSG1L. *Cell Reports* (2012). 6:590-598.

ABSTRACT OF THE DISSERTATION

AMPA Receptor Complexes: Mechanisms of Assembly and Modulation

by

Natalie Frances Shanks

Doctor of Philosophy in Neurosciencs

University of California, San Diego, 2013

Professor Terunaga Nakagawa, Chair

Professor Yishi Jin, Co-Chair

AMPA type glutamate receptors are of fundamental importance for brain function, as they mediate the majority of fast excitatory synaptic transmission. They function by opening their transmembrane ion channel upon binding glutamate in the synapse. In addition to their roles in basal synaptic function, AMPA-Rs have also been implicated in synapse formation and stabilization, and their regulation is a primary mechanism underlying synaptic plasticity, a cellular correlate of learning and memory. Here, in 3 separate studies, I investigate different components of AMPA-R function: mechanisms of AMPA-R assembly, the AMPA-R interactome, and mechanisms of AMPA-R modulation by auxiliary subunits.

In order to better understand the assembly and trafficking of AMPA-Rs, I investigated early AMPA-R subunit assembly mechanisms. Using a recombinant system, I purified and isolated both mature tetrameric AMPA-Rs as well as the transient AMPA-R dimeric biosynthetic intermediates. I determined the three-dimensional single particle EM structures of both of these AMPA-R forms. This work revealed that efficient subunit assembly requires a preferred conformation of the AMPA-R biosynthetic intermediates in order to efficiently progress into the mature form. This proposed model of assembly complements the x-ray crystallography structure of the full length recombinant AMPA-R solved by Eric Gouaux's group perfectly because this structure shows that there is subunit cross over in the tetrameric AMPA-R complex.

In a collaborative proteomics project we utilized mass spectrometry to identify novel proteins that interact with AMPA receptors in the brain. In this way, I came to focus on a predicted protein in the rat genome, GSG1L. Using detailed molecular, cellular, electrophysiological, and biochemical experiments, I validated the interaction between AMPA-Rs and GSG1L and determined that GSG1L enhances AMPA-R surface expression and modulates AMPA-R channel kinetics by slowing desensitization and slowing recovery from desensitization. Thus GSG1L is novel unique modulator of AMPA-R function.

In a third project, I investigate the detailed molecular mechanisms of AMPA-R interaction with and modulation by a known class of AMPA-R auxiliary subunits, the cornichon homologues. I have identified specific domains and clusters of residues involved on both sides of the interaction. Most importantly, I show direct evidence for an interaction between the cornichon extracellular loop and both of the extracellular AMPA-R domains, the ligand binding domain and the N-terminal domain. Functional studies had previously hypothesized that such an interaction might occur with the AMPA-R ligand binding domain, however my work confirms and extends it by demonstrating the additional interaction with the N-terminal domain. Overall, this data suggest a completely novel role for the AMPA-R N-terminal domain in which interactions with auxiliary subunits are involved in allosteric modulation of AMPA-R channel function.

By elucidating the molecular mechanisms of several aspects of AMPA-R function, this work aids our understanding of synaptic transmission and, and may ultimately useful in efforts to develop therapeutic agents for AMPA-R related disorders.

Chapter I

Introduction

The work in this dissertation examines the molecular components that mediate neuronal communication at synapses. The control of neuronal excitability underlies all basic and higher order processes essential for brain function. This dissertation focuses on the regulation of AMPA type glutamate receptors (AMPA-Rs). AMPA-Rs are the primary mediators of fast excitatory transmission in the brain, and their dysfunction is implicated in a large variety of neurological and psychiatric illnesses. In particular, I focus on elucidating the mechanisms of AMPA-R assembly and trafficking as well as the mechanisms of AMPA-R modulation by accessory transmembrane proteins. Ultimately, this work aids our understanding of synaptic transmission and basic brain function, and may ultimately helpful in efforts to develop therapeutic agents for AMPA-R related disorders.

Excitatory glutamatergic transmission in the brain

In mammals, the central nervous system consists of an extremely complicated connectivity between billions of neurons. Neurons connect functionally to each other at synapses, specialized sites of communication allowing for fast processing and the transmission of signals between cells.

This neuronal communication underlies all basic as well as higher order processing essential for function. Neurons can alter their responsiveness to signals from other neurons. This flexibility or plasticity in the in the strength of connectivity between neurons form the molecular basis that underlies experience dependent change in behavior or learning.

Neurons use neurotransmitters to facilitate communication from one cell to another across synapses. Glutamate is the principle excitatory transmitter in the brain. Iontropic glutamate receptors are ligand gated ion channels and are the primary receptive elements that allow one neuron to “listen” to the other neuron during synaptic communication between cells. In synaptic transmission, glutamate is released from the presynaptic specialization of one cell into the synaptic cleft. It can then bind to glutamate receptors present on the closely apposing postsynaptic specialization of another cell. The activation of glutamate receptors allows the passage of cations into the cell through the glutamate receptor ion channel, leading to depolarization of the postsynaptic cell. Spatial or temporal summation of postsynaptic depolarizations may then be sufficient to generate an action potential in this cell, allowing it to transmit information to other neurons in the circuit.

Sites of excitatory transmission

Excitatory glutamatergic synapses are typically present on tiny protrusions of dendrites called dendritic spines (Bourne and Harris, 2008). They are characterized by a morphological and functional specialization called the postsynaptic density (PSD). The PSD, usually at the tip of a dendritic spine, is a well organized structure that apposes the presynaptic terminal, positioned just across the synapse from the presynaptic active zone poised with vesicles of neurotransmitter. The PSD is an incredibly protein rich structure, originally identified using electron microscopy as the electron dense region at the membrane of the post synaptic cell (Gray, 1959; Palay, 1958). The PSD serves to organize the majority of the postsynaptic signaling machinery. The molecular organization includes neurotransmitter receptors like glutamate receptors, other ion channels, actin cytoskeleton, scaffolding proteins, cell adhesion molecules, and a large variety of signaling and regulatory molecules. Together these components function to mediate the cellular processes necessary for synaptic transmission and synaptic plasticity Some of these PSD proteins are discussed in Chapter 3 of this dissertation in the context of glutamate receptor interacting partners.

Glutamate Receptors

There are four subtypes of ionotropic glutamate receptors. These receptors directly respond to the glutamate with a conformational change

which allows ions to pass through the ion channel pore into the cell. Ionotropic glutamate receptors (iGluRs) are pharmacologically characterized into three different categories subfamilies based on their abilities to bind specific agonists. The primary focus of this dissertation work is α-amino-3-hydroxyl-5-methyl-4-isoxazole-propionate (AMPA) receptors, which are the primary mediators of fast excitatory neurotransmission in the brain. The other subtypes are N-methyl-D-aspartic acid (NMDA) receptors, and kainate receptors. Delta (δ) receptors are considered orphan glutamate receptors, as they are structurally related, but the ligands that mediate channel function for these are not known (Lomeli et al., 1993). There are multiple genes that encode the subunits that can make up each iGluR receptor subtype: AMPA-Rs: GluA1-4, NMDA-Rs: GluN1, GluN2A-D, GluN3A-B, kainate receptors: GluK1-4, and delta receptors: GluD1-2.

AMPA-Rs are the primary focus of this dissertation. They mediate fast component of most excitatory neurotransmission, and changes in their numbers and functional properties at synapses underlie forms of synaptic plasticity. They are essential for normal synaptic function and are important for learning any memory (Malinow and Malenka, 2002).

AMPA-R primary structure and subunit composition

The core functional AMPA-R complex is a tetrameric assembly consisting of some combination of the four AMPA-R subunits, GluA1-4 (Rosenmund et al., 1998). The subunit types share the same basic homology and domain organization (shown in Fig 2), but also have key differences. For all subunits, the extracellular portion of the receptor consists of the amino terminal domain (NTD) and the ligand binding domain (LBD). The ligand binding domain consists of two sub domains termed S1 and S2 that are separated by the channel pore segment. These adopt a clamshell like structure composed of two lobes (Armstrong and Gouaux, 2000). The ion channel pore forming transmembrane domain (TMD) consists of three membrane spanning segments (M1, M3, and M4) and one reentrant loop (M2) (Hollmann et al., 1994). The LBD undergoes conformational changes when glutamate in the synapse binds within the clamshell like structure, inducing a closure movement which results in gating of the ion channel (Armstrong and Gouaux, 2000) The small C-terminal domain (CTD) is intracellular and interacts with cytosolic proteins to regulate AMPA-R function including synaptic anchoring and trafficking. GluA1-4 show similarity in their extracellular domains, with the greater variation occurring in their intracellular C-terminal tails. The overall structure of an AMPA-R subunit is shown in Figure 1.

Functional AMPA-Rs can be composed of different combinations and stoichiometries of subunits. Most AMPA-Rs in the brain are heterotetrameric

assemblies. AMPA-R subunits are also subject to multiple forms of alternative splicing which results in flip and flop isoforms, and RNA editing can occur at two different locations within the AMPA-R subunits (Seeburg and Hartner, 2003; Sommer et al., 1990). These factors are highly regulated and can affect the maturation and trafficking as well as the pharmacological and kinetic properties of the AMPA-R ion channel and also change their binding to various intracellular partners (Hollmann and Heinemann, 1994; Monyer et al., 1991; Sommer et al., 1990; Song and Huganir, 2002). Overall, different combinations of differentially spliced and edited subunits contributes to the existence of AMPA-Rs with different functional properties.

AMPA-R Ultrastructure

Structural studies have been critical in understanding the mechanisms of AMPA-R function. The field has only slowly learned about the structural details of AMPA-Rs. This is primarily due to technical issues, as membrane proteins are difficult to work with. Great advances were made in the 90's when the structure of the isolated AMPA-R LBD (referred to as S1S2) was solved (Armstrong et al., 1998). S1S2 adopts a clamshell like structure consisting of two lobes. Glutamate binds in the pocket, inducing a closure of the clamshell. S1S2 exists as a dimer in the crystal structure, and this arrangement is physiologically relevant as the AMPA-R tetramer exists as a

dimer of dimers (Armstrong and Gouaux, 2000). Subsequently similar strategies have been to determine the crystal structure of other glutamate receptor LBDs as well AMPA-R LBDs in complex with other ligands, partial agonists, antagonists, and modulators such as cyclothiazide (CTZ) and in different conformational states (Armstrong and Gouaux, 2000; Armstrong et al., 2006; Armstrong et al., 1998; Inanobe et al., 2005; Mayer, 2005; Mayer et al., 2001; Nanao et al., 2005; Naur et al., 2007). Collectively studies of the isolated LBD of glutamate receptors in the presence of various chemical compounds have suggested mechanisms for both ligand specificity and mechanisms by which ligand binding in the extracellular region translates to channel gating.

It wasn't until many years later, that the structures of the isolated glutamate receptor NTDs were solved, including the NTD of the AMPA-R subunit, GluA2 (Clayton et al., 2009; Farina et al., 2011; Jin et al., 2009; Karakas et al., 2009, 2011; Kumar and Mayer, 2012; Kumar et al., 2009; Rossmann et al., 2011). A common feature of these NTD structures is that, similar to the LBD, the NTD adopts a clamshell like structure. Differences in the extent of conformational change seen in the NTD differs across iGluR subytpes, with the AMPA-R and KA-R NTDs showing limited variation in the extent of NTD closure (Kumar and Mayer, 2013). In contrast, NMDA-R NTDs are proposed to undergo larger conformational changes that are relevant for

allosteric modulation by small molecules (Gielen et al., 2008; Gielen et al., 2009; Hatton and Paoletti, 2005; Karakas et al., 2009; Perin-Dureau et al., 2002). Overall, structures of glutamate receptor NTDs have provided important insight into the processes of both subunit assembly and allosteric modulation (in the case of NMDA-Rs). To date, there is no evidence that the NTDs of AMPA-R or KA-R NTDs are capable of allosteric modulation. The work in Chapter 4 of this dissertation identifies a potential role for the AMPA-R NTD in allosteric modulation.

In 2005, full length native AMPA-Rs purified from rat brain were analyzed using single particle EM. These structures were reported at about 30 Angstroms resolution. They depict the native AMPA-R particles in both the presence and absence of stargazin/TARP auxiliary subunits (Nakagawa et al., 2005; Nakagawa et al., 2006). This study provided the first insight into the global domain arrangement of the AMPA-Rs. They interpreted the EM density using Fab fragment labeling and also by placing the solved crystal structures of isolated domains within the EM map. The sizes and shapes of the globular densities in the EM image are consistent with the crystal structures of the isolated domains (namely the GluA2 LBD and NTD)(Clayton et al., 2009). The same single particle EM studies also revealed global conformational changes in the receptor complex in the presence of pharmacological agents associated with receptor desensitization, namely an apparent lateral displacement of the

two NTD dimers (Nakagawa et al., 2005; Nakagawa et al., 2006) These electron microscopy studies provided the first insight into the ultrastructure of the full length native AMPA-R, and suggested that global conformation changes occur upon channel gating beyond the movements in the LBD predicted by earlier studies.

Later yet, the crystal structure of the nearly intact AMPA-R (GluA2cryst construct) was reported (Sobolevsky et al., 2009). This study was a huge breakthrough for the field as it resolved the atomic structure of the entire tetrameric assembly of the AMPA-R subunits, and proposed many important mechanisms involved in ligand binding, gating, and modulation. In this 3.6 Angstrom resolution structure, the AMPA-R is a homotetrameric assembly of the modified GluA2 subunit (GluA2cryst) in complex with the competitive antagonist ZK00775, representing a closed, nonconductive gating state. The architecture of the complex is subdivided into three layers representing the NTD, LBD, and TMD. The NTD and LBD are consistent with the previous isolated structures of these domains, and both of these extracellular components are represented as dimers, showing two-fold symmetry. This structure provided the first high resolution information about the ion channel forming transmembrane domain of glutamate receptors. This domain is arranged with four-fold symmetry. This structure also revealed that domain swapping and crossover occurs between subunits. That is to say the

combination of conformationally distinct pairs is different depending on the domain. If each subunit in a tetramer is referred to as A-D, in the NTD the dimer pairs are A-B and C-D, however this transitions to A-C and B-D at the level of the LBD, and finally this pairwise arrangement does not exist in the TMD, as here the subunits have four-fold symmetry. This structure also includes (although shortened and modified) the linkers that couple the NTD and LBD and the LBD and TMD. These linkers are essential to accommodate the symmetry mismatches and domain swapping already mentioned and also the transduction of LBD conformational changes upon binding with the TMD channel function as well as alterations in relative NTD conformation. Overall structural studies have provided the field with invaluable insight into the architecture, assembly, and function of AMPA-Rs.

AMPA-R biogenesis, assembly, and trafficking

The synthesis, assembly and trafficking of AMPA-Rs are highly regulated processes required for basic synaptic transmission and synaptic plasticity. The composition of an AMPA-Rs critically affects the receptor trafficking, localization, and functional properties of the receptor. Like all membrane proteins, AMPA-R subunits are synthesized in the endoplasmic reticulum (ER), and are then inserted into the ER membrane. Monomers can combine into dimers, in process in which the NTD portion of the subunits is

critical (Kuusinen et al., 1999). AMPA-R subunit dimers can then come together to form tetramers, which involves the TMD region as well as the LBD region (Ayalon and Stern-Bach, 2001; Greger et al., 2006). AMPA-R tetramers can then exit the ER, entering the trans Golgi network in trafficking vesicles. Speed and efficiency of exit from the ER depends and trafficking to the cell surface depends the subunit composition of the receptor complex (Coleman et al., 2006; Greger et al., 2002). Mechanisms of AMPA-R assembly are addressed in Chapter 2 of this dissertation.

In current models, the recruitment of AMPA-Rs to the synapse takes place in multiple steps. After the exocytosis of intracellular receptors out to the plasma membrane of the cell, lateral diffusion moves receptors to the actual synaptic site, where they can be stabilized in the PSD by scaffolding proteins (Opazo and Choquet, 2011). AMPA-Rs are also removed from the plasma membrane via intracellular vesicles (reviewed in (Shepherd and Huganir, 2007)). This bidirectional trafficking of AMPA-Rs regulateds the number and function of AMPA-Rs at the synapse and is critically involved in synaptic plasticity.

Auxiliary subunits

The core AMPA-R complex is a tetrameric assembly of core subunits forming the ligand gated ion channel. However, in vivo, other membrane proteins associate with this core complex, and modulate trafficking and channel function of the receptor.

Stargazin/TARPs

In characterizing an ataxic mouse with a spontaneous mutation, the small transmembrane protein, stargazin (γ-2), was identified to be critical for the functional expression of AMPA-Rs in cerebellar granule cells (Chen et al., 2000; Hashimoto et al., 1999). Stargazin is the founding member of an entire family of related transmembrane proteins, the TARPs (Tomita et al., 2003), which are tetraspanning membrane proteins with intracellular N- and C-terminal tails. The roles of TARPs as AMPA-R auxiliary subunits have been well studied. The past decade of research has demonstrated that there are at least six TARP isoforms (γ's) with widespread distribution throughout the CNS (Burgess et al., 2001; Klugbauer et al., 2000). TARPs can be divided into several subtypes that are divided by both primary sequence and by the exact functional profile they impart on AMPA-Rs (Cho et al., 2007; Kato et al., 2010; Kato et al.; Kato et al., 2007; Milstein et al., 2007; Tomita et al., 2003).

TARPs contribute to AMPA-R synaptic function as they form stable complexes with AMPA-Rs in the brain, modulate AMPA-R trafficking, and modulate their

channel kinetics. TARPs coimmunoprecipiate with AMPA-R subunits in both the brain and in heterologous cells (Chen et al., 2000; Fukata et al., 2005; Tomita et al., 2003; Tomita et al., 2004; Vandenberghe et al., 2005). TARPs are non pore forming subunits, that stably bind to AMPA-Rs (Fukata et al., 2005; Nakagawa et al., 2005; Vandenberghe et al., 2005). Single particle electron microscopy provided the first evidence for the structural contribution of TARPs to the native AMPA-R, demonstrating that stargazin contributes to the transmembrane density of the tetrameric AMPA-R complex (Nakagawa et al., 2005; Nakagawa et al., 2006). Further chimera domain swapping and mutagenesis experiments further assessed how stargazin interacts with and modulates AMPA-Rs (Tomita et al., 2005a).

TARPs regulate the surface and synaptic targeting of AMPA-Rs. In the stagazer null mice, the cerebellar granule cells almost entirely lack AMPA-R mediated currents compared to wildtype, yet this can be rescued by the overexpression of stargazin (Chen et al., 2000), and other TARP isoforms including γ-3,-4, and -8 ((Tomita et al., 2003). Similarly, in mice that lack γ-8, the primary type isoform in the hippocampus, AMPA-R currents are significantly reduced in hippocampal pyramidal neurons (Chen et al., 2000; Fukaya et al., 2006; Rouach et al., 2005). Such effects have been extensively characterized. Overexpression of TARPs in both neurons and heterologous cells results in an increase in AMPA-Rs at the cell surface. (Chen et al., 2003;

Priel et al., 2005; Rouach et al., 2005; Tomita et al., 2005a; Tomita et al., 2004; Turetsky et al., 2005; Yamazaki et al., 2004).

Beyond helping AMPA-Rs to the cell surface, TARPs also specifically target them to the synapse. The TARP's cytosolic C-terminal region contains a PDZ binding motif that is critical for this function. In stargazer mutant mice, the transfection of stargazin lacking these residues rescues the AMPA-R surface expression, but fails to rescue synaptic localization that was seen with transfection of wildtype (Chen et al., 2000). TARPs interact with scaffolding proteins in the MAGUK family including PSD-95, which are known to be integral parts of the PSD and to be critically involved in AMPA-R stabilization at synapses (Chen et al., 2000; Dakoji et al., 2003; Kim and Sheng, 2004; Schnell et al., 2002). The TARP/PSD-95 interaction is critical for the clustering of AMPA-Rs at synapses by mediating the lateral diffusion of AMPA-Rs from extrasynaptic to synaptic sites (Bats et al., 2007). TARPs are also subject to posttranslational modification events, which influence the modulation of AMPA-Rs. Different residues of the C-terminal portion of TARPs are subject to phosphorylation events by a variety of kinases (Tomita et al., 2005b), the consequences of which are relevant for the regulation of AMPA-R trafficking and localization in synaptic plasticity (Jackson and Nicoll, 2011).

TARPs also modulate AMPA-R channel gating and pharmacology, independent of their trafficking role. In heterologous systems, co-expression of stargazin with AMPA-R subunits enhances the amplitude of steady state currents, slows the rate of receptor deactivation, slows the rate of receptor desensitization in the presence of prolonged glutamate, and also increases the recovery rate from desensitization. In terms of pharmacology, the presence of stargazin potentiates affinity for various agonists including glutamate and kainate (Bedoukian et al., 2008; Priel et al., 2005; Tomita et al., 2005a; Turetsky et al., 2005; Yamazaki et al., 2004). The roles of stargazin in AMPA-R trafficking and gating are mechanistically dissociable, as they are imparted by distinct regions of the stargazin molecule (Tomita et al., 2005a). Later work in the field has demonstrated that different TARP isoforms have slightly different signatures in how and the degree to which they modulate gating kinetics and pharmacology. This is also dependent on the subunit composition of the AMPA-Rs (Cho et al., 2007; Kato et al., 2010; Korber et al., 2007; Kott et al., 2007; Milstein et al., 2007; Soto et al., 2009; Suzuki et al., 2008). Taken together, the TARPs function as auxiliary subunits and increase the functional repertoire of AMPA-R function.

Other AMPA-R auxiliary subunits

More recent screening and proteomic studies have revealed several additional unrelated transmembrane proteins that may also function as AMPA-R auxiliary subunits in the mammalian brain. There are several different families of such proteins currently known. These include cornichon like proteins (CNIHs) (Schwenk et al., 2009), cysteine knot AMPA-R modulating protein 44 (CKAMP44) (von Engelhardt et al., 2010) and synapse differentially induced gene 1 (SynDIG1) (Kalashnikova et al., 2010). Work in this dissertation alongside another independent study also identified germ line specific gene 1 (GSG1L), as a novel AMPA-R auxiliary subunit (Schwenk et al., 2012; Shanks et al., 2012). The auxiliary subunits impart distinct functional properties on the associated receptor, and thus serve to amplify the functional diversity of AMPA-Rs in the brain.

The cornichon family of AMPA-R subunits are the focus of Chapter 3 of this dissertation. CNIH homologues are small three pass transmembrane proteins with an intracellular N-terminus, and extracellular C-terminus. The CNIH homologue, CNIL was originally identified in drosophila, and roles for these proteins in the export of epidermal growth factor receptor ligands from the endoplasmic reticulum is phylogenically conserved (Bokel et al., 2006; Roth et al., 1995). A new function for CNIH-2/3 as AMPA-R auxiliary subunits in the brain was identified in 2009 (Schwenk et al., 2009). Similar to the TARPs, the co-expression of CNIH-2 or CNIH-3 homologues with AMPA-R

subunits in heterologous cells increases AMPA-R surface expression and slows AMPA-R deactivation and desensitization kinetics in response to glutamate application and also alters the pharmacology of various ligands (Kato et al., 2010; Schober et al., 2011; Schwenk et al., 2009; Shi et al., 2010). Recent evidence suggests a role for CNIHs in abolishing the resensitization of AMPA-R mediated current conferred by various TARP subtypes (Kato et al., 2010). Additionally, in AMPA-R complexes with both TARPs and CNIH-2, these two auxiliary proteins appear to compete for interaction with the AMPA-R (Gill et al., 2011). These results suggest that CNIHs and TARPs cooperatively functional as AMPA-R modulators. There is still controversy regarding CNIH function in the brain (Brockie and Maricq, 2010). However in the hippocampus CNIH-2/3 was shown to regulate assembly and stoichiometry of AMPA-Rs (Kim et al., 2010), and more recently, CNIH-2 was suggested to play roles in regulating glial AMPA-Rs (Coombs et al., 2012). In the future, analysis of knockout mice for the cornichon homologues may reveal more about the roles of these proteins in the brain.

CKAMP44 was identified was in AMPA-R interactor in a proteomic screen done in mouse brain (von Engelhardt et al., 2010). Part of the Shisa family, it is a type I transmembrane protein with an intracellular binding motif and a cysteine rich N-terminal domain, that is predicted to form a knot structure similar to that of known peptide neurotoxins (Norton and Pallaghy,

1998). CKAMP44 imparts distinct functional properties on AMPA-Rs, prolonging deactivation and desensitization while slowing the rate of recovery from desensitization. These modulation parameters are unique, and in contrast to the modulation of AMPA-Rs by TARPs and cornichons. The authors also demonstrate relevance of these modulatory effects in hippocampal function.

SynDIG1 was identified through a microarray approach as being a gene associated with neuronal differentiation (Diaz et al., 2002). It is a type II transmembrane protein, that has been proposed to regulate the synaptic localization of AMPA-Rs (Kalashnikova et al., 2010) Further experiments will be necessary to determine whether SynDIG1 is a true AMPA-R auxiliary subunit that can modulate AMPA-R gating properties.

The fact that there are different types of transmembrane AMPA-R accessory proteins enables a very diverse regulation of AMPA-R function. Many of these novel AMPA-R regulators have been identified in recent years, further fueling additional efforts to identify potential novel interactors. The research in Chapter 3 of this dissertation was one such endeavor that successfully resulted in a list of many candidates. This study, and an independent study in parallel identified the novel AMPA-R auxiliary subunit, GSG1L.

Dissertation objectives

The objective of this dissertation work is to provide insight into the molecular mechanisms of AMPA-R function. Chapter 2 examines early AMPA-R subunit assembly mechanisms. The assembly of AMPA-Rs into functional tetramers is a critical determinant in AMPA-R synaptic trafficking and ultimately determines the functional properties at the synapse. While AMPA-R trafficking is a well studied process, the molecular details of the early phases including biosynthesis and assembly are less well understood. The work in Chapter 2 provides insight into the normal assembly process of full length AMPA-R subunits at an ultrastructural level of detail. Using novel approaches, I isolated both mature tetrameric AMPA-Rs as well as the transient AMPA-R dimeric biosynthetic intermediates, and report the single-particle EM three-dimensional structures of both these AMPA-R forms. These structures reveal the global domain arrangement of the both the dimeric and tetrameric AMPA-Rs. Overall, this study revealed that biosynthesis and assembly for AMPA-Rs proceeds by the formation of dimers in which the AMPA-R NTDs and the transmembrane portions are closely coupled, while the LBDs are pushed out and do not contact each other.

Chapter 3 and 4 of this dissertation both address mechanisms of AMPA receptor modulation by auxiliary proteins. The initial objective in Chapter 3 was to investigate the AMPA-R proteome. AMPA-Rs in the brain interact with a large variety of other proteins. Over the years, many researchers have sought to identify novel AMPA-R interacting partners in attempt to learn more about the molecular mechanisms of AMPA-R function. Early studies to this end utilized yeast two-hybrid screens in which small cytosolic regions of the AMPA-R were used as bait to screen cDNA libraries (Dong et al., 1997; Lee et al., 2002; Nishimune et al., 1998; Nuriya et al., 2005; Osten et al., 1998; Schulz et al., 2004; Shen et al., 2000; Song et al., 1998; Xia et al., 1999). More recent studies have favored mass spectrometry in order to gain insight into the AMPA-R proteome (Coombs et al., 2012; Kang et al., 2012; Nakagawa et al., 2005; Schwenk et al., 2012; Schwenk et al., 2009; Shanks et al., 2012; von Engelhardt et al., 2010). As described earlier, many of these recent screening and proteomic studies have resulted in the discovery of additional transmembrane proteins that also function as AMPA-R auxiliary subunits.

Chapter 3 in this dissertation was a collaborative project in which we utilized mass spectrometry to investigate the AMPA-R interactome, with the goal of identifying novel AMPA-R interacting proteins. In this way, we identified the majority of known interacting proteins, validating our methods. More importantly, the resulting interactome data can serve as a resource for others

and provides novel candidates for further studies. Among the candidates, I focused on a predicted protein GSG1L, a membrane protein that co-purified specifically with AMPA-Rs. Using detailed molecular, cellular, electrophysiological, and biochemical experiments, we validated the interaction and determined that GSG1L is unique modulator of AMPA-R function. This study was important because it identified a novel AMPA-R subunit that confers a new functional repertoire to AMPA-Rs.

Chapter 4 in this dissertation focuses on the molecular mechanisms of interaction with and modulation by a known AMPA-R auxiliary subunit type, cornichons. Understanding the molecular details of interactions between AMPA-Rs and auxiliary subunits provides mechanistic insight into their functional importance in AMPA-R modulation, and may in the future provide insight for designing therapeutic agents. Using a variety of techniques I assessed the contribution of cornichons to the AMPA-R structure, and mapped out the complex molecular associations between the two proteins. This study identified loci on the cornichon molecule critical for the interaction with AMPA-Rs down to the level of specific residues. It is also the first work to demonstrate that both of the extracellular domains of the AMPA-R, the LBD and NTD interact with the extracellular loops of cornichon homologues. These results support a new model for the modulation of AMPA-R function by auxiliary subunits in which the AMPA-R NTD can participate.

The work in this dissertation contributes important insights into the molecular mechanisms that govern AMPA-R assembly and AMPA-R functional modulation by auxiliary subunits.

References:

Armstrong, N., and Gouaux, E. (2000). Mechanisms for activation and antagonism of an AMPA-sensitive glutamate receptor: crystal structures of the GluR2 ligand binding core. Neuron *28*, 165-181.

Armstrong, N., Jasti, J., Beich-Frandsen, M., and Gouaux, E. (2006). Measurement of conformational changes accompanying desensitization in an ionotropic glutamate receptor. Cell *127*, 85-97.

Armstrong, N., Sun, Y., Chen, G.Q., and Gouaux, E. (1998). Structure of a glutamate-receptor ligand-binding core in complex with kainate. Nature *395*, 913-917.

Ayalon, G., and Stern-Bach, Y. (2001). Functional assembly of AMPA and kainate receptors is mediated by several discrete protein-protein interactions. Neuron *31*, 103-113.

Bats, C., Groc, L., and Choquet, D. (2007). The interaction between Stargazin and PSD-95 regulates AMPA receptor surface trafficking. Neuron *53*, 719-734.

Bedoukian, M.A., Whitesell, J.D., Peterson, E.J., Clay, C.M., and Partin, K.M. (2008). The stargazin C terminus encodes an intrinsic and transferable membrane sorting signal. J Biol Chem *283*, 1597-1600.

Bokel, C., Dass, S., Wilsch-Brauninger, M., and Roth, S. (2006). Drosophila Cornichon acts as cargo receptor for ER export of the TGFalpha-like growth factor Gurken. Development *133*, 459-470.

Bourne, J.N., and Harris, K.M. (2008). Balancing structure and function at hippocampal dendritic spines. Annu Rev Neurosci *31*, 47-67.

Brockie, P.J., and Maricq, A.V. (2010). In a pickle: is cornichon just relish or part of the main dish? Neuron *68*, 1017-1019.

Burgess, D.L., Gefrides, L.A., Foreman, P.J., and Noebels, J.L. (2001). A cluster of three novel Ca2+ channel gamma subunit genes on chromosome 19q13.4: evolution and expression profile of the gamma subunit gene family. Genomics *71*, 339-350.

Chen, L., Chetkovich, D.M., Petralia, R.S., Sweeney, N.T., Kawasaki, Y., Wenthold, R.J., Bredt, D.S., and Nicoll, R.A. (2000). Stargazin regulates synaptic targeting of AMPA receptors by two distinct mechanisms. Nature *408*, 936-943.

Chen, L., El-Husseini, A., Tomita, S., Bredt, D.S., and Nicoll, R.A. (2003). Stargazin differentially controls the trafficking of alpha-amino-3-hydroxyl-5-methyl-4-isoxazolepropionate and kainate receptors. Mol Pharmacol *64*, 703-706.

Cho, C.H., St-Gelais, F., Zhang, W., Tomita, S., and Howe, J.R. (2007). Two families of TARP isoforms that have distinct effects on the kinetic properties of AMPA receptors and synaptic currents. Neuron *55*, 890-904.

Clayton, A., Siebold, C., Gilbert, R.J., Sutton, G.C., Harlos, K., McIlhinney, R.A., Jones, E.Y., and Aricescu, A.R. (2009). Crystal structure of the GluR2 amino-terminal domain provides insights into the architecture and assembly of ionotropic glutamate receptors. J Mol Biol *392*, 1125-1132.

Coleman, S.K., Moykkynen, T., Cai, C., von Ossowski, L., Kuismanen, E., Korpi, E.R., and Keinanen, K. (2006). Isoform-specific early trafficking of AMPA receptor flip and flop variants. J Neurosci *26*, 11220-11229.

Coombs, I.D., Soto, D., Zonouzi, M., Renzi, M., Shelley, C., Farrant, M., and Cull-Candy, S.G. (2012). Cornichons modify channel properties of recombinant and glial AMPA receptors. J Neurosci *32*, 9796-9804.

Dakoji, S., Tomita, S., Karimzadegan, S., Nicoll, R.A., and Bredt, D.S. (2003). Interaction of transmembrane AMPA receptor regulatory proteins with multiple membrane associated guanylate kinases. Neuropharmacology *45*, 849-856.

Diaz, E., Ge, Y., Yang, Y.H., Loh, K.C., Serafini, T.A., Okazaki, Y., Hayashizaki, Y., Speed, T.P., Ngai, J., and Scheiffele, P. (2002). Molecular analysis of gene expression in the developing pontocerebellar projection system. Neuron *36*, 417-434.

Dong, H., O'Brien, R.J., Fung, E.T., Lanahan, A.A., Worley, P.F., and Huganir, R.L. (1997). GRIP: a synaptic PDZ domain-containing protein that interacts with AMPA receptors. Nature *386*, 279-284.

Farina, A.N., Blain, K.Y., Maruo, T., Kwiatkowski, W., Choe, S., and Nakagawa, T. (2011). Separation of domain contacts is required for heterotetrameric assembly of functional NMDA receptors Journal of Neuroscience.

Fukata, Y., Tzingounis, A.V., Trinidad, J.C., Fukata, M., Burlingame, A.L., Nicoll, R.A., and Bredt, D.S. (2005). Molecular constituents of neuronal AMPA receptors. J Cell Biol *169*, 399-404.

Fukaya, M., Tsujita, M., Yamazaki, M., Kushiya, E., Abe, M., Akashi, K., Natsume, R., Kano, M., Kamiya, H., Watanabe, M.*, et al.* (2006). Abundant distribution of TARP gamma-8 in synaptic and extrasynaptic surface of hippocampal neurons and its major role in AMPA receptor expression on spines and dendrites. Eur J Neurosci *24*, 2177-2190.

Gielen, M., Le Goff, A., Stroebel, D., Johnson, J.W., Neyton, J., and Paoletti, P. (2008). Structural rearrangements of NR1/NR2A NMDA receptors during allosteric inhibition. Neuron *57*, 80-93.

Gielen, M., Siegler Retchless, B., Mony, L., Johnson, J.W., and Paoletti, P. (2009). Mechanism of differential control of NMDA receptor activity by NR2 subunits. Nature *459*, 703-707.

Gill, M.B., Kato, A.S., Roberts, M.F., Yu, H., Wang, H., Tomita, S., and Bredt, D.S. (2011). Cornichon-2 modulates AMPA receptor-transmembrane AMPA receptor regulatory protein assembly to dictate gating and pharmacology. J Neurosci *31*, 6928-6938.

Gray, E.G. (1959). Axo-somatic and axo-dendritic synapses of the cerebral cortex: an electron microscope study. J Anat *93*, 420-433.

Greger, I.H., Akamine, P., Khatri, L., and Ziff, E.B. (2006). Developmentally regulated, combinatorial RNA processing modulates AMPA receptor biogenesis. Neuron *51*, 85-97.

Greger, I.H., Khatri, L., and Ziff, E.B. (2002). RNA editing at arg607 controls AMPA receptor exit from the endoplasmic reticulum. Neuron *34*, 759-772.

Hashimoto, K., Fukaya, M., Qiao, X., Sakimura, K., Watanabe, M., and Kano, M. (1999). Impairment of AMPA receptor function in cerebellar granule cells of ataxic mutant mouse stargazer. J Neurosci *19*, 6027-6036.

Hatton, C.J., and Paoletti, P. (2005). Modulation of triheteromeric NMDA receptors by N-terminal domain ligands. Neuron *46*, 261-274.

Hollmann, M., and Heinemann, S. (1994). Cloned glutamate receptors. Annu Rev Neurosci *17*, 31-108.

Hollmann, M., Maron, C., and Heinemann, S. (1994). N-glycosylation site tagging suggests a three transmembrane domain topology for the glutamate receptor GluR1. Neuron *13*, 1331-1343.

Inanobe, A., Furukawa, H., and Gouaux, E. (2005). Mechanism of partial agonist action at the NR1 subunit of NMDA receptors. Neuron *47*, 71-84.

Jackson, A.C., and Nicoll, R.A. (2011). The expanding social network of ionotropic glutamate receptors: TARPs and other transmembrane auxiliary subunits. Neuron *70*, 178-199.

Jin, R., Singh, S.K., Gu, S., Furukawa, H., Sobolevsky, A.I., Zhou, J., Jin, Y., and Gouaux, E. (2009). Crystal structure and association behaviour of the GluR2 amino-terminal domain. EMBO J *28*, 1812-1823.

Kalashnikova, E., Lorca, R.A., Kaur, I., Barisone, G.A., Li, B., Ishimaru, T., Trimmer, J.S., Mohapatra, D.P., and Diaz, E. (2010). SynDIG1: an activity-regulated, AMPA- receptor-interacting transmembrane protein that regulates excitatory synapse development. Neuron *65*, 80-93.

Kang, M.G., Nuriya, M., Guo, Y., Martindale, K.D., Lee, D.Z., and Huganir, R.L. (2012). Proteomic analysis of alpha-amino-3-hydroxy-5-methyl-4-isoxazole propionate receptor complexes. J Biol Chem *287*, 28632-28645.

Karakas, E., Simorowski, N., and Furukawa, H. (2009). Structure of the zinc-bound amino-terminal domain of the NMDA receptor NR2B subunit. EMBO J *28*, 3910-3920.
Karakas, E., Simorowski, N., and Furukawa, H. (2011). Subunit arrangement and phenylethanolamine binding in GluN1/GluN2B NMDA receptors. Nature *475*, 249-253.

Kato, A.S., Gill, M.B., Ho, M.T., Yu, H., Tu, Y., Siuda, E.R., Wang, H., Qian, Y.W., Nisenbaum, E.S., Tomita, S.*, et al.* (2010). Hippocampal AMPA Receptor Gating Controlled by Both TARP and Cornichon Proteins. Neuron *68*, 1082-1096.

Kato, A.S., Gill, M.B., Yu, H., Nisenbaum, E.S., and Bredt, D.S. TARPs differentially decorate AMPA receptors to specify neuropharmacology. Trends Neurosci *33*, 241-248.

Kato, A.S., Zhou, W., Milstein, A.D., Knierman, M.D., Siuda, E.R., Dotzlaf, J.E., Yu, H., Hale, J.E., Nisenbaum, E.S., Nicoll, R.A.*, et al.* (2007). New transmembrane AMPA receptor regulatory protein isoform, gamma-7, differentially regulates AMPA receptors. J Neurosci *27*, 4969-4977.

Kim, E., and Sheng, M. (2004). PDZ domain proteins of synapses. Nat Rev Neurosci *5*, 771-781.

Kim, K.S., Yan, D., and Tomita, S. (2010). Assembly and stoichiometry of the AMPA receptor and transmembrane AMPA receptor regulatory protein complex. J Neurosci *30*, 1064-1072.

Klugbauer, N., Dai, S., Specht, V., Lacinova, L., Marais, E., Bohn, G., and Hofmann, F. (2000). A family of gamma-like calcium channel subunits. FEBS Lett *470*, 189-197.

Korber, C., Werner, M., Kott, S., Ma, Z.L., and Hollmann, M. (2007). The transmembrane AMPA receptor regulatory protein gamma 4 is a more effective modulator of AMPA receptor function than stargazin (gamma 2). J Neurosci *27*, 8442-8447.

Kott, S., Werner, M., Korber, C., and Hollmann, M. (2007). Electrophysiological properties of AMPA receptors are differentially modulated depending on the associated member of the TARP family. J Neurosci *27*, 3780-3789.

Kumar, J., and Mayer, M.L. (2012). Functional insights from glutamate receptor ion channel structures. Annu Rev Physiol *75*, 313-337.

Kumar, J., and Mayer, M.L. (2013). Functional insights from glutamate receptor ion channel structures. Annu Rev Physiol *75*, 313-337.

Kumar, J., Schuck, P., Jin, R., and Mayer, M.L. (2009). The N-terminal domain of GluR6-subtype glutamate receptor ion channels. Nat Struct Mol Biol *16*, 631-638.

Kuusinen, A., Abele, R., Madden, D.R., and Keinanen, K. (1999). Oligomerization and ligand-binding properties of the ectodomain of the alpha-amino-3-hydroxy-5-methyl-4-isoxazole propionic acid receptor subunit GluRD. J Biol Chem *274*, 28937-28943.

Lee, S.H., Liu, L., Wang, Y.T., and Sheng, M. (2002). Clathrin adaptor AP2 and NSF interact with overlapping sites of GluR2 and play distinct roles in AMPA receptor trafficking and hippocampal LTD. Neuron *36*, 661-674.

Lomeli, H., Sprengel, R., Laurie, D.J., Kohr, G., Herb, A., Seeburg, P.H., and Wisden, W. (1993). The rat delta-1 and delta-2 subunits extend the excitatory amino acid receptor family. FEBS Lett *315*, 318-322.

Malinow, R., and Malenka, R.C. (2002). AMPA receptor trafficking and synaptic plasticity. Annu Rev Neurosci *25*, 103-126.

Mayer, M.L. (2005). Crystal structures of the GluR5 and GluR6 ligand binding cores: molecular mechanisms underlying kainate receptor selectivity. Neuron *45*, 539-552.
Mayer, M.L., Olson, R., and Gouaux, E. (2001). Mechanisms for ligand binding to GluR0 ion channels: crystal structures of the glutamate and serine complexes and a closed apo state. J Mol Biol *311*, 815-836.

Milstein, A.D., Zhou, W., Karimzadegan, S., Bredt, D.S., and Nicoll, R.A. (2007). TARP subtypes differentially and dose-dependently control synaptic AMPA receptor gating. Neuron *55*, 905-918.

Monyer, H., Seeburg, P.H., and Wisden, W. (1991). Glutamate-operated channels: developmentally early and mature forms arise by alternative splicing. Neuron *6*, 799-810.

Nakagawa, T., Cheng, Y., Ramm, E., Sheng, M., and Walz, T. (2005). Structure and different conformational states of native AMPA receptor complexes. Nature *433*, 545-549.

Nakagawa, T., Cheng, Y., Sheng, M., and Walz, T. (2006). Three-dimensional structure of an AMPA receptor without associated stargazin/TARP proteins. Biol Chem *387*, 179-187.

Nanao, M.H., Green, T., Stern-Bach, Y., Heinemann, S.F., and Choe, S. (2005). Structure of the kainate receptor subunit GluR6 agonist-binding domain complexed with domoic acid. Proc Natl Acad Sci U S A *102*, 1708-1713.

Naur, P., Hansen, K.B., Kristensen, A.S., Dravid, S.M., Pickering, D.S., Olsen, L., Vestergaard, B., Egebjerg, J., Gajhede, M., Traynelis, S.F.*, et al.* (2007). Ionotropic glutamate-like receptor delta2 binds D-serine and glycine. Proc Natl Acad Sci U S A *104*, 14116-14121.

Nishimune, A., Isaac, J.T., Molnar, E., Noel, J., Nash, S.R., Tagaya, M., Collingridge, G.L., Nakanishi, S., and Henley, J.M. (1998). NSF binding to GluR2 regulates synaptic transmission. Neuron *21*, 87-97.

Norton, R.S., and Pallaghy, P.K. (1998). The cystine knot structure of ion channel toxins and related polypeptides. Toxicon *36*, 1573-1583.
Nuriya, M., Oh, S., and Huganir, R.L. (2005). Phosphorylation-dependent interactions of alpha-Actinin-1/IQGAP1 with the AMPA receptor subunit GluR4. J Neurochem *95*, 544-552.

Opazo, P., and Choquet, D. (2011). A three-step model for the synaptic recruitment of AMPA receptors. Mol Cell Neurosci *46*, 1-8.

Osten, P., Srivastava, S., Inman, G.J., Vilim, F.S., Khatri, L., Lee, L.M., States, B.A., Einheber, S., Milner, T.A., Hanson, P.I.*, et al.* (1998). The AMPA receptor GluR2 C terminus can mediate a reversible, ATP-dependent interaction with NSF and alpha- and beta-SNAPs. Neuron *21*, 99-110.

Palay, S.L. (1958). The morphology of synapses in the central nervous system. Exp Cell Res *14*, 275-293.

Perin-Dureau, F., Rachline, J., Neyton, J., and Paoletti, P. (2002). Mapping the binding site of the neuroprotectant ifenprodil on NMDA receptors. J Neurosci *22*, 5955-5965.

Priel, A., Kolleker, A., Ayalon, G., Gillor, M., Osten, P., and Stern-Bach, Y. (2005). Stargazin reduces desensitization and slows deactivation of the AMPA-type glutamate receptors. J Neurosci *25*, 2682-2686.

Rosenmund, C., Stern-Bach, Y., and Stevens, C.F. (1998). The tetrameric structure of a glutamate receptor channel. Science *280*, 1596-1599.

Rossmann, M., Sukumaran, M., Penn, A.C., Veprintsev, D.B., Babu, M.M., and Greger, I.H. (2011). Subunit-selective N-terminal domain associations organize the formation of AMPA receptor heteromers. EMBO J *30*, 959-971.

Roth, S., Neuman-Silberberg, F.S., Barcelo, G., and Schupbach, T. (1995). cornichon and the EGF receptor signaling process are necessary for both anterior-posterior and dorsal-ventral pattern formation in Drosophila. Cell *81*, 967-978.

Rouach, N., Byrd, K., Petralia, R.S., Elias, G.M., Adesnik, H., Tomita, S., Karimzadegan, S., Kealey, C., Bredt, D.S., and Nicoll, R.A. (2005). TARP gamma-8 controls hippocampal AMPA receptor number, distribution and synaptic plasticity. Nat Neurosci *8*, 1525-1533.

Schnell, E., Sizemore, M., Karimzadegan, S., Chen, L., Bredt, D.S., and Nicoll, R.A. (2002). Direct interactions between PSD-95 and stargazin control synaptic AMPA receptor number. Proc Natl Acad Sci U S A *99*, 13902-13907.

Schober, D.A., Gill, M.B., Yu, H., Gernert, D.L., Jeffries, M.W., Ornstein, P.L., Kato, A.S., Felder, C.C., and Bredt, D.S. (2011). Transmembrane AMPA receptor regulatory proteins and cornichon-2 allosterically regulate AMPA receptor antagonists and potentiators. J Biol Chem *286*, 13134-13142.

Schulz, T.W., Nakagawa, T., Licznerski, P., Pawlak, V., Kolleker, A., Rozov, A., Kim, J., Dittgen, T., Kohr, G., Sheng, M.*, et al.* (2004). Actin/alpha-actinin-dependent transport of AMPA receptors in dendritic spines: role of the PDZ-LIM protein RIL. J Neurosci *24*, 8584-8594.

Schwenk, J., Harmel, N., Brechet, A., Zolles, G., Berkefeld, H., Muller, C.S., Bildl, W., Baehrens, D., Huber, B., Kulik, A.*, et al.* (2012). High-resolution proteomics unravel architecture and molecular diversity of native AMPA receptor complexes. Neuron *74*, 621-633.

Schwenk, J., Harmel, N., Zolles, G., Bildl, W., Kulik, A., Heimrich, B., Chisaka, O., Jonas, P., Schulte, U., Fakler, B.*, et al.* (2009). Functional proteomics identify cornichon proteins as auxiliary subunits of AMPA receptors. Science *323*, 1313-1319.

Seeburg, P.H., and Hartner, J. (2003). Regulation of ion channel/neurotransmitter receptor function by RNA editing. Curr Opin Neurobiol *13*, 279-283.

Shanks, N.F., Savas, J.N., Maruo, T., Cais, O., Hirao, A., Oe, S., Ghosh, A., Noda, Y., Greger, I.H., Yates, J.R., 3rd*, et al.* (2012). Differences in AMPA and Kainate Receptor Interactomes Facilitate Identification of AMPA Receptor Auxiliary Subunit GSG1L. Cell Rep *1*, 590-598.

Shen, L., Liang, F., Walensky, L.D., and Huganir, R.L. (2000). Regulation of AMPA receptor GluR1 subunit surface expression by a 4. 1N-linked actin cytoskeletal association. J Neurosci *20*, 7932-7940.

Shepherd, J.D., and Huganir, R.L. (2007). The cell biology of synaptic plasticity: AMPA receptor trafficking. Annu Rev Cell Dev Biol *23*, 613-643.
Shi, Y., Suh, Y.H., Milstein, A.D., Isozaki, K., Schmid, S.M., Roche, K.W., and Nicoll, R.A. (2010). Functional comparison of the effects of TARPs and cornichons on AMPA receptor trafficking and gating. Proc Natl Acad Sci U S A *107*, 16315-16319.

Sobolevsky, A.I., Rosconi, M.P., and Gouaux, E. (2009). X-ray structure, symmetry and mechanism of an AMPA-subtype glutamate receptor. Nature *462*, 745-756.

Sommer, B., Keinanen, K., Verdoorn, T.A., Wisden, W., Burnashev, N., Herb, A., Kohler, M., Takagi, T., Sakmann, B., and Seeburg, P.H. (1990). Flip and flop: a cell-specific functional switch in glutamate-operated channels of the CNS. Science *249*, 1580-1585.

Song, I., and Huganir, R.L. (2002). Regulation of AMPA receptors during synaptic plasticity. Trends Neurosci *25*, 578-588.

Song, I., Kamboj, S., Xia, J., Dong, H., Liao, D., and Huganir, R.L. (1998). Interaction of the N-ethylmaleimide-sensitive factor with AMPA receptors. Neuron *21*, 393-400.

Soto, D., Coombs, I.D., Renzi, M., Zonouzi, M., Farrant, M., and Cull-Candy, S.G. (2009). Selective regulation of long-form calcium-permeable AMPA receptors by an atypical TARP, gamma-5. Nat Neurosci *12*, 277-285.

Suzuki, E., Kessler, M., and Arai, A.C. (2008). The fast kinetics of AMPA GluR3 receptors is selectively modulated by the TARPs gamma 4 and gamma 8. Mol Cell Neurosci *38*, 117-123.

Tomita, S., Adesnik, H., Sekiguchi, M., Zhang, W., Wada, K., Howe, J.R., Nicoll, R.A., and Bredt, D.S. (2005a). Stargazin modulates AMPA receptor gating and trafficking by distinct domains. Nature *435*, 1052-1058.

Tomita, S., Chen, L., Kawasaki, Y., Petralia, R.S., Wenthold, R.J., Nicoll, R.A., and Bredt, D.S. (2003). Functional studies and distribution define a family of transmembrane AMPA receptor regulatory proteins. J Cell Biol *161*, 805-816.

Tomita, S., Fukata, M., Nicoll, R.A., and Bredt, D.S. (2004). Dynamic interaction of stargazin-like TARPs with cycling AMPA receptors at synapses. Science *303*, 1508-1511.

Tomita, S., Stein, V., Stocker, T.J., Nicoll, R.A., and Bredt, D.S. (2005b). Bidirectional synaptic plasticity regulated by phosphorylation of stargazin-like TARPs. Neuron *45*, 269-277.

Turetsky, D., Garringer, E., and Patneau, D.K. (2005). Stargazin modulates native AMPA receptor functional properties by two distinct mechanisms. J Neurosci *25*, 7438-7448.

Vandenberghe, W., Nicoll, R.A., and Bredt, D.S. (2005). Stargazin is an AMPA receptor auxiliary subunit. Proc Natl Acad Sci U S A *102*, 485-490.

von Engelhardt, J., Mack, V., Sprengel, R., Kavenstock, N., Li, K.W., Stern-Bach, Y., Smit, A.B., Seeburg, P.H., and Monyer, H. (2010). CKAMP44: a brain-specific protein attenuating short-term synaptic plasticity in the dentate gyrus. Science *327*, 1518-1522.

Xia, J., Zhang, X., Staudinger, J., and Huganir, R.L. (1999). Clustering of AMPA receptors by the synaptic PDZ domain-containing protein PICK1. Neuron *22*, 179-187.

Yamazaki, M., Ohno-Shosaku, T., Fukaya, M., Kano, M., Watanabe, M., and Sakimura, K. (2004). A novel action of stargazin as an enhancer of AMPA receptor activity. Neurosci Res *50*, 369-374.

Figures

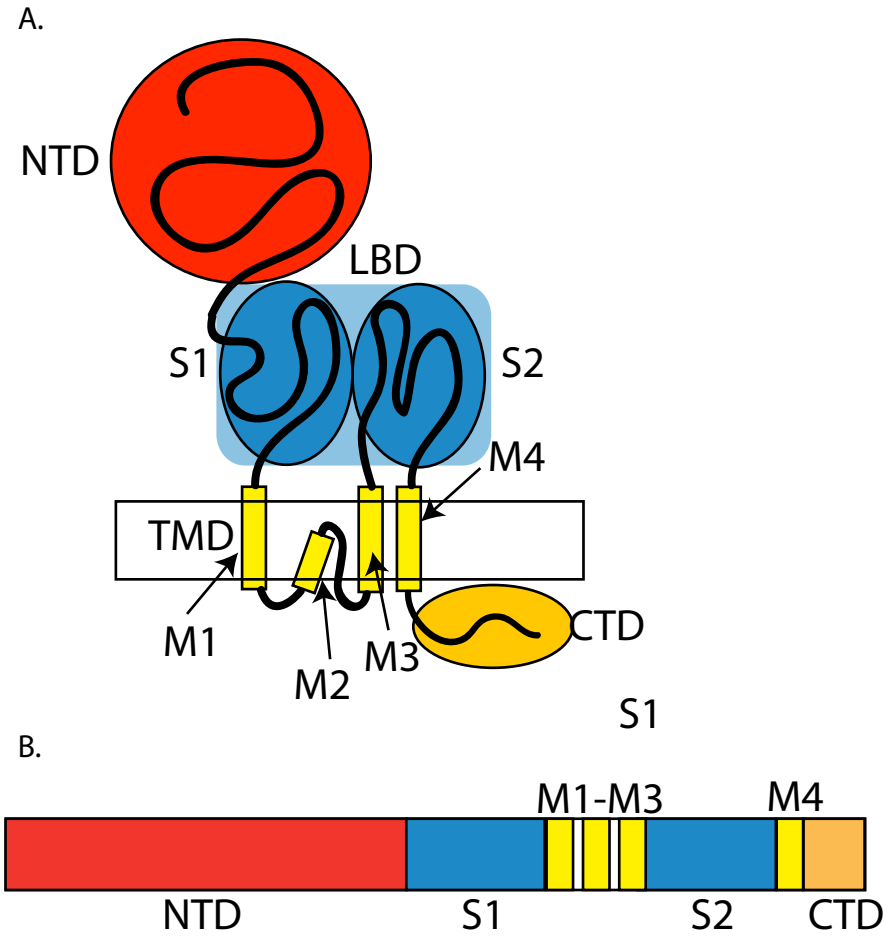

Figure 1_1. AMPA-R subunit topology
(A) Cartoon schematic depicting the topology and domain organization of an AMPA-R subunit. NTD = N-terminal domain; LBD = ligand-binding domain; and TMD = transmembrane domain. The box represents the lipid bilayer. M1–4 indicate the sub-domains within the TMD. CTD = C-terminal domain. (S1 and S2 are the subdomains of the ligand binding domain**.**

Chapter II

Contribution of the global subunit structure and stargazin on the maturation of AMPA receptors

Abstract

Subunit assembly governs regulation of AMPA receptor (AMPA-R) synaptic delivery and determines biophysical parameters of the ion channel. However, little is known about the molecular pathways of this process. Here we present single particle electron microscopy (EM) 3D structures of dimeric biosynthetic intermediates of the GluA2 subunit of AMPA-Rs. Consistent with the structures of intact tetramers, the amino terminal domains of the biosynthetic intermediates form dimers. Transmembrane domains also dimerize despite the two ligand binding domains (LBD) being separated. A significant difference was detected between the dimeric structures of the wildtype and the L504Y mutant, a point mutation that blocks receptor trafficking and desensitization. In contrast to the wildtype, whose LBD is separated, the LBD of the L504Y mutant was detected as a single density. Our results provide direct structural evidence that separation of the LBD within the intact dimeric subunits is critical for efficient tetramerization in the endoplasmic reticulum and further trafficking of AMPA-Rs. The contribution of stargazin on the subunit assembly of AMPA-R was examined. Our data suggests that stargazin affects AMPA-R trafficking at a later stage of receptor maturation.

Introduction

The majority of fast excitatory synaptic transmission in the brain is mediated by AMPA (a-amino-3-hydroxy-5-methyl-4-isoxazole propionic acid) receptors (AMPA-Rs), a subset of ligand-gated ion channels of the glutamate receptor family. Trafficking, anchoring, and gating of AMPA-Rs form the molecular basis for certain types of synaptic plasticity involved in learning and memory (Barry and Ziff, 2002; Malinow and Malenka, 2002; Nicoll et al., 2006). Dysfunction of AMPA-Rs is implicated in a variety of neurological and psychiatric disorders, including X-linked mental retardation, Alzheimer's disease, amyotrophic lateral sclerosis, and Rasmussen's encephalitis (Rogers et al., 1994; Shepherd and Huganir, 2007; Wu et al., 2007).

AMPA-R subunits are encoded by four different genes (GluA1-4). (Hollmann et al., 1989; Keinanen et al., 1990; Nakanishi et al., 1990). Each subunit consists of four domains (Fig 1A). The N-terminal domain (NTD) and ligand binding domain (LBD) are both extracellular. The LBD, made of S1 and S2 subdomains, undergoes conformational changes resulting in channel gating upon glutamate binding. The polypeptide chain forming the LBD is interrupted by the channel pore-forming transmembrane domain (TMD), which consists of three membrane spanning segments (M1, M3, and M4) and one re-entrant loop (M2) (Hollmann et al., 1994). A small C-terminal domain (CTD)

extends into the cytoplasm, interacting with cytosolic proteins that regulate receptor anchoring and trafficking. (Scannevin and Huganir, 2000; Sheng and Lee, 2001; Malinow and Malenka, 2002; Ziff, 2007). Cumulative evidence suggests an AMPA-R subunit assembly model in which two dimers come together to form a tetramer, hence a dimer-of-dimer organization for mature tetrameric AMPA-Rs. (Armstrong et al., 1998; Gouaux, 2004; Mayer, 2006). In the brain, AMPA-R auxiliary subunits of the stargazin/TARP (transmembrane AMPA-R regulatory protein) family and the cornichon family are physically associated with the channel and regulate their trafficking and gating (Chen et al., 2000; Nakagawa et al., 2005; Nicoll et al., 2006; Ziff, 2007; Schwenk et al., 2009).

Trafficking of both newly synthesized and recycling AMPA-Rs is a critical component of synaptic plasticity (Malinow and Malenka, 2002; Ju et al., 2004; Park et al., 2004; Matsuo et al., 2008). The molecular anatomy of early phases of AMPA-R trafficking, including biosynthesis, is largely unknown. Studies have identified point mutations and splice variants that alter receptor trafficking and, together with the crystal structures of the mutated S1S2 domains, have provided insight into what might be happening at the ultrastructural level of the intact subunits during receptor assembly (Greger et al., 2002; Greger et al., 2003; Coleman et al., 2006; Greger et al., 2006). It is not clear how the domains are organized during the normal assembly of full-

length subunits and how mutant subunits interfere with this process. In addition, how the auxiliary subunit stargazin influences biosynthesis of AMPA-R remains controversial.

Here we investigate AMPA-R subunit assemply and report single particle EM structures of newly synthesized AMPA-Rs in dimeric states. The study reveals that efficient subunit assembly requires a preferred conformation of AMPA-R biosynthetic intermediates and stargazin affects AMPA-R trafficking at the later stages of receptor maturation.

Results

Simplified biochemical preparation to study AMPA receptor assembly

To obtain pure intact AMPA-Rs for EM analyses, we stably expressed FLAG epitope tagged GluA2 *flop* (Fig 1A) in HEK cells. Recombinant GluA2 was solubilized in dodecylmaltoside (DDM) in the presence of 1 mM kynurenic acid and purified by affinity chromatography using a sepharose column conjugated with anti-FLAG M2 monoclonal antibody (Fig 1C). The purity was further improved by gel filtration chromatography. The majority of purified GluA2 existed as tetramers (Supplementary Fig 1C). Because of glycosylation, the purified protein migrated in the SDS-PAGE as a doublet (Fig 1C). Only the tetrameric species were glycosylated (Supplementary Fig 1B-D). Based on the yield of purification we estimate that at least 15,000~20,000 GluA2 tetramers are expressed per cell.

Recombinant GluA2 tetramers were homogeneous in shape and size when imaged by negative stain EM (Fig 1D, left panel). The projection structures (class averages) of GluA2 tetramers were very similar to those of native AMPA-Rs from rat brain (compare Fig 1B and 1D). The NTD, LBD and TMD were clearly identified as distinct features (Fig 1E). The TMD of native

AMPA-Rs is larger than that of recombinant GluA2, a difference caused by the presence or absence of auxiliary stargazin/TARP subunits (Chen et al., 2000). Consistently we did not detect stargazin/TARP protein in the purified recombinant GluA2 fraction when examined by western blotting or by protein identification using liquid chromatography followed by tandem mass spectroscopy (LC/MS/MS, data not shown). Glycosylation did not affect the overall structure of tetrameric GluA2. The shapes of negative stained glycosylated GluA2 tetramers were very similar to GluA2 tetramers purified from the GnTI(-) HEK cell line, a line defective in complex mannose glycosylation (Reeves et al., 2002) (Supplementary Fig 1E). Altogether, our stable HEK cell line is a simple, robust and highly reproducible system to study AMPA-Rs using single particle EM.

Isolation of dimer intermediates of newly synthesized AMPA receptors

To enrich biosynthetic intermediates that have a shorter lifetime than mature and targeted proteins, we induced expression of GluA2-FLAG in HEK cells and purified them at an early time point. In this system, HEK cells stably express a reverse Tet transcriptional activator that enhances transcription from the minimal CMV promoter upstream of the GluA2-FLAG transgene only in the presence of doxycycline (DOX) (Fig 2A). We named this cell line TetONGluA2. GluA2 protein expression reached a maximum 24 hr after DOX application

(Fig 2B). The magnitude of GluA2 expression in DOX inducible system was similar to that of the constitutive expression when the expression was induced for 24 hr at 7.5 mg/ml DOX. Enrichment of the glycosylated band became prominent 12 to 24 hr after transcription initiation (emergence of the upper band in Fig 2B).

When GluA2 was purified 20 hr after addition of DOX and resolved by gel filtration, equal amounts of tetramers and dimers were detected (Fig 2C solid line). The tetramer peak increased relative to the dimer peak 20 hr to 24 hr after DOX induction. At earlier time points (15 hr post induction) the majority of GluA2 existed as dimers (Supplementary Fig 2). Collectively, this suggests that the dimer population precedes the formation of the tetramer population, and thus represents a biosynthetic intermediate of pre-assembled GluA2 tetramers.

Interestingly, even at 15 hr after DOX induction we were unable to detect a distinct population that represents the monomeric subunits (Supplementary Fig 2). Because the appearance of the monomers should in theory precede the dimers, we interpret that at a given moment, the monomer population is much lower relative to the dimer population. It is thus difficult to detect monomers in our experimental system. Such an interpretation is

consistent with an idea that the dimer-to-tetramer transition is the rate-limiting step compared to the monomer-to-dimer transition.

Projection structures of the GluA2 wildtype dimers

When GluA2 biosynthetic dimer intermediates were imaged by negative stain EM, the particles were homogeneous in size but existed in a variety of shapes (Fig 2D, upper panel). Approximately 7,000 particles were analyzed by multivariate statistical analysis, classification and multi reference alignment. Representative class averages are shown in Fig 2D, lower panels. There is an elongated bipartite density at the top of the particle, and a featureless globular density at the bottom of the particle. In some class averages the upper bipartite density appears as a squarish density with a weaker density in the center (Fig 2D). Between these structures two small round densities are positioned at both sides. The arrangement of the bipartite density relative to the small round densities on the sides differs significantly between class averages, and as a result, the heights of the particles vary between class averages.

The projection structures were interpreted by molecular labeling. To immunolabel the C-terminal FLAG epitope, antigen binding fragments (Fabs) were generated by proteolytic digest from IgG of anti-FLAG monoclonal

antibody (Fig 2E left). Anti-FLAG Fab consistently labeled the bottom featureless density of the particles (Fig 2E right panels). Consistent with our interpretation that these particles are dimers, some particles were labeled with two Fabs (Fig 2E, far right). Because the CTD is small and attached to the TMD, we interpret that the bottom round density represents the TMD and CTD (Fig 2G).

In order to GFP label the NTD, we purified particles from a DOX inducible HEK cell line that expresses a GluA2 construct whose amino terminal end of the NTD is fused to GFP (Fig 2F). The timecourse of GFP-GluA2 expression after DOX induction and the elution profile of purified GFP-GluA2 in gel filtration chromatography were similar to those without the GFP tag (data not shown), suggesting that GFP does not affect overall processing. In the class averages of GFP-GluA2 dimers, two GFP densities were always attached to each side of the bipartite density (Fig 2F). The small round densities between the NTD and the TMD were neither labeled by anti-FLAG Fab or GFP, so we interpret that they are the LBDs (Fig 2G).

Contrasting vesicle trafficking of GluA2 wildtype and L504Y

Maturation and trafficking are tightly coupled processes in membrane proteins. To understand the functional significance of the dimer structure, we

decided to study the structure of the L504Y mutant, which has trafficking and maturation deficits (Fig 3A). This mutation within the LBD was originally identified in the GluR3 subunit because it blocks receptor desensitization (Stern-Bach et al., 1998). L504Y mutation is located in helix D in the S1 subdomain and the mutated tyrosine interacts with helix J in the S2 subdomain of the adjacent subunit (Sun et al., 2002). This interaction stabilizes the LBD dimer interface, and thus blocks the receptor from entering into the desensitized state. Recently it was found that surface expression of the GluA2L504Y mutant is impaired (Greger et al., 2006). Consistently, we observe significantly reduced surface expression of GluA2L504Y compared to GluA2 wildtype when expressed for 4 days starting from DIV14 in primary rat hippocampal neurons (Fig 3B).

We created stable HEK cell lines in which expression of GFP-GluA2 wildtype or GFP-GluA2L504Y is DOX inducible. In both cell lines, the timecourses of protein expression after DOX induction were similar to those without the GFP tag (data not shown), suggesting that the GFP has minimal effect on protein turnover. At 30 hr after DOX induction, there was significantly less GFP-GluA2L504Y on the cell surface compared to GFP-GluA2 wildtype, while the total expression levels of each protein were the same (Fig 3C). This suggests that the defect in surface expression of GluA2L504Y can be replicated in our simplified HEK cell system.

To gain further insight into the differential dynamics of newly synthesized GFP-tagged GluA2 wildtype and L504Y, we conducted time-lapse confocal imaging of HEK cells. We imaged a thin layer of cytoplasm between the bottom of the nucleus and the bottom of the cell that provides clear images of receptor trafficking (yellow volume in Fig 3D). For the first 24 hours following DOX induction, GluA2 wildtype and GluA2L504Y showed similar subcellular distribution, localized predominantly in the endoplasmic reticulum (ER) (data not shown). After 24 hours dynamic punctate structures emerged in the GluA2 wildtype cells but not in the GluA2L504Y cells (compare Fig 3E and F). The vesicles appeared at time points after the majority of receptor maturation was complete. More than 50 % of the punctate structures in GluA2 wildtype cells were dynamic and translocated rapidly (Fig 3G and supplementary movies). These punctate structures were absent from GluA2L504Y cells even 48 hrs after DOX induction, suggestive of differential vesicle trafficking patterns caused by the mutation (Supplementary Fig 3). Double staining GFP-GluA2 puncta with the known organelle markers revealed no co-localization with EEA1 (an early endosomal marker), transferrin (a recycling endosomal marker), nor lysotracker (a lysosomal marker). However, a subpopulation of GFP-GluA2 vesicles co-localized with rab6 (a small GTPase localized to a subset of the post Golgi vesicles), GM130 (a Golgi marker), and PDI (a ER marker) (Supplemental Fig 4). In addition, the GFP-GluA2 puncta partially co-

localized with a population of GFP-GluA2 that underwent endocytosis while they were live-labeled for 1 hr with anti-GluA2NTD antibody. These data suggest that the GFP-GluA2 puncta are a mixture of vesicles that belong to the ER or Golgi apparatus, or are involved in post-Golgi trafficking and endocytic pathways (Supplemental Fig 4). The time lag between tetramer formation and the appearance of puncta of GFP-GluA2 wildtype may also suggest the possibility that tetrameric GFP-GluA2 is not readily competent to exit the ER. Collectively, these results suggest that vesicle trafficking is severely reduced in GluA2L504Y cells compared to wildtype. Next, we tested if there is also a maturation deficit in this mutant.

Inefficient tetramerization of GluA2L504Y mutant

The timecourse of GluA2L504Y protein expression following DOX induction was similar to that of GluA2 wildtype. However, unlike GluA2 wildtype, GluA2L504Y was detected as a single band by SDS-PAGE when purified 24 hr after induction (Fig 4A and B). Furthermore, the mobility of GluA2L504Y was identical to that of GluA2 wildtype purified from GnTI(-)HEK cells deficient in complex mannose glycosylation (data not shown), indicating that the majority of GluA2L504Y is not glycosylated within 24 hr of expression.

Next, we tested if tetramerization was affected by the L504Y mutation. Interestingly, even 24 hour after induction, the majority of GluA2L504Y remained as dimers when resolved by gel filtration chromatography (Fig 4C blue). In contrast, GluA2 wildtype exists primarily as tetramers 24 hr after DOX induction (Fig 4C compare red and blue). Western blotting of the gel filtration fractions suggests that the glycosylated species of GluA2 wildtype are tetramers whereas the non-glycosylated species are primarily enriched as dimers (Fig 4D). In contrast to GluA2 wildtype, GluA2L504Y exists mostly as dimers, although a small quantity is detected as tetramers. These results are in keeping with the observation that GluA2L504Y mutant has high degree of aberrant multimerization of subunits including limited tetramer formation in HEK cells (Penn et al., 2008).

The projection structure of the negative stained tetrameric GluA2L504Y is very similar to that of GluA2 wildtype (Supplementary Fig 5A and B). The yield of these particles was extremely low, so despite our efforts, it was not feasible to obtain 3D structures of GluA2L504Y tetramers. We considered the possibility that the yield was low because tetramers in the non-desensitizing state might be less stable in detergent. However, this is unlikely because our previous study showed that brain derived AMPA-R locked in the non-desensitized state by treatment with 330 mM cyclothiazide (CTZ) and 1 mM glutamate had similar structures to the untreated receptors (Nakagawa et al.,

2005). Collectively, these results suggest that the GluA2L504Y mutation causes defects in the dimer-to-tetramer transition.

Projection structures of the GluA2L504Y dimer

To gain further insight into the difference in tetramerization between GluA2 wildtype and L504Y, EM images were taken from negative stained GluA2L504Y dimers. GluA2L504Y dimer particles were homogeneous in size, but had less conformational heterogeneity and were more elongated than wildtype dimers (Fig 5A). Representative class averages show three layers of domains stacked on top of each other. Similar to the GluA2 wildtype dimer structures, the top domain of GluA2L504Y was bipartite and elongated or appeared squarish with a weaker density in the center in some class averages. (Fig 5A, bottom right panels). The bottom domain was a featureless globular density. In contrast to the wildtype dimer, in most class averages, the middle portion existed as a single density, and was split into two in only a minority of the class averages (Fig 5A, bottom row, second from right).

Fab labeling and GFP tagging were used for domain assignment. Similar to GluA2 wildtype dimers, anti-FLAG epitope Fabs consistently decorated the bottom round featureless density of the particles (Fig 5B) and two Fabs sometimes bound to a single particle (Fig 5B, right panel).

Moreover, two extra densities representing N-terminal GFP tags were detected at the top of the elongated bipartite density of GFP-GluA2L504Y dimers. From these experiments we interpret the bottom density as the TMD and CTD dimer, the middle density as the LBD dimer, and the top elongated bipartite domain as the NTD dimer (Fig 5D).

The particles were quantified based on LBD separation. Approximately 7,000 particles from negative stained EM images were classified into 100 classes by multivariate statistical analysis and multi-reference alignment. We assigned each class average (and the particles in these classes) either to “LBD separated” or “LBD fused”. All classes that could not unambiguously be assigned to either were termed “unclassifiable”. In GluA2 wildtype dimers, 71.3% had a separated LBD, 2.3% had a fused LBD, and 26.4% were unclassifiable. In contrast, of GluA2L504Y dimers, 66 % had a fused LBD, 20% had a separated LBD, and 14% were unclassifiable. Among the 66% of GluA2L504Y dimers that adopted fused LBD, 33.3% had shapes exhibiting two-fold symmetry, while 66.7% had asymmetric shapes. Among the classifiable particles of GluA2 wildtype and L504Y dimers, 7.8% and 12.1% adopted squarish NTDs, respectively, indicating that the particles that adopt squarish NTDs are the minority. These results demonstrate a robust difference in the molecular shapes between dimers of GluA2 wildtype and L504Y (Fig

2D, 5A, and 6). Furthermore, the difference in molecular shapes is correlated with their contrasting ability to transition from dimer-to-tetramer (Fig 4).

3D EM maps of GluA2 wildtype and L504Y dimer

To confirm that the structural differences seen in the projection structures indeed reflect structural differences in 3D, the 3D density maps of the GluA2 wildtype and L504Y dimers were calculated using random conical tilt reconstruction (Frank, 1996; Frank et al., 1996). For this purpose, particle images were recorded as tilt pairs at specimen tilt angles of 0^o and 60^o. Raw particle images recorded at 0^o were analyzed by multivariate statistical analysis, classification and multi reference alignment. Well aligned and highly represented class averages were chosen (Fig 6A and C, left box) and corresponding tilted images of particles in the selected class were used to calculate the 3D structure. Refinement was done in three steps using backprojection refinement, angular refinement (implemented in SPIDER) (Frank et al., 1996) and FREALIGN refinement (Grigorieff, 2007). Three different views of the final reconstruction of wildtype and L504Y dimers are shown in Fig 6A and C, respectively. The resolution of the final reconstruction was 35Å (wildtype) and 34 Å (L504Y) at FSC = 0.5, and with the less conservative criteria 29Å (wildtype) and 28Å (L504Y) (FSC = 0.142) (Rosenthal and Henderson, 2003). The images shown in Fig 6 are filtered at

the resolution determined by FSC = 0.5, the more conservative resolution criteria. In addition, to demonstrate the structural contrast between immature and mature receptors, the 3D maps of GluA2 wildtype dimer and AMPA-R tetramer are compared side-by-side in Fig 6E.

The 3D maps of wildtype and L504Y dimers were significantly different. The projection structures and the 3D EM maps viewed from the front correspond well for both wildtype and L504Y dimers (Fig 6A and C). We assigned each globular feature in the 3D maps to individual domains of the subunit based on the domain labeling experiments (Fig 2G and 5D). The wildtype dimer has the bipartite NTD dimer at the top and two smaller globular LBD densities attached at both sides of the NTD dimer. The following dimensions are the maximal distances. The height of the particle is 14.5 nm and the width is 14.6 nm. The central empty cavity of the particle suggests a clear physical separation of the two LBDs. The dimensions of the cavity are 3.7 nm in height and 5.6 nm in width. In contrast, the height and width of the L504Y dimer is 17.0 nm and 8.7 nm, and the L504Y dimer has no LBD separation.

Similar to the class averages (Fig 6A and C), the overall 3D structures did not reveal global two fold symmetry, despite that they represent homodimeric subunits of GluA2 wildtype or L504Y. The linker between the

NTD and LBD consists of 16 amino acids, and we predict it has structural flexibility to accommodate twist that may exist between the NTD and LBD dimers. Consistently, the NTD was observed as an elongated bipartite density in some class averages, whereas in the others it appeared as a squarish density (Fig 2D and 5A). We believe that the different appearance of the NTD in different class averages results from viewing the NTD dimer from different angles. A variety of orientations of the NTD relative to LBD can be explained by the structural flexibility present in the linker connecting these domains.

To interpret our 3D density map, we used known crystal structures of AMPA-R subunit domains. The crystal structure of the NTD of GluA2 (Jin et al., 2009) fits nicely in the NTD density of our EM structure (Fig 6B, and D). Additionally, the two separated small globular densities of the wildtype dimer can each accommodate the crystal structure of the GluA2 LBD monomer (Armstrong et al., 1998), while the density that corresponds to the LBD in the L504Y dimer is consistent with the dimeric crystal structure of the LBD (Fig 6B and D) (Sun et al., 2002). Because of the limited resolution of our EM map, we did not refine the position of the crystal structures using computational algorithms. However, placing crystal structures into our 3D reconstruction demonstrates that the size and shape of the densities of the extracellular domains of dimeric GluA2 wildtype and L504Y are compatible with known crystal structures. Thus, we conclude that the structural differences of the

class averages between GluA2 wildtype and GluA2L504Y do not reflect different views of an identical 3D structure but represent true structural differences. Specifically, the structural difference between the wildtype and L504Y dimers can be attributed to the different global arrangement of the LBDs.

Interaction of GluA2 and stargazin during the subunit assembly of AMPA-Rs

Stargazin/TARPs are auxiliary subunits of native AMPA-Rs in the brain. Because endogenous stargazin/TARPs were not detected in HEK cells, we investigated the effect of stargazin on subunit assembly of GluA2 by introducing stargazin into the parental stable HEK cell that DOX-dependently expresses FLAG-tagged GluA2 *flop* (TetONGluA2 cell, Fig 2A). The new stable HEK cell lines, which we named TetONGluA2-stg cells, constitutively express stargazin-IRES-mCherry using the elongation factor (EF) promoter, and DOX-dependently express GluA2 *flop* (Fig 7A and B). The mCherry was co-expressed (not as a fusion protein) with stargazin to facilitate the visual isolation of stable clones by fluorescent microscopy.

The four stable TetONGluA2-stg cell lines (clone #2, 8, 9, and 10), express stargazin at different levels. Interestingly, these cells started to die

after 24 hr of DOX induction, suggesting that the expression of GluA2 induced cytotoxicity in the presence of stargazin. The cytotoxicity was stronger in the clones that express higher levels of stargazin and, as a result, all the cells died within 48 hr in clone#10 and 8. The cytotoxicity was suppressed when the cells were cultured with 30 mM of NBQX, an antagonist of AMPA-Rs. Because the same level of GluA2 expression was not cytotoxic in TetONGluA2 cells, we interpret that the glutamate in the media caused cell death by activating AMPA-Rs whose function was enhanced by stargazin. These observations suggest that both GluA2 and stargazin are functional in these cells.

First, we investigated if stargazin alters the biosynthesis of GluA2. All the TetONGluA2-stg cell lines expressed similar levels of GluA2 24hr after DOX induction. To assess the effect of stargazin on GluA2 maturation, we induced GluA2 expression in various TetONGluA2-stg cells and compared the timecourse of expression with the parental TetONGluA2 cells that lack stargazin. We were unable to detect any significant difference in the rate of GluA2 expression (Fig 7B). Thus, in HEK cells stargazin is not the rate limiting molecular chaperone for GluA2 biosynthesis.

When GluA2 was purified from clone #10, 12 hr after DOX application, no detectable amount of stargazin was co-purified. However, when purification was done 24 hr after DOX induction, stargazin co-purified with GluA2 and

associated only with the tetrameric forms of GluA2, as determined by Superdex 200 gel filtration (Fig 7C). Consistently both proteins co-localized at the cell periphery when clone#10 cells were double stained 24 hr after induction (Fig 7D).

Discussion

This study establishes a new approach to investigate subunit assembly of AMPA-Rs using a combination of genetic engineering and single particle EM. We utilize recombinant GluA2 tetramers obtained from HEK cells whose structures (at the resolution of our current study) are indistinguishable from those purified from rat brain (Nakagawa et al., 2005; Nakagawa et al., 2006) (Fig 1). This system has several advantages because the subunit composition can be precisely controlled, genetic manipulation is feasible, and the protocol is simple and highly reproducible. While AMPA-Rs form heterotetramers in the brain (Wenthold et al., 1996), it has been established that homotetrameric receptors are functional ion channels when expressed in HEK cells (Swanson et al., 1997). Many structural studies of AMPA-Rs are done using the GluA2 subunit. In addition, this subunit renders AMPA-Rs impermeable to calcium, therefore they are less toxic when overexpressed in cells. Insights obtained from homomeric GluA2 may therefore also apply to the heteromeric AMPA-Rs.

Recombinant AMPA-Rs were structurally more homogeneous than the AMPA-R particles purified from the brain (Nakagawa et al., 2005; Nakagawa et al., 2006). Because application of glutamate to the purified AMPA-R induces conformational changes of the NTD, we speculate that the structural heterogeneity observed in brain derived AMPA-Rs is caused by exposure of

the particles to the endogenous glutamate during purification. Consistently, it is critical to include antagonist kynurenic acid (or NBQX) during the detergent solubulization and subsequent immunoaffinity chromatography to obtain structurally homogeneous recombinant AMPA-R tetramers.

The AMPA-R auxiliary subunit stargazin/TARP was not detected in HEK cells, nor from fractions of purified GluA2 from HEK cells that should in principal enrich endogenous stargazin/TARPs if they are present (Note, however, that two proteins co-purified when stargazin was introduced into the system (Fig 7C)). We estimate that there is very little, if any, and that possible endogenous stargazin/TARPs in HEK cells contribute little to tetrameric assembly of AMPA-R subunits. Consistently, stargazin/TARPs form a stable complex with GluA2 tetramers but not with the dimer intermediates during biogenesis (Fig 7C). In addition, the timecourse of expression of the newly synthesized GluA2 was not affected by the presence of stargazin in these cell lines. Stargazin functions as a molecular chaperone for AMPA-Rs in the presence of the ER stress response (Vandenberghe et al., 2005a). Because our expression level of GluA2 was modest, it is unlikely that the ER stress response was elicited. Taken together, it is likely that stargazin functions as a chaperone only when there is a high demand to synthesize AMPA-Rs. The lack of accumulation of AMPA-R dimers in the *stargazer* mutant mice is likely due to the fact that the ER is unlikely to be in a stress state (Vandenberghe et

al., 2005b). Cornichons are newly identified auxiliary subunits of AMPA-Rs that modulate receptor trafficking (Schwenk et al., 2009). This suggests the possibility that they are also involved in the assembly process of AMPA-Rs. However, no definitive data is currently available.

Trafficking intermediates of membrane receptors are typically not easily accessible. By harvesting GluA2 within a short period after induction of transcription, we were able to enrich the biosynthetic intermediates. GluA2 protein expression reached a plateau more than 24 hr after DOX induction in HEK cells. Interestingly, the half-life of an AMPA-R subunit is 18 hr as determined by radioisotope metabolic labeling in cortical neurons (O'Brien et al., 1998). As the duration of protein turnover and molecular structures are consistent between AMPA-Rs expressed in HEK cells and endogenous receptors in neurons, HEK cells likely have the necessary molecular chaperones to correctly assemble AMPA-Rs.

The ratio of tetramer to dimer increased as a function of time after GluA2 induction by DOX. When determined by negative stain EM, purified AMPA-R tetramers remained in tetrameric form up to 5 days in buffer containing 0.1% DDM, suggesting that the tetrameric complexes are relatively stable (data not shown). Thus, it is unlikely that the dimers we purified are an artifact of detergent solubilization. Dimeric GluA2, a biogenic trafficking intermediate, is

a previously uncharacterized molecular species of AMPA-Rs from a structural point of view. We speculate that stable dimers are common biosynthetic intermediates of AMPA-Rs, regardless of subunit composition. Such an idea is consistent with the preferential interaction of GluA1 with GluA1 NTD relative to GluA2 NTD (Leuschner and Hoch, 1999).

The 3D structure of dimeric GluA2 revealed that the LBDs are spatially separated, a novel feature that was not previously observed in AMPA-R structures. The NTD and TMD form dimers but the LBD remains separated. This observation provides a structural basis for a previous model derived from electrophysiological experiments in which the NTD and TMD are critical determinants for the formation of functional channels (Ayalon and Stern-Bach, 2001). Our structural finding suggests that dimerization of both the NTD and TMD precedes tetramerization. This agrees with the interruption of the polypeptide sequence of the LBD by the TMD, which implies that folding of the TMD coordinates with that of the LBD during translation.

To study the functional significance of the structure of GluA2 wildtype dimers, we identified GluA2L504Y as a mutant defective in tetramerization, determined the structure of the dimers of this mutant, and compared the structure with the wildtype. GluA2L504Y and analogous mutants in other AMPA-R subunits have been studied extensively as non-desensitizing mutants (Rosenmund et al.,

1998; Stern-Bach et al., 1998; Robert et al., 2001; Sun et al., 2002). The tetramerization defect, however, was not observed when GluA2L504Y was exogenously expressed in neurons (Greger et al., 2006). This can be explained by the possible co-assembly of exogenous mutant GluA2L504Y subunits with endogenous wildtype AMPA-R subunits. However it remains unclear why heterotetramers that contain GluA2L504Y did not exit the ER. Additional mechanisms such as sampling of gating motion in the ER may regulate this process (Penn et al., 2008).

In the dimers of GluA2L504Y, all three domains (NTD, LBD, and TMD) appear to be dimerized or at least in close proximity. The dimeric modules are arranged linearly, thus making the overall shape of the complex elongated compared to wildtype structures (compare Fig 2, 5, and 6). The compact structure of the LBD in dimeric GluA2L504Y is consistent with the high affinity dimer formed by the S1S2 construct of the LBD that carries the same mutation (Sun et al., 2002). Our data is also consistent with previous results indicating that native tetrameric AMPA-Rs treated with 1 mM glutamate have more compact structures in the presence of 330 mM cyclothiazide, an allosteric inhibitor of desensitization (Nakagawa et al., 2005).

The two LBDs are separated in the GluA2 wildtype dimers and therefore, intermolecular dimerization of the LBDs can potentially occur

between two GluA2 wildtype dimers during assembly of a tetramer. In contrast, the LBDs are fused in the GluA2L504Y dimers. Since this mutation causes a defect in dimer-to-tetramer transition, it is conceivable that the separation of LBD dimers is required to drive tetramerization (Fig 8A). Thus, our results support a new model for the subunit assembly pathway of AMPA-Rs in which the dimer-to-tetramer transition accompanies formation of two new LBD dimers between the two molecular dimers of subunits (Fig 8B). This suggests an unexpected domain arrangement in tetrameric AMPA-Rs, in which the NTD and LBD of each subunit forms a dimer with a different neighboring subunit.

As with any structural approaches, technical artifacts must always be considered. The carbon support and the negative stain can potentially introduce a small distortion in the molecular structure. Even if we assume the presence of a small distortion, the robust structural differences between the GluA2 wildtype dimer and L504Y dimer were detected when both specimens were prepared under identical experimental procedures. Therefore the observed structural differences of the particles on EM grid should reflect the structural differences in solution. In addition, when carefully inspected, the peak elution volume of wildtype and L504Y dimers are different (Fig 4C and D). Because the molecular weights of the wildtype and the L504Y mutant are nearly identical, this small difference in the peak elution volume suggests a

structural difference between the two molecular forms. The direct structural inspection by single particle EM and the hydrodynamic properties obtained from quantitative gel filtration chromatography both support the presence of a structural difference between the wildtype and L504Y dimers, thus experimental artifacts are an unlikely explanation for the observed gross structural differences.

In both AMPA-Rs and kainite receptors, point mutations that prevent receptor desensitization also result in decreased surface delivery (Greger et al., 2006; Priel et al., 2006). Accordingly, it has been proposed that glutamate receptors sense glutamate prior to being delivered to the cell surface, which can prevent non-desensitizing and non-functional subunits from going to the surface (Mah et al., 2005; Valluru et al., 2005) (Penn et al., 2008). Because globular LBDs are clearly detected in immature AMPA receptors, glutamate might be used as a tool to facilitate progression through the subunit assembly pathway of AMPA-Rs as well. All in all we have created a system that has allowed us to study molecular details of AMPA-R assembly. Comparison of wildtype and mutant receptors has provided insight into the domain arrangements of the dimeric intermediates which are conducive to the receptor transitioning into mature tetrameric form.

Note added in proof:

While this manuscript was being reviewed, a paper reporting the X-ray crystal structure of GluA2cryst was published (Sobolevsky et al., 2009). Despite the fact that 6 out of 16 amino acids in the wildtype GluA2 were deleted from the linker that connects the NTD and LBD, the domain arrangement reported for the X-ray crystal structure of GluA2cryst is consistent with our model described in Figure 8.

Supplementary text

Detailed characterization of HEK cell based recombinant GluA2 tetramers

To obtain pure and intact AMPA-R for EM analyses, we expressed in HEK cells a construct of the GluA2 *flop* subunit of AMPA-Rs that contains a FLAG epitope tag near the c-terminus. When this construct was expressed by transient transfection, the majority of purified GluA2 aggregated and emerged in the void volume in gel filtration chromatography (Supplementary Fig 1C). Only a small portion of the purified protein eluted in the fraction that corresponds to tetramers (Supplementary Fig 1C, asterisk). Aggregation of recombinant GluA2 was prevented when we expressed the construct by creating a stable cell line. These cells remained stable for more than 6 months of continuous culture (Supplementary Fig 1A).

Recombinant GluA2 was solubilized in dodecylmaltoside (DDM) in the presence of 1 mM kynurenic acid and purified by affinity chromatography using a sepharose column conjugated with anti FLAG M2 monoclonal antibody. Proteins were removed from the column by competitive elution using a FLAG epitope peptide. The purity was further improved by gel filtration chromatography (Supplementary Fig 1C). The majority of purified GluA2

eluted from the Superdex200 gel filtration column as a tetramer (Supplementary Fig 1C, asterisk).

Recombinant GluA2 is purified as a doublet despite the single transgene introduced into the stable HEK cell line (Supplementary Fig 1B, right). SDS-PAGE followed by silver staining resolved the higher and the lower molecular weight bands from the fractions obtained from gel filtration chromatography (Supplementary Fig 1D, asterisk corresponds to the peak fractions with asterisk in Supplementary Fig 1C). When we expressed GluA2 in a mutant GnTI(-)HEK cell line, a cell line defective in complex mannose glycosylation (Reeves et al., 2002), GluA2 was detected as a single band (Supplementary Fig 1B, left). The mobility of this band was identical to the lower molecular weight band detected in GluA2 that was purified from wildtype HEK cells, indicating that the doublet band is caused by complex mannose glycosylation. The glycosylated species were only detected in the fractions corresponding to tetramers (asterisk in Supplementary Fig 1C and D).

Complex glycosylation did not affect the overall structure of tetrameric GluA2. The shapes of negative stained GluA2 tetramers purified from the GnTI(-) cell line are very similar to those purified from the wildtype HEK cells (Supplementary Fig 1E, compare with Fig 1D and E).

Methods

Recombinant DNA

The GluA2 *flop* splice variant was used for all experiments. The L504Y mutation was introduced by *in vitro* mutagenesis using Quick change kit (Stratagene). The GFP-GluA2 fragment was a gift from Y.Hayashi and GFP was inserted immediately after the signal peptide, following the exact design as previously described (Hayashi et al., 2000). The FLAG epitope tag was inserted in the C-terminal domain of GluA2 (FAT**DYKDDDDK**EGYNVYGIESVKI, where bold case indicates FLAG epitope) and placement preserves the original anti-GluA2CT epitope.

Generation of stable HEK cell line

Wildtype HEK cells, GnTI(-)HEK cells, and the transformants created were maintained in a base media that consists of high glucose DMEM, 100 units/ml penicillin, 100 mg/ml streptomycin, and 10 % fetal calf serum. To isolate stable clones, we co-transfected a plasmid vector that expresses GluA2 under the CMV promoter and another plasmid vector that expresses a hygromycin resistant gene. Transfection was done by calcium phosphate methods and the selection of clones was done over two weeks in the presence of 160 mg/ml hygromycin. Isolated colonies were cultured until morphologically homogeneous cultures were established. Expression of GluA2-FLAG was

tested for each clone using western blotting of the whole cell lysate by probing with custom made antibodies raised against the C-terminal peptide of GluA2 (EGYNVYGIESVKI) (Nakagawa et al., 2005). Through screening ~200 colonies we identified several clones that meet the criteria of optimal growth speed and expression. There was a tendency for highly expressing clones to be slow growing, consistent with toxicity to the host cell caused by overexpressing an ion channel. To assess stability, we kept culturing the established clones for seven months, and detected by immunofluorescence microscopy that 65% of the cells maintain expression of GluA2 (Supplemental Fig 1A). Thus the stable cell line we established can be used for large scale culture to produce recombinant GluA2 in large quantities. Typically a 1 liter culture of HEK cells was used for each purification in this study.

Generation of stable HEK cell lines that expresses GluA2-FLAG by DOX induction

A neomycin (G418) resistant TetON-HEK cell line (Clontech) has in its genome the expression module to produce rtTA (see Fig 2A). GluA2-FLAG, GluA2L504Y-FLAG, GFP-GluA2-FLAG, and GFP-GluA2L504Y-FLAG were subcloned into pTREtight vector (Clontech). TetON-HEK cells were co-transfected with a plasmid that expresses a hygromycin resistant gene and a GluA2 construct in pTREtight described above. Transfection was done by calcium phosphate and selection of clones was done over two weeks in the

presence of 120 mg/ml hygromycin. The remaining procedure follows the generation of the stable HEK cell lines described above, except that we detected the expression of GluA2 using western blotting after inducing the isolated clones with 5 mg/ml DOX for 24 hours.

Generation of TetOnGluA2-stg stable HEK cells

Stargazin-IRES-mCherry cassette was subcloned into pBOSS vector (a gift from Shigekazu Nagata and Hideki Sakahira) downstream of the elongation factor promoter. pBOSS-stg-IRES-mCherry vector and pCMVZeocin (Invitrogen) were co-transfected into the parental TetONGluA2 stable HEK cell and stable clones were isolated by selecting with antibiotics 125 mg/ml zeocin, 150 mg/ml hygromycin, and 125 mg/ml neomycin (G418). mCherry positive colonies were visually identified using an epi-fluorescent microscope, isolated, and subcultured. 80% of the mCherry positive clones also expressed stargazin as determined by Western blotting. DOX inducible GluA2 expression was also re-confirmed in all of the isolated cell lines.

Harvesting HEK cell monolayer from a large number of plates

Five confluent 15 cm dishes were taken from the CO_2 incubator at a time. Media was aspirated off and 6 ml of ice-cold phosphate buffered saline (PBS) was added to each plate. The plates were tapped strongly from the side about 10 – 15 times to dislodge all cells from the bottom of the dish. Cells were

pooled in a 250 ml centrifuge tube on ice. The dishes were further rinsed with 3 ml of PBS twice to collect all remaining cells. Cells collected from 20 plates fill up the 250 ml centrifuge tube. We centrifuged the cells at 1000 rpm at 4 ^{o}C for 10 min. After discarding the supernatant the pellet was resuspended in 50 ml of PBS and further centrifuged. After discarding the supernatant the cell pellet was flash frozen in liquid nitrogen and stored at -80 ^{o}C until use.

Purification of recombinant GluA2.

All purification procedures were conducted on ice or in the cold room to maintain specimen temperature below 4 ^{o}C. 1 liter of HEK cell culture (6 ml of cell pellet) was resuspended in 50 ml of buffer containing 50 mM K-HEPES pH7.4, 100 mM NaCl, 1mM Kynurenic acid, protease inhibitors (1 mM PMSF, 10 mg/ml leupeptin, atropinin, benzamidine, and pepstatin A). The cells were extracted with the detergent, DDM (0.25%) at 4 ^{o}C for three hours. Solubulization yield was above 90%, which is unsurprising given that AMPA-Rs from brain solubulize efficiently when synaptosomal fractions are extracted with mild detergents (Leonard et al., 1998). After clearing the lysate by ultracentrifugation (Beckman 45 Ti) at 45,000 rpm for 1 hour at 4 ^{o}C, the supernatant was applied to a column made of protein A sepharose beads (GE Amersham) crosslinked using DMP (Pierce) with anti-FLAG M2 monoclonal antibody (Sigma) at a concentration of 2 mg/ml. Following washing, bound proteins were released from the column using a buffer containing 0.5 mg/ml of

FLAG epitope peptide. The peak fraction from the peptide elution was further separated by Superdex 200 gel filtration column (GE Amersham) in a buffer that contains 50 mM K-HEPES pH 7.4, 100 mM NaCl, and 0.1% DDM.

Detection of stargazin from the preparation of recombinant GluA2

Purified GluA2 was resolved in 7.5% SDS-PAGE and Western blotting was done using the custom made anti-panTARP antibody as described (Nakagawa et al., 2005). In the case of the mass spectrometry, the gel was stained with CBB. All the bands between 30-60 kDa were cut out and digested with trypsin. The identity of each band was determined by liquid chromatography followed by tandem mass spectrometry (LC/MS/MS) at UCSD mass spectrometry facility.

Negative staining of purified proteins and EM

400 mesh copper grids were coated with carbon to create a substrate for proteins to bind. 4 ml of protein solution was applied to a glow discharged grid and left for 30 sec to 5 min to allow the proteins to bind. The excess water was blotted on filter paper and the specimen was washed twice in water droplets to remove excess detergents. Purified proteins were negatively stained with 0.75% (w/v) uranyl formate as described (Ohi et al., 2004). Images were recorded using a FEI Sphera electron microscope equipped with a LaB_6 filament operated at an acceleration voltage of 200 keV. Images were taken at

a magnification of 50,000 X and defocus value = -1.5 mm. Specimens were imaged at 0° and 60° tilt for random conical tilt 3D reconstruction; the defocus value for 0° = -1.5 ~ -1.8 mm and 60° tilt = -2.0 ~ -2.2 mm. All images were recorded using SO-163 film and developed with a Kodak D-19 developer at full strength for 12 min at 20 °C. Particle images were taken at room temperature and under low dose conditions (20 e/Å^2) to minimize radiation damage.

Fab labeling

Fabs were purified using the Immunopure IgG1 F(ab') and the F(ab')$_2$ Fab purification kit (Pierce) followed by gel filtration on a Superdex 200 column (Pharmacia). Anti-FLAG M2 monoclonal antibody (Sigma) was used as source. Labeling was performed by incubating dimeric AMPA-Rs with Fab fragments at a molar ratio of 1:4 to 1:8 overnight at 4^{o}C in 50 mM HEPES, pH 7.4, 100 mM NaCl, 0.1% DDM.

Image processing

Electron micrographs were digitized with a CoolScan 9000 (Nikon) using a step size of 6.35 mm and 3 x 3 pixels were binned so the specimen level pixel size used was 3.81 Å. Projection averages were calculated from windowed small images of 100 x 100 pixels over 10 cycles of K-means classification and multi-reference alignment specifying 100 classes. For 3D reconstruction of GluA2wildtype dimer, 269 tilt pairs (total of 538 micrographs) were recorded

on film from which 178 tilt pairs were selected based on image quality. A total of 13,345 particle pairs were interactively selected using WEB display program for SPIDER (Frank et al., 1996) and windowed, and the untilted particles were averaged into 100 classes as before. In the case of the GluA2L504Y dimer, 238 tilt pairs (total of 476 micrographs) were recorded from which 159 tilt pairs were selected based on image quality. A total of 9,000 particle pairs were selected and used for further analysis. Raw particle images were visually inspected after classification to make sure that tetramers were not mistakenly introduced into our dimer 3D reconstruction. Images of the tilted specimens for each class were used to calculate initial 3D reconstructions of individual classes by backprojection, backprojection refinement, and angular refinement (implemented in SPIDER). The final volume obtained by angular refinement with SPIDER was used as the input model for FREALIGN (Grigorieff, 2007); this was used for refinement of orientation parameters of individual particles and for individual image contrast transfer function correction based upon the defocus value. The tilt angles and defocus values of the center of each micrograph were determined with CTFTILT (Mindell and Grigorieff, 2003). The defocus of each particle was deduced from its position on the micrograph. Particles selected from tilted and untilted specimens were used for FREALIGN refinement (500 and 800 particles were used in the final reconstruction for wildtype and L504Y, respectively). To ensure that the final 3D reconstruction

agreed with the raw data, the particle images were compared with reprojections.

Surface labeling of HEK cells

Expression of GFP-GluA2 wildtype and GFP-GluA2L504Y was induced with 7.5 mg/ml DOX. 30 hr after induction cells were live labeled using an anti-GluA2 NTD monoclonal antibody for 15 min (Chemicon, MAB397). Cells were washed with warm DMEM and fixed with 4% formaldehyde in 0.1 M phosphate buffer pH 7.4. Surface GluA2 was detected using Alexa 568 conjugated anti-mouse IgG secondary antibody (Invitrogen). Total GluA2 was detected by the GFP fluorescence signal. Imaging was performed using an Olympus Fluoview confocal microscope using the 60X objective lens.

Subcellular colocalization of total GFP-GluA2 and internalized GFP-GluA2

GFP-GluA2 expression was induced for 30 hrs with 7.5mg/ml DOX followed by labeling with 10 mg/ml anti-GluA2NTD monoclonal antibody (Chemicon, MAB397) in the CO_2 incubator at for 1 hr. During the 1 hr incubation period, GFP-GluA2 labeled with the antibody undergoes endocytosis. Unbound antibodies were washed with DMEM (37 ^{o}C) and the cells were fixed with 4% formaldehyde. Alexa 568 conjugated anti-mouse IgG antibody (Invitrogen) was used as secondary antibody to label the primary antibodies. All the

images were taken on an Olympus Fluoview confocal microscope, as described in the above section.

Time-lapse imaging

HEK cells were grown on a glass bottom dish for 24 hr before 7.5 mg/ml DOX was added. Time-lapse imaging occurred 30 hr after induction using an Olympus Fluoview confocal microscope mounted with a temperature (37 ^{o}C), CO_2 (5%) and humidity controlled chamber was used equipped with a 60X objective lens (Olympus PLAPON, N.A. = 1.42) was used. 0.5 mm thick optical sections were obtained up to 4 mm from the bottom of the cell. Recording was done continuously, resulting in 20 sec time intervals between each Z-stack.

Neuron culture and immunostaining

Primary cultures of rat hippocampal neurons were prepared from E18 rat embryos as previously described (Sala et al., 2003). HA-tagged GluA2 constructs were introduced into neurons at DIV14 using calcium phosphate transfection. Surface HA-GluA2 was stained while neurons were alive. Specifically, after labeling the DIV 18 neurons with anti-HA monoclonal antibody (HA.11, Covance), neurons were washed in DMEM to remove unbound antibodies and fixed with 4% formaldehyde in 0.1 M phosphate buffer pH 7.4. After washing with PBS, internal HA-GluA2 was labeled using anti-HA polyclonal antibody (Y-11, Santa Cruz) diluted in 1XGBD (0.2%

gelatin, 0.6% TritonX-100, 33mM phosphate buffer pH 7.4, and 0.9M NaCl). Alexa 488 conjugated anti-mouse IgG (Invitrogen) and Alexa 568 conjugated anti-rabbit IgG (Invitrogen) were used as secondary antibodies. Neurons were imaged using an Olympus Fluoview confocal microscope using the 60X objective lens (Olympus PLAPON, N.A. = 1.42). Z-projections of confocal stacks are shown in Figure 3B.

Timecourse of GluA2 expression in TetOnGluA2-stg cell lines.

Four clones (#2, 8, 9, and 10) of TetOnGluA2-stg cell lines and the parental TetONGluA2 cell were plated on the 6 well plates at a density of 0.6 x 10^6 cells/well, and incubated 24 hr to allow the cells to attach. At this point the cells were near confluent and 7.5 mg/ml DOX was added with 30 mM of NBQX to induce GluA2 expression. Cells were harvested 0, 6, 12, 18, and 24 hr after induction. Equal amounts of protein sample from each time point were loaded into each well of the SDS-PAGE gel (12.5% and 7.5% gels were used to resolve stargazin and GluA2, respectively). Western blotting was done using anti-panTARP and anti-GluA2C-terminal polyclonal antibodies (both generated in (Nakagawa et al., 2005)).

Immunostaining of HEK cells expressing stargazin and GluA2.

TetOnGluA2-stg Clone#10 cells were fixed as above 24hr after DOX induction. Anti-FLAG monoclonal (Sigma) and anti-panTARP polyclonal antibodies

(Nakagawa et al., 2005) were used to detect GluA2 and stargazin, respectively. Cy5 conjugated anti-mouse IgG (Jackson ImmunoResearch laboratories) and Alexa 488 conjugated anti rabbit (Invitrogen) were used as secondary antibodies. Confocal Z-stack images of the cells were recorded as above.

Supplemental Methods

Subcellular colocalization of GFP-GluA2 and the various membrane markers

Labeling with organelle specific antibodies: GFP-GluA2 expression was induced for 30 hrs with 7.5mg/ml DOX and the cells were fixed with 4% formaldehyde. The following primary antibodies were used for staining; anti-PDI monoclonal antibody (ER marker; from Affinity BioReagents), anti-rab6 monoclonal antibody (post-Golgi vesicle marker; a gift from Casper Hoogenraad), anti-GM130 monoclonal antibody (Golgi apparatus marker; from BD Transduction Laboratories), anti-EEA1 monoclonal antibody (early endosome marker; BD Transduction Laboratories). Alexa 568 conjugated anti-mouse IgG antibodiy (Invitrogen) was used as a secondary antibody to label the primary antibodies.

Labeling with lyotracker: 30 hrs after inducing GFP-GluA2 expression with 7.5mg/ml DOX, cells were incubated with 50 nM of Lysotracker Red (Invitrogen) for 1hr at 37 ^{o}C in the CO_2 incubator. The excess dyes were removed by washing with DMEM and the cells were fixed with 4% formaldehyde.

Labeling with Alexa568 conjugated transferrin: 30 hrs after inducing GFP-GluA2 expression with 7.5mg/ml DOX, cells were incubated with 50 ng/ml

Alexa 568 conjugated transferrin (Invitrogen) for 1 hr at 37 ^{o}C in the CO_2 incubator. The excess dyes were removed by washing with DMEM and the cells were fixed with 4% formaldehyde.

All the images were taken on an Olympus Fluoview confocal microscope. Z-projections of the confocal stacks are shown. GFP signal was used to detect GFP-GluA2 and was pseudo-colored with green in the confocal images, whereas signals from Alexa 568 and Lysotracker Red were pseudo-colored with red. Superposition of the green and red channels are shown the merged images.

References

Armstrong N, Sun Y, Chen GQ, Gouaux E (1998) Structure of a glutamatreceptor ligand-binding core in complex with kainate. Nature 395:913-917.

Ayalon G, Stern-Bach Y (2001) Functional assembly of AMPA and kainate receptors is mediated by several discrete protein-protein interactions. Neuron 31:103-113.

Barry MF, Ziff EB (2002) Receptor trafficking and the plasticity of excitatory synapses. Curr Opin Neurobiol 12:279-286.

Chen L, Chetkovich DM, Petralia RS, Sweeney NT, Kawasaki Y, Wenthold RJ, Bredt DS, Nicoll RA (2000) Stargazin regulates synaptic targeting of AMPA receptors by two distinct mechanisms. Nature 408:936-943.

Coleman SK, Moykkynen T, Cai C, von Ossowski L, Kuismanen E, Korpi ER, Keinanen K (2006) Isoform-specific early trafficking of AMPA receptor flip and flop variants. J Neurosci 26:11220-11229.

Frank J (1996) Three-dimensional Electron Microscopy of Macromolecular Assemblies.: Academic Press.

Frank J, Radermacher M, Penczek P, Zhu J, Li Y, Ladjadj M, Leith A (1996) SPIDER and WEB: processing and visualization of images in 3D electron microscopy and related fields. J Struct Biol 116:190-199.

Gouaux E (2004) Structure and function of AMPA receptors. J Physiol 554:249-253.

Greger IH, Khatri L, Ziff EB (2002) RNA editing at arg607 controls AMPA receptor exit from the endoplasmic reticulum. Neuron 34:759-772.

Greger IH, Khatri L, Kong X, Ziff EB (2003) AMPA receptor tetramerization is mediated by Q/R editing. Neuron 40:763-774.

Greger IH, Akamine P, Khatri L, Ziff EB (2006) Developmentally regulated, combinatorial RNA processing modulates AMPA receptor biogenesis. Neuron 51:85-97.

Grigorieff N (2007) FREALIGN: high-resolution refinement of single particle structures. J Struct Biol 157:117-125.

Hayashi Y, Shi SH, Esteban JA, Piccini A, Poncer JC, Malinow R (2000) Driving AMPA receptors into synapses by LTP and CaMKII: requirement for GluR1 and PDZ domain interaction. Science 287:2262-2267.

Hollmann M, Maron C, Heinemann S (1994) N-glycosylation site tagging suggests a three transmembrane domain topology for the glutamate receptor GluR1. Neuron 13:1331-1343.

Hollmann M, O'Shea-Greenfield A, Rogers SW, Heinemann S (1989) Cloning by functional expression of a member of the glutamate receptor family. Nature 342:643-648.

Jin R, Singh SK, Gu S, Furukawa H, Sobolevsky AI, Zhou J, Jin Y, Gouaux E (2009) Crystal structure and association behaviour of the GluR2 amino-terminal domain. Embo J 28:1812-1823.

Ju W, Morishita W, Tsui J, Gaietta G, Deerinck TJ, Adams SR, Garner CC, Tsien RY, Ellisman MH, Malenka RC (2004) Activity-dependent regulation of dendritic synthesisand trafficking of AMPA receptors. Nat Neurosci 7:244-253.

Keinanen K, Wisden W, Sommer B, Werner P, Herb A, Verdoorn TA, Sakmann B, Seeburg PH (1990) A family of AMPA-selective glutamate receptors. Science 249:556-560.

Leonard AS, Davare MA, Horne MC, Garner CC, Hell JW (1998) SAP97 is associated with the alpha-amino-3-hydroxy-5-methylisoxazole-4-propionic acid receptor GluR1 subunit. J Biol Chem 273:19518-19524.

Leuschner WD, Hoch W (1999) Subtype-specific assembly of alpha-amino-3-hydroxy-5-methyl-4-isoxazole propionic acid receptor subunits is mediated by their n-terminal domains. J Biol Chem 274:16907-16916.

Mah SJ, Cornell E, Mitchell NA, Fleck MW (2005) Glutamate receptor trafficking: endoplasmic reticulum quality control involves ligand binding and receptor function. J Neurosci 25:2215-2225.

Malinow R, Malenka RC (2002) AMPA receptor trafficking and synaptic plasticity. Annu Rev Neurosci 25:103-126.
Matsuo N, Reijmers L, Mayford M (2008) Spine-type-specific recruitment of newly synthesized AMPA receptors with learning. Science 319:1104-1107.

Mayer ML (2006) Glutamate receptors at atomic resolution. Nature 440:456-462.

Mindell JA, Grigorieff N (2003) Accurate determination of local defocus and specimen tilt in electron microscopy. J Struct Biol 142:334-347.

Nakagawa T, Cheng Y, Sheng M, Walz T (2006) Three-dimensional structure of an AMPA receptor without associated stargazin/TARP proteins. Biol Chem 387:179-187.

Nakagawa T, Cheng Y, Ramm E, Sheng M, Walz T (2005) Structure and different conformational states of native AMPA receptor complexes. Nature 433:545-549.

Nakanishi N, Shneider NA, Axel R (1990) A family of glutamate receptor genes: evidence for the formation of heteromultimeric receptors with distinct channel properties. Neuron 5:569-581.

Nicoll RA, Tomita S, Bredt DS (2006) Auxiliary subunits assist AMPA-type glutamate receptors. Science 311:1253-1256.

O'Brien RJ, Kamboj S, Ehlers MD, Rosen KR, Fischbach GD, Huganir RL (1998) Activity-dependent modulation of synaptic AMPA receptor accumulation. Neuron 21:1067-1078.

Ohi M, Li Y, Cheng Y, Walz T (2004) Negative staining and image classification - powerful tools in modern electron microscopy. Biol Proced Online 6:23-34.

Park M, Penick EC, Edwards JG, Kauer JA, Ehlers MD (2004) Recycling endosomes supply AMPA receptors for LTP. Science 305:1972-1975.

Penn AC, Williams SR, Greger IH (2008) Gating motions underlie AMPA receptor secretion from the endoplasmic reticulum. Embo J 27:3056-3068.

Priel A, Selak S, Lerma J, Stern-Bach Y (2006) Block of kainate receptor desensitization uncovers a key trafficking checkpoint. Neuron 52:1037-1046.

Reeves PJ, Callewaert N, Contreras R, Khorana HG (2002) Structure and function in rhodopsin: high-level expression of rhodopsin with restricted and homogeneous N-glycosylation by a tetracycline-inducible N-acetylglucosaminyltransferase I-negative HEK293S stable mammalian cell line. Proc Natl Acad Sci U S A 99:13419-13424.

Robert A, Irizarry SN, Hughes TE, Howe JR (2001) Subunit interactions and AMPA receptor desensitization. J Neurosci 21:5574-5586.

Rogers SW, Andrews PI, Gahring LC, Whisenand T, Cauley K, Crain B, Hughes TE, Heinemann SF, McNamara JO (1994) Autoantibodies to glutamate receptor GluR3 in Rasmussen's encephalitis. Science 265:648-651.

Rosenmund C, Stern-Bach Y, Stevens CF (1998) The tetrameric structure of a glutamate receptor channel. Science 280:1596-1599.

Rosenthal PB, Henderson R (2003) Optimal determination of particle orientation, absolute hand, and contrast loss in single-particle electron cryomicroscopy. J Mol Biol 333:721-745.

Sala C, Futai K, Yamamoto K, Worley PF, Hayashi Y, Sheng M (2003) Inhibition of dendritic spine morphogenesis and synaptic transmission by activity-inducible protein Homer1a. J Neurosci 23:6327-6337.

Scannevin RH, Huganir RL (2000) Postsynaptic organization and regulation of excitatory synapses. Nat Rev Neurosci 1:133-141.

Schwenk J, Harmel N, Zolles G, Bildl W, Kulik A, Heimrich B, Chisaka O, Jonas P, Schulte U, Fakler B, Klocker N (2009) Functional proteomics identify cornichon proteins as auxiliary subunits of AMPA receptors. Science 323:1313-1319.

Sheng M, Lee SH (2001) AMPA receptor trafficking and the control of synaptic transmission. Cell 105:825-828.

Shepherd JD, Huganir RL (2007) The cell biology of synaptic plasticity: AMPA receptor trafficking. Annu Rev Cell Dev Biol 23:613-643.

Sobolevsky AI, Rosconi MP, Gouaux E (2009) X-ray structure, symmetry and mechanism of an AMPA-subtype glutamate receptor. Nature 462:745-756.

Stern-Bach Y, Russo S, Neuman M, Rosenmund C (1998) A point mutation in the glutamate binding site blocks desensitization of AMPA receptors. Neuron 21:907-918.

Sun Y, Olson R, Horning M, Armstrong N, Mayer M, Gouaux E (2002) Mechanism of glutamate receptor desensitization. Nature 417:245-253.

Swanson GT, Kamboj SK, Cull-Candy SG (1997) Single-channel properties of recombinant AMPA receptors depend on RNA editing, splice variation, and subunit composition. J Neurosci 17:58-69.

Valluru L, Xu J, Zhu Y, Yan S, Contractor A, Swanson GT (2005) Ligand binding is a critical requirement for plasma membrane expression of heteromeric kainate receptors. J Biol Chem 280:6085-6093.

Vandenberghe W, Nicoll RA, Bredt DS (2005a) Interaction with the unfolded protein response reveals a role for stargazin in biosynthetic AMPA receptor transport. J Neurosci 25:1095-1102.

Vandenberghe W, Nicoll RA, Bredt DS (2005b) Stargazin is an AMPA receptor auxiliary subunit. Proc Natl Acad Sci U S A 102:485-490.

Wenthold RJ, Petralia RS, Blahos J, II, Niedzielski AS (1996) Evidence for multiple AMPA receptor complexes in hippocampal CA1/CA2 neurons. J Neurosci 16:1982-1989.

Wu Y et al. (2007) Mutations in ionotropic AMPA receptor 3 alter channel properties and are associated with moderate cognitive impairment in humans. Proc Natl Acad Sci U S A 104:18163-18168.

Ziff EB (2007) TARPs and the AMPA receptor trafficking paradox. Neuron 53:627-633.

Figures

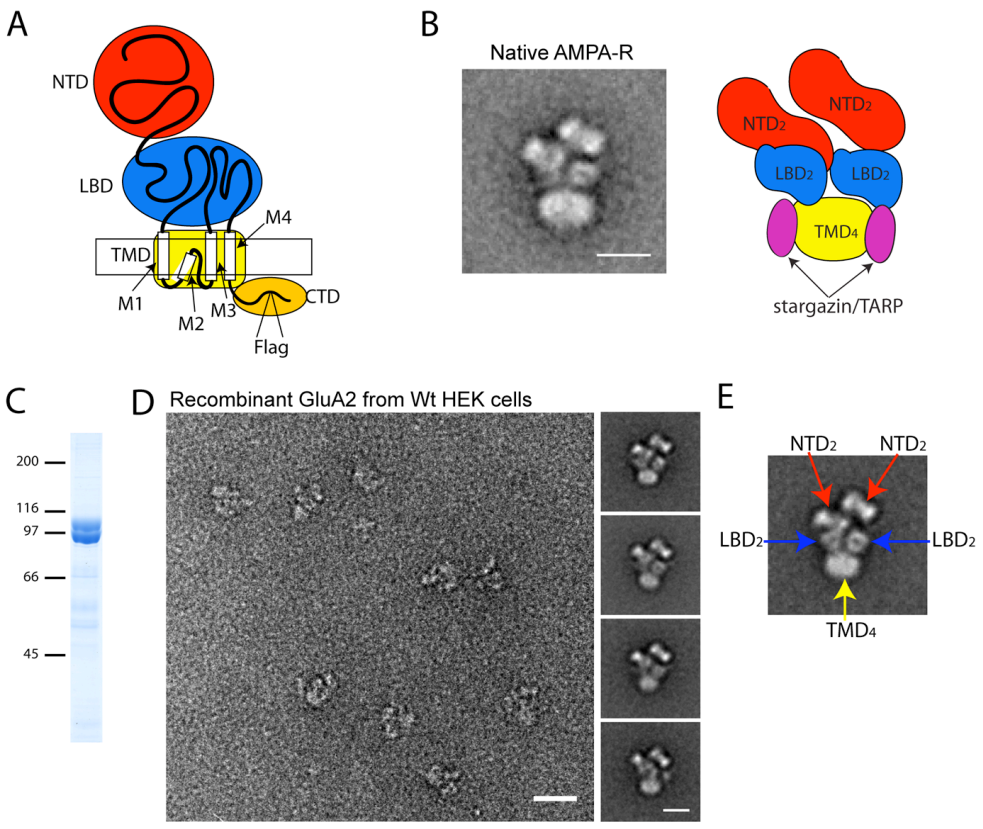

Figure 2_1. Characterization of recombinant GluA2 homotetramers
(A) Cartoon depicting domain organization of an AMPA-R subunit. NTD = N-terminal domain; LBD = ligand-binding domain; and TMD = transmembrane domain. The box represents the lipid bilayer. M1–4 indicate the sub-domains within the TMD. CTD = C-terminal domain. **(B)** Representative class average of negative stained native heterotetrameric AMPA-R particles purified from rat brain with schematic representation. TMD density includes stargazin/TARP protein(s). Scale bar = 10 nm. **(C)** 7.5% SDS-PAGE gel of GluA2 doublet purified from constitutively expressing HEK cells (coomassie brilliant blue stained gel). Numbers on left indicate positions of the molecular weight marker in kDa. **(D)** Left panel: Raw particle images of negatively stained recombinant GluA2 homotetramers purified from stably expressing HEK cells. Scale bar = 20 nm. Right small panels: Representative class averages. Scale bar = 10 nm. **(E)** Class average of recombinant tetrameric GluA2 particle labeled with domain designations.

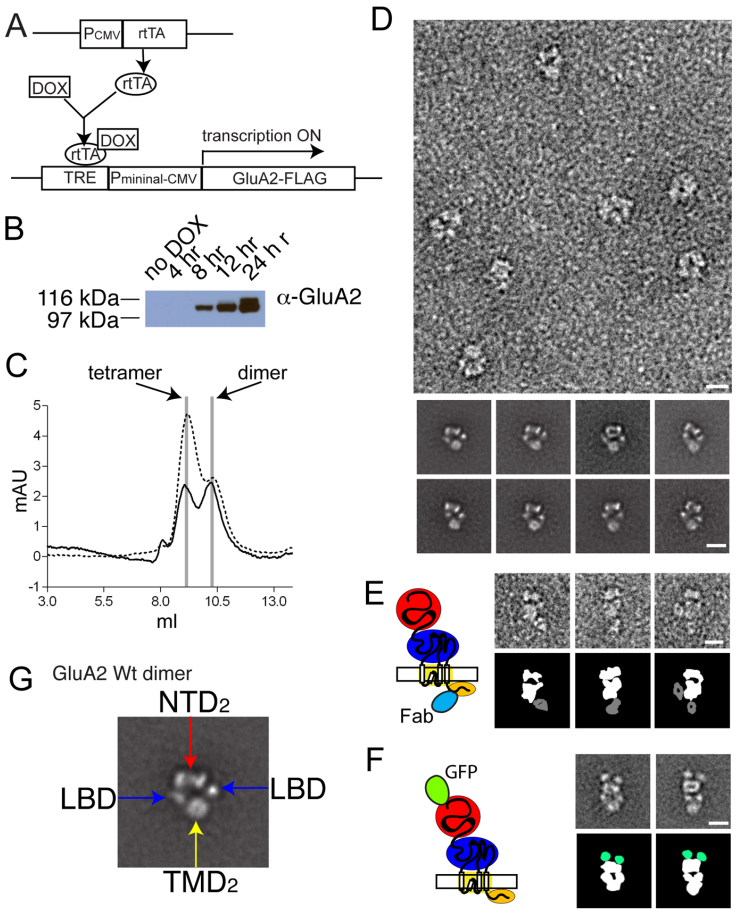

Figure 2_2. Purification and EM imaging of GluA2 dimers
(A) Schematic of TetON system of protein induction. Addition of DOX promotes GluA2 production. **(B)** Western blot depicting the timecourse of GluA2 protein expression after induction. Note the formation of double band after 24 hr. **(C)** Gel filtration chromatograph for GluA2 expressed and purified at 20 hr (solid line) and 24 hr (dotted line) after induction. Positions of tetramer and dimer are indicated. (**D)** Raw particle images of GluA2 dimers (top) and representative class averages (bottom small panels) purified from TetONGluA2 HEK cells. Scale bar = 10 nm. **(D)** Cartoon of Fab fragment labeled GluA2 subunit (left). Raw particle images GluA2 dimer labeled with Fab fragment. Under each class average is a representation to facilitate interpretation. Receptor complex is in white, and Fabs in gray. Fab labels C-terminal portion. Scale bar = 10 nm. **(E)** Cartoon of GFP tagged GluA2 subunit (left). Class averages of GFP-GluA2 dimer particles (right upper panels). Under each class average is a representation facilitate interpretation. The receptor complex is in white and GFP in green. GFP labels the N-terminal portion. Scale bar = 10 nm. **(F)** Summary of domain labeling. Class average of a dimeric AMPA-R particle labeled with domain designations.

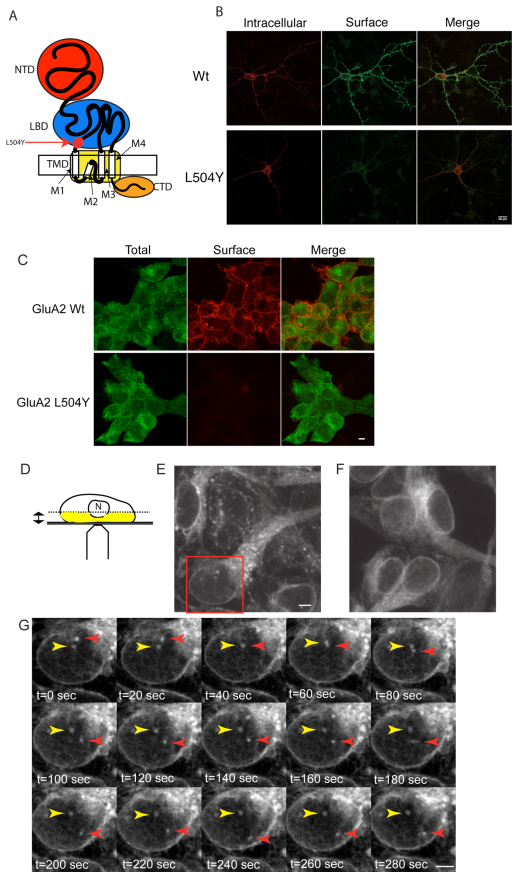

Figure 2_3. Contrasting dynamics of GFP-GluA2 wildtype and L504Y
(A) Cartoon showing position of the L504Y mutation in GluA2 subunit. **(B)** Fluorescent confocal images of primary rat hippocampal neurons overexpressing HA-GluA2 wildtype (top) or HA-GluA2L504Y (bottom). Surface GluA2 (green) was live-labeled with anti-HA monoclonal antibody. Fixed and permeablized neurons were labeled with anti-HA polyclonal antibody (red) to stain intracellular GluA2. Scale bar = 20 mm. **(C)** Fluorescent confocal images of HEK cells expressing GFP-GluA2 wildtype (top) or GFP-GluA2L504Y (bottom). Surface expression of the L504Y mutant is reduced in our inducible expression system. Surface labeling (red) was done 30 hr after induction. Total GluA2 was detected by the GFP signal (green). Scale bar = 5 mm. **(D)** Scheme of time-lapse imaging. The 4 mm between the bottom of the nucleus and the bottom of the cell attached to the coverglass (yellow volume) provided the clearest images of receptor trafficking. **(E)** Confocal Z-stack projection of GFP-GluA2 wildtype in HEK cells. Imaged 30 hr after GluA2 induction. Scale bar = 4 mm. **(F)** Confocal Z-stack projection of GFP-GluA2L504Y. Imaged 30 hr after GluA2 induction. Same magnification as in E. **(G)** Time-lapse image taken from the red square in (E) Note difference in dynamics between the puncta pointed out by red and yellow arrows. Scale bar = 4 mm.

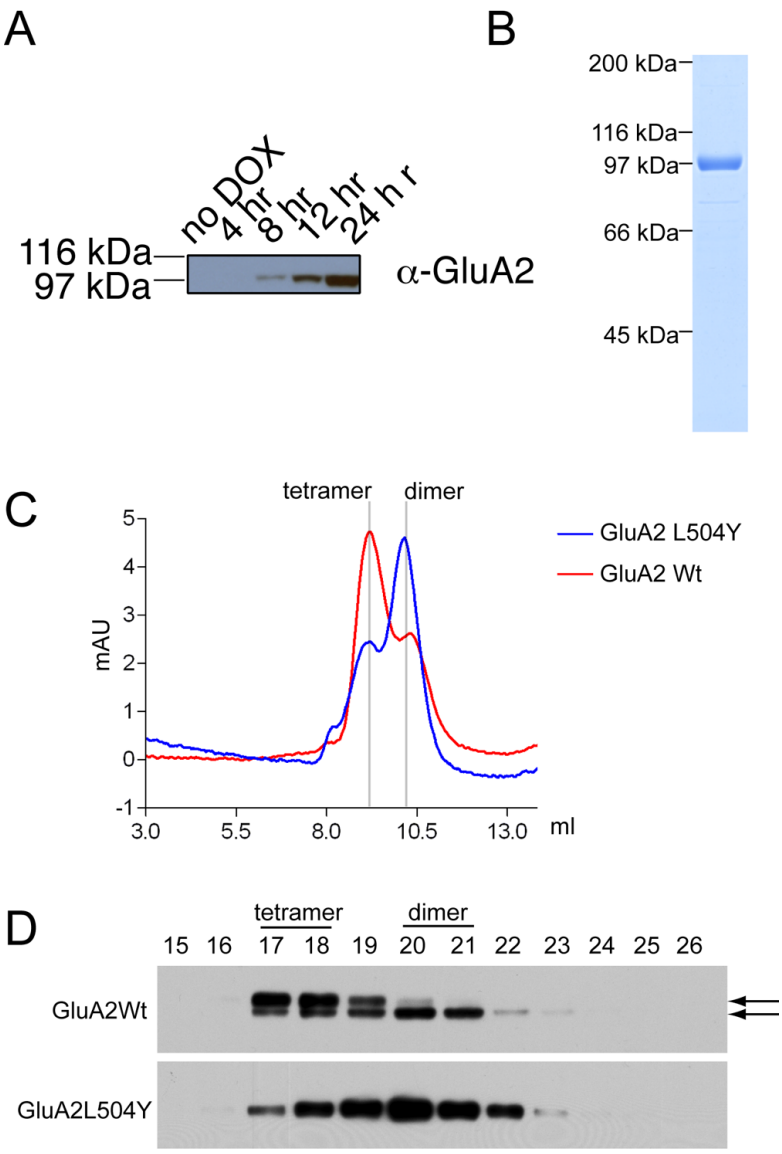

Figure 2_4. Inefficient tetramerization of GluA2 L504Y
(A) Western blot depicting timecourse of GluA2L504Y protein expression after induction. **(B)** Coomassie brilliant blue stained 7.5% SDS-PAGE of GluA2 purified from TetOnGluA2L504Y HEK cells. Note only single band is present.
(C) Gel filtration chromatograph of GluA2 wildtype (red) and L504Y (blue) purified from TetONGluA2 and TetONGluA2L504Y HEK cells, respectively. Proteins were harvested 24 hr after induction. Peaks corresponding to tetramer and dimer are indicated.

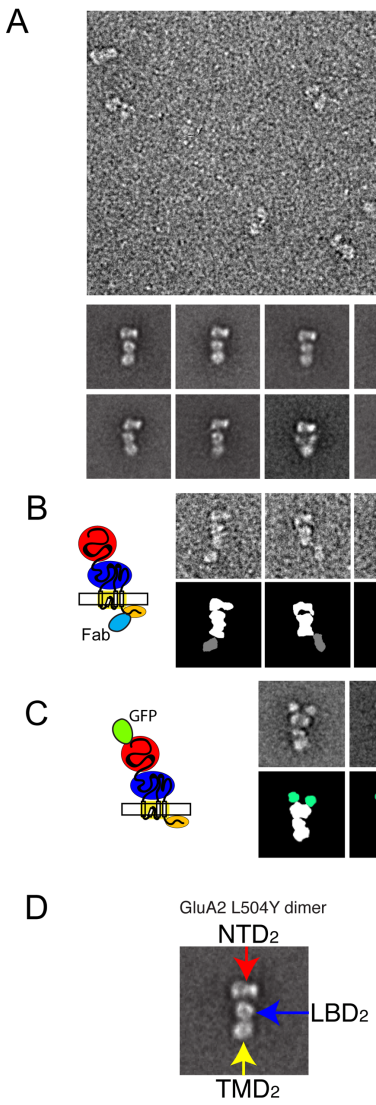

Figure 2_5. EM imaging of GluA2L504Y dimers
(A) Raw particle images of the GluA2L504Y dimer (upper large panel) and representative class averages (lower small panels). Scale bar = 10 nm.
(B) Cartoon of Fab fragment labeled GluR subunit (left). Raw particle images of GluA2L504Y dimer labeled with Fab fragment (right upper panels). Under each class average is a representation to facilitate interpretation. Receptor complex is in white, and Fabs in gray. Fabs label the C-terminus. Scale bar = 10 nm. **(C)** Cartoon of GFP tagged GluA2L504Y subunit (left). Class averages of GFP-GluA2L504Y dimer particles (right upper panels). Under each class average is a representation to facilitate interpretation. Receptor complex is in white and GFP in green. GFP labels the N-terminus. Scale bar = 10 nm. **(D)** Summary of domain labeling. Class average of dimeric GluA2L540Y particle labeled with domain designations.

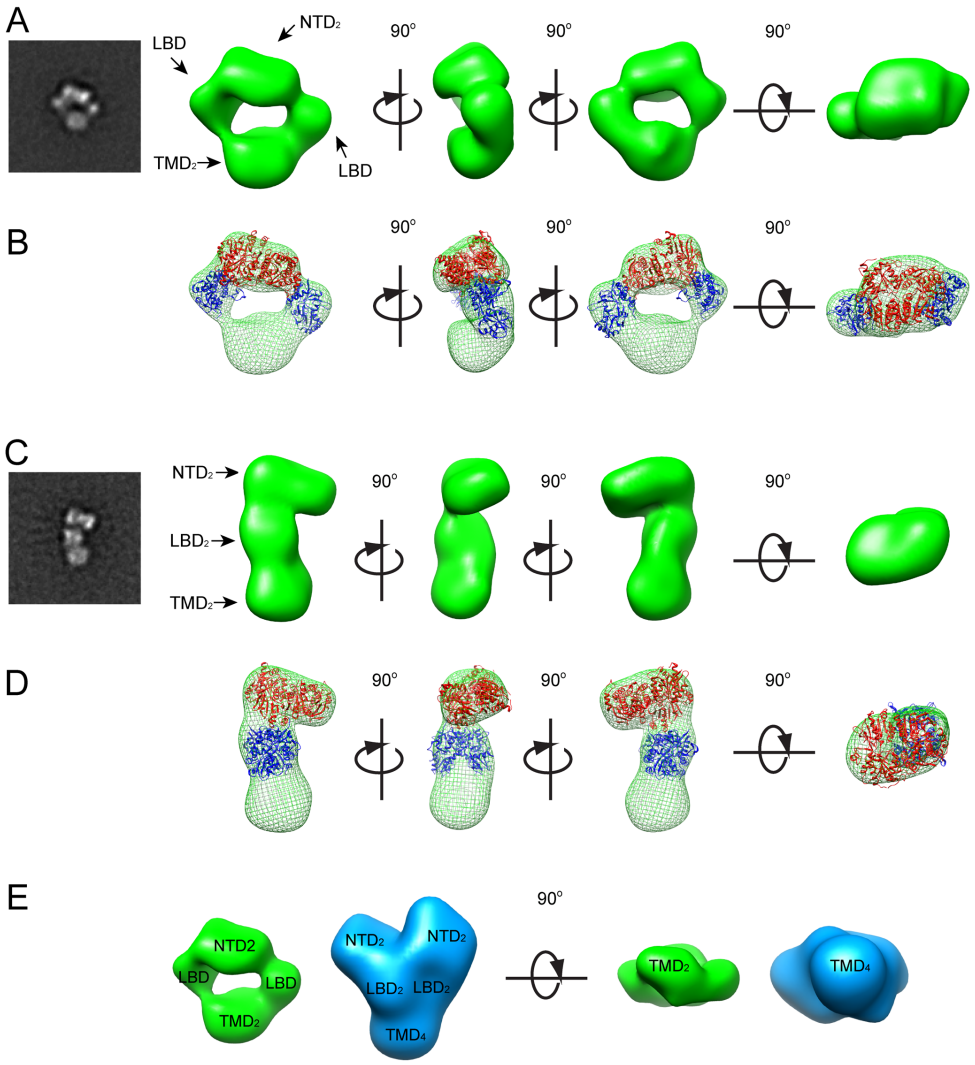

Figure 2_6. 3D structures of GluA2 wildtype and L504Y dimers
(A) Structures of GluA2 wildtype dimers. Left box: Class average of untilted particles used for random conical tilt reconstruction. Right: four different views of 3D density map calculated from particles classified into the class average on left left. **(B)** Placement of known crystal structures into the EM density map for the GluA2 wildtype dimer. Red: NTD of GluA2 (PDB:3H5W); blue: LBD of GluA2 S1S2 wildtype (PDB:1FTJ). Scale bar = 7.3nm. **(C)** Structures of GluA2L504Y dimers. Left box: Class average of untilted particles used for random conical tilt reconstruction. Right: four different views of the 3D density map calculated from particles classified into the class average shown on left. **(D)** Placement of known crystal structures into the EM density map for GluA2L504Y dimer. Red: NTD of GluA2 (PDB:3H5W),;blue: LBD of GluA2 S1S2 L483Y (PDB:1LB8). Scale bar = 7.3 nm. 3D map in A-D are shown at the same scale. **(E)** Juxtaposition of GluA2 wildtype dimer and brain derived tetrameric AMPA-R devoid of stargazin/TARPs (Nakagawa et al., 2006). Two different views are shown. Note the TMD is smaller in the dimer than in the tetramer when the density map is viewed from the bottom. Scale bar = 7.3 nm.

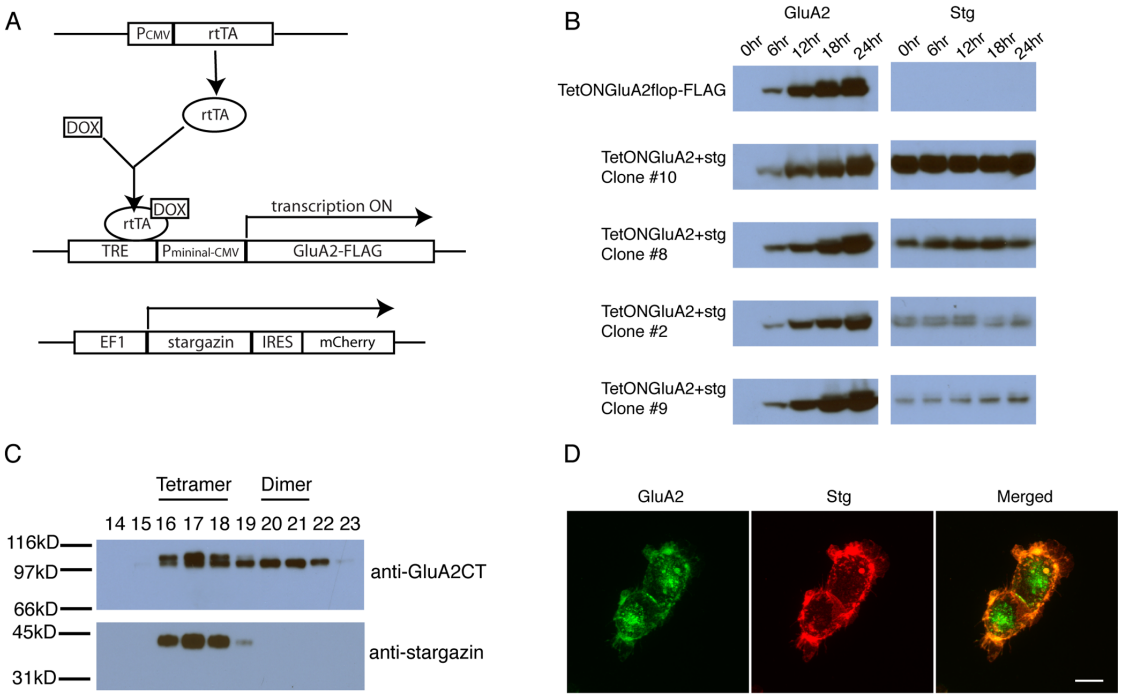

Figure 2_7. Stargazin forms a stable complex with GluA2 tetramers but not with dimers **(A)** Schematic of our strategy used to co-express GluA2 and stargazin in HEK cells which we named TetONGluA2-stg cells. **(B)** Western blotting showing timecourse of GluA2 (left) and stargazin (right) expression in the cell lines indicated on the left of each row. **(C)** Western blotting of the fractions eluted from Superdex200 gel filtration column. Membranes were probed with anti-GluA2C-terminal antibidy (upper panel) and anti-stargazin (lower panel) antibodies. Fractions corresponding to the tetramers and dimers are indicated. (D) Confocal immunofluorescent Z-stack projections of clone#10 24hr after induction. Red is stargazin and green is GluA2. Superposition of the two colors is shown in merged image on the right. Scale bar 15 mm.

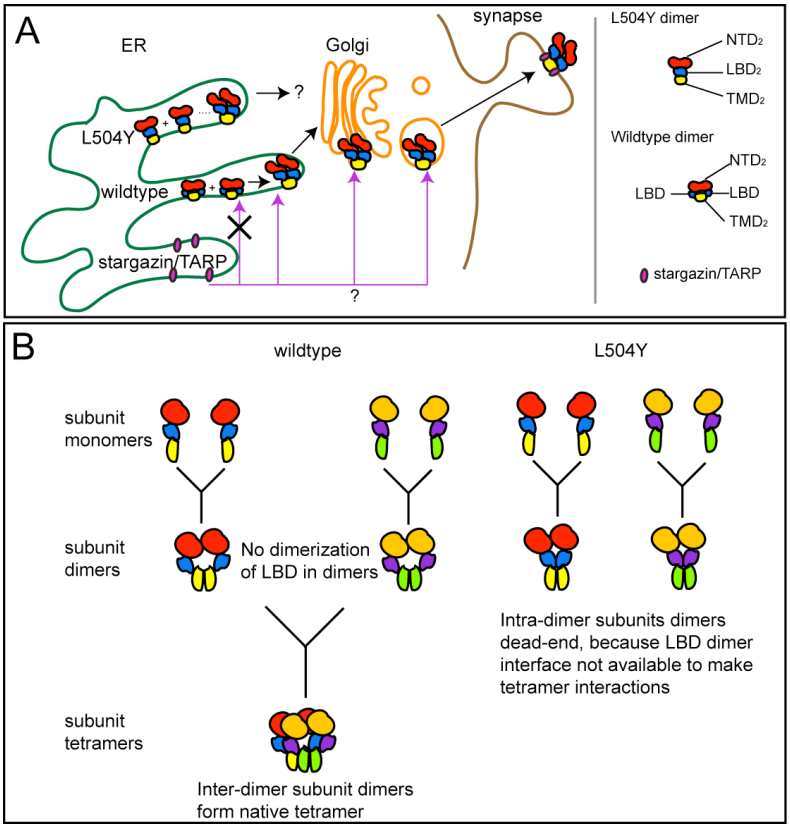

Figure 2_8. Working model of AMPA-R tetramerization and trafficking
(A) In the ER, dimers of AMPA-R subunits are formed and transition into tetramers. With dimeric wildtype subunits, the NTD and TMD form dimers but the LBD is separated. In contrast, the NTD, LBD, and TMD are all compactly dimerized in the GluA2L504Y mutant, which transition into tetramers much less efficiently. The domain organization seen in the structure of the wildtype dimer is critical for efficient tetramerization. A small quantity of GluA2L504Y tetramers are formed and reach the cell surface by an unknown mechanism. The majority of GluA2L504Y is not complex mannose glycosylated, suggesting that it did not receive modification in the Golgi apparatus. It is likely that most GluA2L504Y cannot even exit the ER or reach the cis-Golgi. Stargazin/TARPs are associated with the mature AMPA-Rs. Stargazin preferentially forms a stable complex with GluA2 tetramers but not with dimers. Cornichons are another subset of AMPA-R auxiliary proteins in the membrane. The precise timing of incorporation into the AMPA-R complex remains to be determined.
(B) Proposed AMPA-R subunit assembly pathways are shown. In the wildtype subunit dimers, the LBDs are not dimerized. We propose that the LBD dimers in wildtype subunits are formed during the dimer-to-tetramer transition. On the other hand, the LBDs in the L504Y mutant subunits form intra-dimer dimers that may prevent efficient dimer-to-tetramer transition. NTD = red and orange, LBD = blue and purple, TMD = yellow and green.

Supplementary Figures

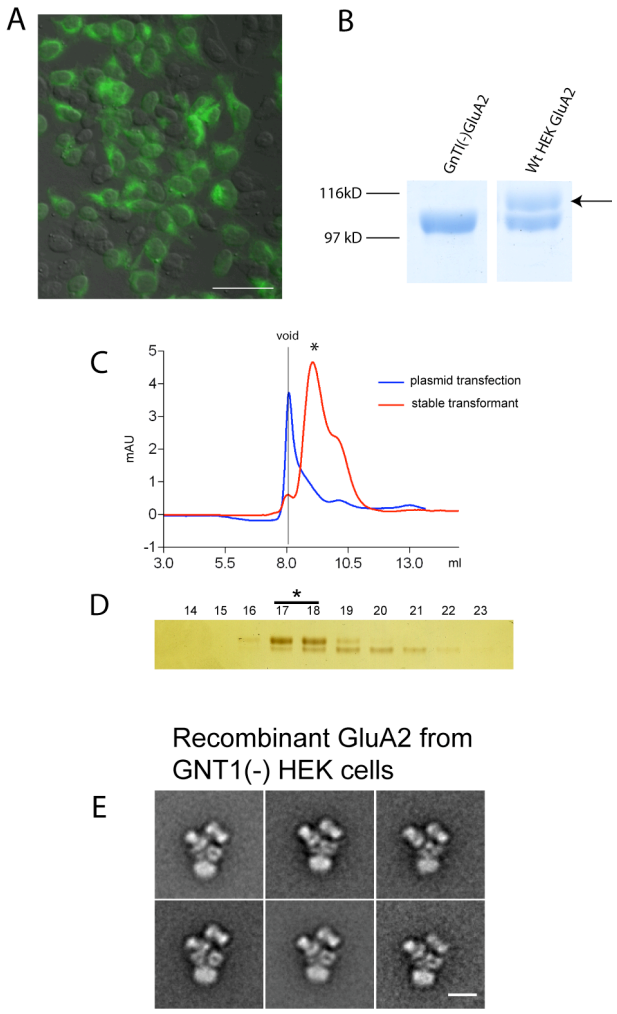

Figure 2_S1. Detailed characterization of the HEK cell based recombinant GluA2 tetramers

(A) HEK cells constitutively express GluA2. Immunostaining represents total GluA2. Overlay of DIC and immunofluorescence image is shown. Scale bar = 50 mm. **(B)** Recombinant GluA2 was resolved by SDS-PAGE gel. Right: GluA2 purified from wild type stable HEK cells. The doublet represents glycosylated and unglycosylated forms. Left: GluA2 purified from GnT1(-) (glycosylation mutant) stable HEK cells. Only a single band is resolved. (**C)** Gel filtration chromatograph for transiently (blue) vs. stably expressed (red) GluA2 in HEK cells. Position of void volume is marked. Asterisk represents the major GluA2 tetramer peak. **(D)** Silver stained SDS-PAGE gel. Fractions near the peak fraction shown in (C) were resolved. Numbers indicate the fraction number. Fractions indicated by the asterisk correspond to the fractions around the peak indicated by asterisk in (C). **(E)** Representative class averages of recombinant GluA2 homotetramers purified from stably expressing GnT1(-) HEK cells.

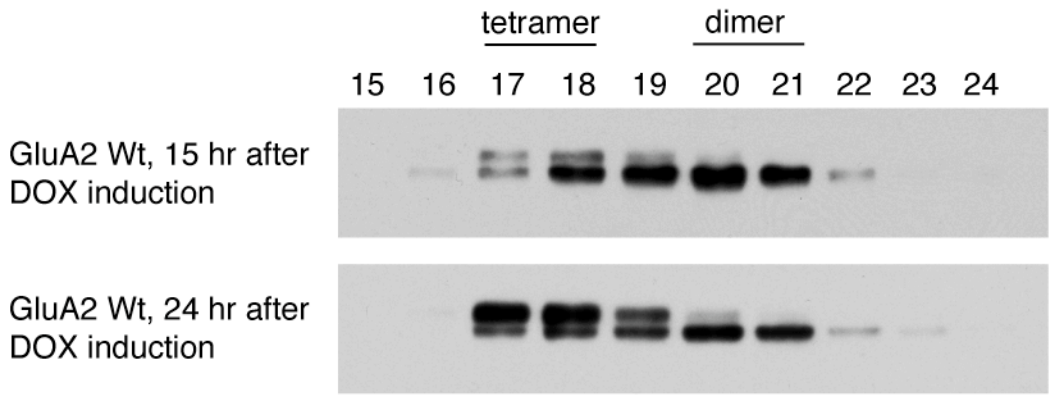

Figure 2_S2. Dimeric species appear before the tetrameric species of GluA2
Recombinant GluA2 purified either 15 or 24 hours after Dox-induction, and further separated into dimeric and tetrameric species by gel filtration. Fractions (#15 to #24) from gel filtration resolved by 7.5% SDS-PAGE and processed probed by Western blotting. The tetramer peak corresponded to fraction 17 and 18, and dimer peak corresponded to fractions 20 and 21. Upper blot: 15 hr after induction. Lower blot: 24 hr after induction. Note that the majority of the protein obtained from HEK cells that were harvested after 15 hr of DOX induction is in the form of dimers. The dimer population precedes the formation of tetramers, and the dimers represent a biosynthetic intermediate of pre-assembled GluA2 tetramers.

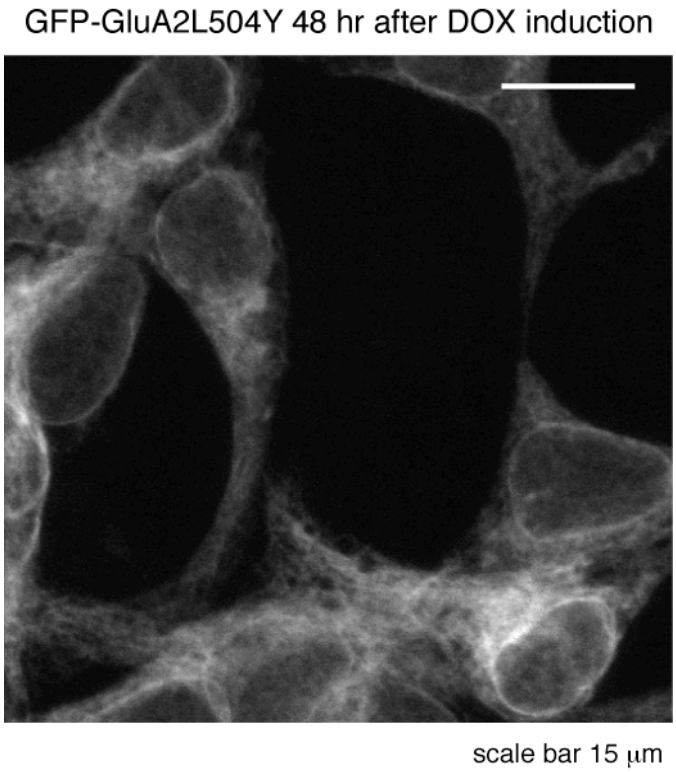

Figure 2_S3. Subcellular localization of GFP-GluA2L504Y mutant at 48 hr after DOX induction
Expression of GFP-tagged GluA2L504Y mutant was induced for 48 hr using DOX. Z-projections of the confocal stack are shown. Scale bar= 15mm. Even at 48 hr after DOX induction no punctate GFP signal was detectable.

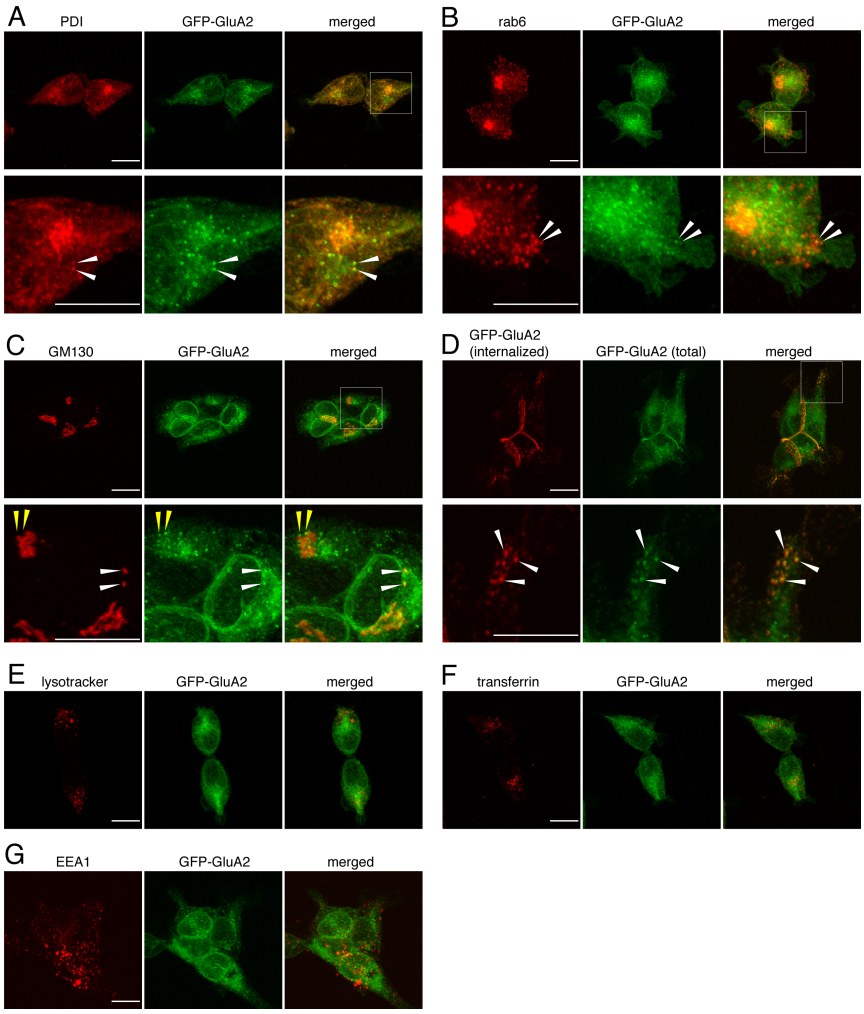

Figure 2_S4. Subcellular localization of GFP-GluA2 in HEK cells.
Fluorescent confocal Z-stack images are shown. For all: Scale bars = 15 mm. Superposition of the green and red channel is shown in the right of each row as a merged image. Higher resolution images of the white rectangle are shown in the lower row. White arrowheads indicate co-localization. **(A)** Subcellular localization of PDI (an ER maker) (red) and GFP-GluA2 (green). **(B)** Subcellullar localization of rab6 (a sub-population of post-Golgi vesicle maker) (red) and GFP-GluA2 (green). (**C)** Subcellular localization of GM130 (a Golgi apparutus maker) (red) and GFP-GluA2 (green). Yellow arrowheads indicate GFP-GluA2 puncta associated with the Golgi apparatus. (**D)** Subcellular localization of internalized GFP-GluA2 (red) and GFP-GluA2 (green). (**E)** Subcellular localization of lysotracker (a lysosome marker) (red) and GFP-GluA2 (green). (**F)** Subcellular localization of transferrin (a recycling endosome marker) (red) and GFP-GluA2 (green). (**G)** Subcellular localization of EEA1 (an early endosome marker) (red) and GFP-GluA2 (green).

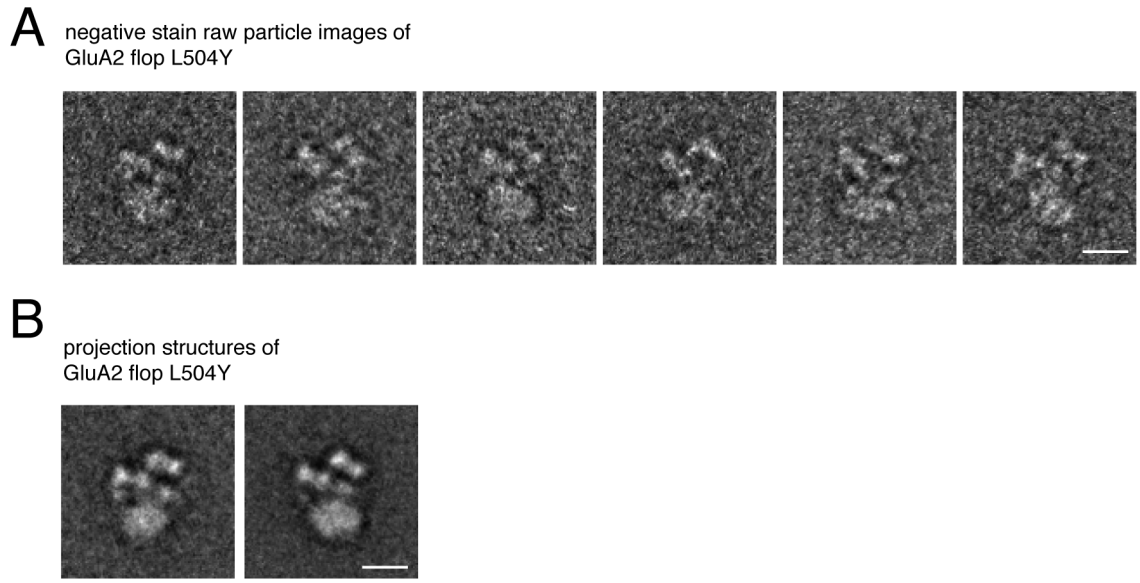

Figure 2_S5. Projection structures of tetrameric GluA2L504Y. Tetramers of GluA2L504Y were purified and imaged by negative stain EM.
(A) Raw particle images are shown. The size of the rectangular boxes is 38 nm x 38 nm. Scale bar = 10 nm. (**B)** Representative class averages of tetrameric GluA2L504Y. Note that the tetrameric GluA2L504Y adopts structures that are very similar to the tetramers of GluA2 wildtype (compare with Fig 1D). Scale bar = 10 nm

Acknowledgments

Chapter II, in full, is a reproduction of the material as it appears in Journal of Neuroscience 2010. Shanks, Natalie F.; Maruo, Tomohiko; Farina, Anthony N.; Ellisman, Mark H.; Nakagawa, Terunaga, the Society for Neuroscience, 2012. The dissertation author was the primary contributor to the investigation and writing of the manuscript. Permission of all authors has been obtained.

Chapter III

Differences of AMPA and kainate receptor interactomes identify a novel AMPA receptor auxiliary subunit, GSG1L

Abstract

AMPA receptor (AMPA-R) complexes consist of channel forming subunits, GluA1-4 and auxiliary proteins including TARPs, CNIHs, synDIG1, and CKAMP44, which can modulate AMPA-R function in specific ways. Combinatorial effects of four GluA subunits binding to various auxiliary subunits amplify the functional diversity of AMPA-Rs. The significance and magnitude of molecular diversity, however, remain elusive. To gain insight into the molecular complexity of AMPA and kainate receptors (KA-Rs), we compared the proteins that co-purify with each receptor type in rat brain. This interactome study identified the majority of known interacting proteins and more importantly, provides novel candidates for further studies. We validate the claudin homologue GSG1L as a novel binding protein and unique modulator of AMPA-R gating, as determined by detailed molecular, cellular, electrophysiological, and biochemical experiments. GSG1L extends the functional variety of AMPA-R complexes and further investigation of other candidates may reveal additional complexity of ionotropic glutamate receptor function.

Introduction

AMPA-R and KA-R are members of the ionotropic glutamate receptor (iGluR) family, functioning as ligand-gated ion channels that mediate excitatory synaptic transmission and plasticity in the brain (Traynelis et al., 2010). Their functions are regulated by the composition of channel forming core subunits, association with auxiliary proteins, phosphorylation, receptor trafficking, and interaction with cytoplasmic scaffolds (Jackson and Nicoll, 2011; Kim and Sheng, 2004; Shepherd and Huganir, 2007). Defining molecules that mediate receptor modulation is critical in understanding basic brain function and disease mechanisms. The molecular composition of AMPA and KA-Rs are diverse and the complete landscape is currently unclear.

The iGluR's channel core is a tetrameric assembly of receptor subunits, GluA1-4 for AMPA-Rs and GluK1-5 for KA-Rs (Collingridge et al., 2009). Auxiliary transmembrane subunits bind to core iGluR subunits. They are found across species (Wang et al., 2008), and include stargazin (stg)/TARPs (Chen et al., 2000; Tomita et al., 2003), SOL-1 (Zheng et al., 2004), cornichon2/3 (CNIH-2/3) (Schwenk et al., 2009), synDIG1 (Kalashnikova et al., 2010), and CKAMP44 (von Engelhardt et al., 2010) for AMPA-Rs, and Neto1-2 (Zhang et al., 2009) for KA-Rs. The combinatorial effect of various auxiliary subunits binding to channel forming core subunits extends the architectural and

functional complexity of iGluRs in the brain (Farrant and Cull-Candy, 2010; Jackson and Nicoll, 2011).

iGluR complexes are extensively studied, yet new binding proteins are continuously reported. Biochemical hurdles in handling intact membrane proteins have been overcome for AMPA and KA-Rs by robust purification protocols (Nakagawa et al., 2005; Zhang et al., 2009). In combination with liquid chromatographic separations in line with tandem mass spectrometers (LC-MS/MS), peptide analysis can identify nearly all proteins present in a low complexity sample (Savas et al., 2011).

In this study, we wished to identify new iGluR interactors that are less abundant or difficult to find. Specifically, we compared the interactomes of native AMPA and KA-Rs and identified a new AMPA-R auxiliary subunit, GSG1L. GSG1L modifies AMPA-R channel function very differently from the known auxiliary modulators, revealing a new functional repertoire of AMPA-Rs. This study provides a proof-of-principal for identifying novel interactors of iGluRs using our interactome data. Our results may further reveal previously unexpected molecular and functional diversity of iGluR complexes.

Results

Identification of candidate proteins that co-purify with AMPA-Rs and KA-Rs in rat brain

We performed immuno-affinity purification of native AMPA and KA-Rs followed by shotgun LC-MS/MS protein analysis (AP-MS/MS). The co-purifying proteins were directly analyzed by multidimensional protein identification technology (MudPIT) (Washburn et al., 2001). As a negative control, we performed a parallel purification with normal rabbit IgG. Any protein binding to IgG was excluded from analysis.

A summary and complete list of the proteins that co-purify with brain AMPA and KA-Rs are shown in Table 1 and S1 (http://www.cell.com/cell-reports/fulltext/S2211-1247(12)00128-3#suppinfo), respectively. Our purification was highly enriched for the target proteins containing the epitopes of the antibodies used for affinity purification, as demonstrated by numerous spectrum counts (s.c.) and peptides counts (p.c.) for GluA2 (2526 s.c./193 p.c.) and GluK2 (790 s.c./88 p.c.). Nearly all known AMPA-R interacting membrane proteins, such as TARPs (stg/g-2, g-3, g-4, g-5, g-7, and g-8), CNIH2/3, and CKAMP44 were identified in our AMPA-R preparation. While we did not find synDIG1 itself, we identified homologues (Fig 1A and C). Among

the known auxiliary subunits, stg/TARPs were most abundantly detected, while fewer s.c.'s and p.c's were observed for the others. Furthermore, the known KA-R auxiliary subunits Neto-1 and 2 were detected with KA-Rs (Fig 1B and C). These results indicate that our purification was robust and thus, further investigation of the list may identify novel interactors. Our results extend current knowledge on the interactomes of AMPA and KA-Rs.

Predicted protein GSG1L is expressed and binds to AMPA-Rs

Among the candidates, we focused on a predicted protein GSG1L, a membrane protein specifically co-purifying with AMPA-Rs (Fig 1A). It is a distant homologue of stg/TARPs belonging to the extended claudin family (Fig 1B). Furthermore, its peptide counts were comparable to known AMPA-R auxiliary subunits (Fig 1A and Table 1). GSG1L was reproducibly identified from rat brain (Table 1 and S1 (http://www.cell.com/cell-reports/fulltext/S2211-1247(12)00128-3#suppinfo)) and also co-purified with AMPA-Rs from human cortex (Fig S1A-C), indicative of evolutionary conservation of the interactome. Collectively, this evidence provided confidence for further investigation.

While it is in the claudin family, GSG1L is distinct from stg/TARPs, as there is a large evolutionary distances between GSG1L and stg/TARPs. The nearest family member of GSG1L is the product of germ line specific gene 1

(GSG1) whose transcript is specifically expressed in the germ line and whose function is unknown (Tanaka et al., 1994).

Similar to claudins, the predicted topology of GSG1L has a cytoplasmic N-terminus, four transmembrane segments, two extracellular loops, and a cytoplasmic C-terminus (Fig 1C). Loop1 is ~50% longer in GSG1L than in TARPs. The extracellular and cytoplasmic domains of GSG1L are not conserved with stg/TARPs (Fig S1D). These regions are responsible for modulating AMPA-R function in stg/TARPs (Tomita et al., 2005), and thus GSG1L may potentially have unique modulatory function.

GSG1L was annotated as a predicted protein in the rat genome. Its protein existence was unknown and two alternatively spliced transcripts were predicted (Genbank entries XP_002725730.1 and XP_574558.2; predicted molecular weights, 26 and 36 kDa). The shorter variant lacks the first 102 amino acids including the first transmembrane domain. We first created three polyclonal antibodies against different epitopes of the predicted GSG1L protein (Fig S1D). The first epitope Lp1 is only present in the product of longer spliced variant. When we purified native AMPA-Rs from rat brain and examined GSG1L by Western blot, all three antibodies detected a band at the molecular weight of 43 kDa, consistent with the long isoform (Fig 1D1 and D2).

These results establish that GSG1L is a protein expressed in rat brain and co-purifies with native AMPA-Rs.

GSG1L interacts specifically with AMPA-R subunits *in vitro*

To reconstitute the interaction in non-neuronal cells, we transfected HA-tagged GSG1L into stable HEK cell lines that express either GluA2 or GluK2, and immunoprecipitated (IPed) using an anti-HA antibody. GluA2 co-IPed with GSG1L whereas GluK2 did not (Fig 1E1 and E2). Under the same conditions the known KA-R auxiliary subunit Neto-2 specifically interacted with GluK2 but not GluA2. Conversely, the specific interaction of GSGIL with GluA2 and not GluK2 was also observed when the IP was done using antibodies against each glutamate receptor subunit (Fig S2A1 and 2). Furthermore, GSG1L and GluA2 partially co-localize near the plasma membrane when co-expressed in a stable HEK cell line using a DOX inducible expression system (Fig 1F). Similar results were obtained when the two proteins were co-expressed using transient transfection (Fig S2B). GluA1 also forms a complex with GSG1L, as determined by co-IP experiments (Fig 1G). These observations establish the physical interaction between GSG1L and AMPA-R subunits.

Functional interaction of GSG1L with AMPA-Rs

We next investigated functional interactions between GSG1L and AMPA-Rs. Transfection of GSG1L into a stable HEK cell line that expresses GluA2 increased surface expression of GluA2 compared to EGFP. In fact, GSG1L increased surface GluA2 as efficiently as stg (Fig 2A and B), indicating that surface expression of AMPA-Rs is positively modulated by GSG1L.

A functional interaction was also detected by a cell death assay (Sans et al., 2003; Shanks et al., 2010) (Fig S3). For this purpose, we created stable TetON HEK cell lines that DOX dependently express GluA2 and constitutively express GSG1L or stg (Fig S3A). Cell death was observed after GluA2 expression was induced by DOX in the cell line constitutively expressing stg or GSG1L. Cytotoxicity was blocked by AMPA-R antagonist NBQX and was not detected in the absence of stg or GSG1L (Fig S3C). Glutamate in the media thus triggered the cell death by activating AMPA-Rs whose function was enhanced by stg or GSG1L.

GSG1L profoundly slows AMPA-R recovery from the desensitized state

TARPs, which are distantly related to GSG1L (Fig 1B and C), alter AMPA-R gating kinetics (Tomita et al., 2005). Specifically, deactivation and desensitization rates are slowed by both Type I and II TARPs (with the

exception of γ-5; (Jackson and Nicoll, 2011) and recovery from desensitization is accelerated (Priel et al., 2005).

To examine its potential function, GSG1L was co-expressed with GluA2-Q (flip) in HEK293T cells. Channel kinetics were assessed by ultrafast agonist application to outside-out membrane patches. In response to a sustained L-glutamate pulse (10 mM for 100 ms), the GSG1L AMPA-R complex desensitized approximately 2-fold slower (data were fitted with two exponentials, weighted τ_{des} : 4.76 ± 0.16 ms, n = 27; versus 9.50 ± 0.21 ms, n = 10; $p < 0.0001$; t-test) (Fig 2C, D left). This difference is largely due to an increase in the relative amplitude of the slow component of the decay (A_{slow} = 10 ± 2 % and 47 ± 5 % without and with GSG1L, respectively) and, to a lesser extent, to an increase in the time constants of the individual components (τ_{fast} and τ_{slow} shift from 4.09 ± 0.13 ms and 11.58 ± 0.85 ms to 4.86 ± 0.40 ms and 15.18 ± 0.82, respectively). In addition, the 20-80% rise time of these responses was also slightly slower with GSG1L (0.23 ± 0.02 ms vs. 0.19 ± 0.01 ms; $p < 0.05$; t-test).

A more dramatic effect surfaced when analyzing recovery from desensitization via a two-pulse protocol. Whereas GluA2 recovered with a time constant of 18 ± 1 ms (n = 10), the presence of GSG1L slowed recovery by ~10-fold (τ_{rec} = 196 ± 28 ms, n = 6; $p < 0.005$, Mann-Whitney U test) (Fig 2D

right, E). Interestingly, despite their structural similarity (Fig 1C and S1D), this recovery phenotype is in fact opposite to what has been described for TARPs but parallels the effect of CKAMP44, a structurally unrelated Cys-knot protein (von Engelhardt et al., 2010). However, GSG1L and CKAMP44 have opposite effects on modulating desensitization. Therefore, GSG1L is an auxiliary factor which confers novel gating properties, further increasing the AMPA-R functional repertoire. Collectively, these data establish the existence of functional interaction between GSG1L and AMPA-Rs.

Localization of GSG1L in neurons

The *in situ* hybridization data in Allen Brain Atlas indicates GSG1L RNA signal in the hippocampus, striatum, and cortex (Lein et al., 2007). Consistently, GSG1L immunoreactivity was detected in CA3 pyramidal neurons, and partially co-localized with excitatory synaptic marker PSD-95 (Fig 3A). Despite our efforts none of the antibodies generated could detect endogenous GSG1L in dissociated cultured cortical nor hippocampal neurons. However, our antibodies could detect GSG1L when it was moderately overexpressed in cultured neurons. Taken together, we speculate that our antibodies do not have high enough affinity to detect the endogenous proteins in cultured neurons and/or the expression level of GSG1L in culture is lower than in brain tissue.

To gain insight into the distribution of GSG1L in neurons, we analyzed the subcellular localization of GSG1L transfected into cortical neurons. To detect GSG1L at the neuronal cell surface, we used a GSG1L construct with an HA epitope tag in the extracellular loop1 (see methods). Consistent with the physical and functional interactions described above, surface GSG1L co-localized with endogenous AMPA-R subunits GluA1 and 2 (Fig 3B and C). The punctate subcellular distribution of surface GSG1L also co-localized with the excitatory synaptic marker PSD-95 (Fig 3D). These results suggest that GSG1L exists at the excitatory synapses in neurons where AMPA-Rs are present.

Discussion

Interactome data identifies novel candidates forming the iGluR complex

By searching through the dataset for membrane proteins that specifically co-purify with AMPA-Rs and homologues of known interactors, we reduced the list of candidates significantly. After taking into account the s.c.'s and p.c.'s, we thought it likely that GSG1L is a primary AMPA-R interactor (Fig 1A). Validation of the interaction is the rate-limiting step, requiring multiple experimental approaches. Further investigations of other candidates from our data are expected to validate novel components of AMPA and KA-R complexes (see supplementary material for further discussions).

GSG1L is a new AMPA-R specific auxiliary subunit

The GSG1L gene is implicated to play roles in the nervous system. Its transcript level increases during synapse formation (Bruses, 2010; Lai et al., 2011), and decreases in Huntington's disease (Becanovic et al., 2010).

Both GSG1L and TARPs are members of the tetraspanin superfamily, with GSG1L belonging to the evolutionarily distant claudin family. The extracellular loop1 of GSG1L is least conserved (19% homology and 6.25%

identity) when compared with stg/TARPs and is substantially longer (~50%) (Fig 1C and S1D). Because this loop is essential for ion channel modulation by stg/TARPs (Menuz et al., 2008; Tomita et al., 2005), divergence in channel modulation may be due to mechanistic differences in how the loop interacts with AMPA-Rs. Indeed, whereas TARPs largely speed recovery from the desensitized state, GSG1L slows this parameter, mimicking the structurally unrelated Cys-knot protein CKAMP44 (von Engelhardt et al., 2010). Since desensitization and recovery from the desensitized state impact on high-frequency transmission (Arai and Lynch, 1998), synaptic AMPA-Rs associated with GSG1L are not expected to follow high-frequency trains with great fidelity. Further experiments are necessary to define the mechanisms of binding and functional modulation between GSG1L and TARPs with AMPA-Rs.

Despite that stg/TARPs increase surface expression of AMPA-Rs in HEK cells, there was no change in the amplitude of the AMPA-R mediated current in neurons overexpressing stg (Kessels et al., 2009). Increased surface expression of AMPA-Rs by GSG1L in HEK cells may not warrant that such modulation occurs in neurons. Further experiments are needed to investigate the differences and similarities between GSG1L and stg/TARPs in modulating synaptic physiology.

GSG1L is structurally related to stg/TARPs yet confers completely different function to AMPA-Rs; therefore investigating homologues of known interactors may reveal novel functional repertoire of AMPA-Rs. In fact, we identified many related proteins of known interactors (Table 1 and S1 (http://www.cell.com/cell-reports/fulltext/S2211-1247(12)00128-3#suppinfo)). For example, the LRRC and Shisa family of proteins are related to known AMPA-R interactors, LRRTM2 and CKAMP44 (de Wit et al., 2009; Pei and Grishin, 2012). Similarly, PRRT 1 (NG5 and synDIG4), and pancortin-3 (Olfm1) are shown to co-purify with AMPA-Rs (von Engelhardt et al., 2010). Our study extends the interactome by identifying homologues such as PRRT 2 and
Olfm-3.

Given the large number of auxiliary subunits identified for AMPA-Rs, questions regarding their distribution in brain and their stoichiometry remain to be addressed. Different auxiliary subunits simultaneously interact with a single tetramer of GluA subunits (Kato et al., 2010). AMPA-R complexes with different molecular composition may be used during spatio-temporal regulation in specific neurons and synapses. Exactly how this extensive diversity contributes to the activity of neural circuits and behavior remains unclear and is an important question that still needs to be solved.

Supplementary text

Candidates for future discovery

Many proteins that were previously reported to play roles in neurological and psychiatric disorders and synaptic plasticity were found in our interactome. For example, in Table S1 (http://www.cell.com/cell-reports/fulltext/S2211-1247(12)00128-3#suppinfo), IL1RAPL1 known as X-linked interleukin-1 receptor accessory protein-like 1 precursor was found together with its ligand RPTPdelta in the AMPA-R preparation (Yoshida et al., 2011).

Fewer interacting partners are known for KA-Rs compared to AMPA-Rs. Neto1-2, MAGUK scaffolds, and Kelch interact with and modulate KA-R function (Garcia et al., 1998; Marshall et al., 2011; Zhang et al., 2009). Consistently, these proteins were among the most abundant hits in our KA-R interctome (Fig 1A2, and Table 1). The actin based motor myosin XVIII (Foth et al., 2006) was also represented abundantly in the KA-R interactome. Given the localization of KA-Rs in sophisticated actin rich spine architectures in CA3 pyramidal cells, myosin XVIII may potentially be an important candidate. Interestingly, myosin XVIII has a PDZ domain next to the motor domain. The C-termini of KA-R subunits are known PDZ ligands and thus it will be

interesting to test if interactions exist between the PDZ domains of myosin XVIII and KA-Rs.

The secreted pentraxins are known interactors of AMPA-Rs (O'Brien et al., 1999; Sia et al., 2007). However, our results indicate that they are more abundantly found with KA-Rs, indicating the possibility of pentraxin function in modulating KA-R function. We also find significant peptide counts of neuronal secreted protein Olfm specifically found with AMPA-Rs.

4. References of the known and candidate interactors in Table1.

A. Known interactors

TARPs, CNIH, CKAMP44, Netos are reviewed in (Jackson and Nicoll, 2011)

PSD-95, PSD-93, SAP97, SAP-102, GRIPs are reviewed in (Kim and Sheng, 2004)

Protein 4.1 (Shen et al., 2000)

AP-2, NSF (Lee et al., 2002)

Kelch (Salinas et al., 2006)

B. Candidate interactors

MAGUK p55, CASK, Lin7 are major synaptic scaffold protein and is justifiable as potential indirect interactors (Kim and Sheng, 2004).

Liprin interacts with AMPA-R via GRIP (Wyszynski et al., 2002) and is an indirect interactor.

NGL-3 (LRRC4b) binds directly to PSD-95 (Woo et al., 2009). Because PSD-95 binds to stg/TARPs (Bats et al., 2007; Schnell et al., 2002), which binds directly to GluA2, NGL-3 is a candidate indirect interactor.

Leucine-rich transmembrane protein, LRRTM2 interacts with AMPA-Rs (de Wit et al., 2009) and is part of a large protein family. It is then plausible that members of the LRRTM family identified in our interactomes would be prime candidates for further experimental verification. Those include proteins listed as LRRC family in Table 1.

FLRT-2 and Latrophilin functionally interact with AMPA-Rs (O'Sullivan et al., 2012).

Neurexin (Nrxn) and neuroligin (Nlgn) form complex and interacts with PSD-95 (Irie et al., 1997), while PSD-95 interacts with stargazing/TARPs (Bats et al., 2007; Schnell et al., 2002).

Eph receptors and their ligands ephrins functionally intersect with AMPA-Rs in synapses (Ethell et al., 2001) and were detected with AMPA-Rs.

Myosin18 was the most abundantly found protein in the GluK2 interactome and thus was included in Table 1 as candidate.

DHHC5 interacts with GRIP (Thomas et al., 2012), which interacts with GluA2 (Dong et al., 1997), and thus considered as an indirect interactor.

RTRT family is related to LAR which binds to liprin (Dunah et al., 2005). LAR is also a receptor for NGL-3 (Woo et al., 2009), which is described above.

Shisa-6 belongs to the Shisa family (Pei and Grishin, 2012) that includes the well established AMPA-R binding partner CKAMP44 (von Engelhardt et al., 2010).

Pentraxins are described as AMPA-R binding proteins in the literature (O'Brien et al., 1999; Sia et al., 2007). Interestingly we find these proteins associating preferentially with kainite receptors.

SynDIG1 is a known interactor of AMPA-R and belongs to the PRRT family of proteins. PRRT 1 (NG5 and synDIG4), and pancortin-3 (Olfm1) are known to co-purify with AMPA-Rs in the supplementary figure of (von Engelhardt et al., 2010). Our study extends the interactome by identifying their homologues such as PRRT 2 and Olfm-3 (Table1).

Methods

Antibodies

Anti-GluA2CT antibody and ProteinA sepharose beads conjugated with this antibody were described previously (Nakagawa et al., 2005). Anti-GluK2CT antibody was affinity purified from rabbit serum obtained from rabbits that were immunized with the following peptide antigen, CVKTEEVINMHTFNDRRLPGKEMTA. CNBr-activated Sepharose beads (GE Healthcare) were conjugated with a GST fusion protein that contains the antigen sequence, and used for affinity purification column. Normal rabbit IgG was purchased from Pierce. The purified antibody was covalently conjugated with ProteinA Sepharose using DMP (Pierce).

The Lp1, Ct1, and Ct2, peptide antigens for anti-GSG1L antibodies were, RFHTGIWYSCEEELGGPGEKC, CRSSAHEAAELNRQCWVLGHWV, and CKVFEQGYREEPTFIDPEAIKYFR respectively, and were synthesized. Each antigen was conjugated to maleimide activated KLH via cysteine and used to immunize rabbits (Genscript). The antibodies were affinity purified using columns conjugated via CNBr, purified GST fusion proteins expressed in bacteria. The amino acid sequences of GSG1L fused to GST using pGEX4T-1 plasmid were GST-Lp1: TYWCQGTQRVPKPGCGQGGGANCPNSGANATANSTAAPVAASPAGAPYS

WEAGDERFQLRRFHTGIWYSCEEELGGPGEKCRSFIDLAPASEK, GST-Ct3: GDSWPRSSAHEAAELNRQCWVLGHWV , and GST-Ct8: TKTVIEFRHKRKVFEQGYREEPTFIDPEAIKYFRERIEKGDVSEEED, respectively. The antigens are underlined.

Purification of AMPA and KA-Rs from rat brain

Using Protein A Sepharose beads covalently conjugated with antibodies that specifically recognize GluA2 andGluK2, we purified native AMPA-R and KA-R complexes from CHAPS extracted brain membranes obtained from P15 rats that were anesthetized with isofluorane and decapitated. Protocols approved by IACUC of UCSD were followed. Beads conjugated with normal rabbit IgG were prepared similarly and used during purification as negative control. The adopted purification protocol was similar to what was used for purifying native AMPA-R complexes for EM studies (Nakagawa et al., 2005). Rat brains were homogenized in 20 mM HEPES, pH 7.4, 320 mM sucrose, 5 mM EDTA, 5 mM EGTA, 30 μM NBQX supplemented with protease inhibitors (1 mM PMSF, 10 μg/ml aprotinin, 10 μg/ml leupetin, 1 μg/ml pepstatin, and 500 μM benzamidine). Supernatant was obtained by centrifuging the homogenate at 3,000 g for 15 min was further spun at 38,400 g for 15 min to obtain a membrane pellet (P2 fraction). P2 was resuspended in SB1 (20 mM HEPES, pH 7.4, 1 M KI, 5 mM EDTA, 5 mM EGTA, and 30 μM NBQX) and membranes were collected by centrifugation. Membranes were further washed with WB

(20 mM HEPES, pH 7.4, 5 mM EDTA, 5 mM EGTA, 30 μM NBQX) to remove KI. Finally, membranes were solublized in RB (20 mM HEPES, pH 7.4, 100 mM NaCl, 5 mM EDTA, 5 mM EGTA, 1 % CHAPS, 30 μM NBQX, with protease inhibitors) for 3hr with gentle stirring at 4 ^{o}C and ultracentrifuged at 100,000 g to remove insoluble material. The final supernatant was applied to appropriate antibody affinity column (0.25 ml bed volume, antibody concentration 2 mg/ml). After washing the column with 3 ml of sample buffer, bound proteins were eluted with 100 mM glycine pH 2.5, 1% CHAPS and each eluted fractions were immediately mixed with 1/10 volume of 1M TrisHCl pH8.5. The affinity purified material was then precipitated with 15% *TCA* (*trichloroacetic acid*). The experiment was duplicated using smaller number of rat brains (at approximately 1/2 scale). The duplicate results are summarized in the Compare_all tab. For experiments shown in Figure 1D, the column elution was conducted using 20 mM HEPES, pH 7.4, 150 mM NaCl, 5 mM EDTA, 5 mM EGTA, 1% CHAPS, 30 μM NBQX, 0.5 μg/ml GluA2 C-terminal epitope peptide (GYNVYGIESVKI).

Purification of AMPA-R from human brain

Human brain (cortex) was obtained through the National Disease Research Interchange (NDRI), Researcher: Yates (code YAJ2), TSRI: IRB-11-5719. The antigen of the antibody against GluA2 is conserved in rat and human. GluA2

from human cortex was immunoaffinity purified using identical purification protocol used to purify rat GluA2.

Mass spectrometry

Sample Preparation: TCA precipitate was resuspended in 8M urea. Next the extracts were processed with ProteasMAX (Promega, Madison, WI, USA) per the manufacturer's instruction. The samples were subsequently reduced by 20 minute incubation with 5mM TCEP (*tris*(2 carboxyethyl)phosphine) at room temperature and alkylated in the dark by treatment with 10mM Iodoacetamide for 20 additional minutes. The proteins were digested over-night at 37 degrees with Sequencing Grade Modified Trypsin (Promega, Madison, WI, USA) and the reaction was stopped by acidification.

Multidimensional Protein Identification Technology (MudPIT) and LTQ and LTQ Orbitrap Mass Spectromtery: The protein digest was pressure-loaded onto a 250--µm i.d capillary packed with 2.5cm of 10-µm *Jupiter C18 resin* (Phenomenex, Torrance, CA, USA) followed by an additional 2.5cm of 5-µm Partisphere strong cation exchanger (Whatman, Clifton, NJ). The column was washed with buffer containing 95% water, 5% acetonitrile, and 0.1% formic acid. After washing, a 100--µm i.d capillary with a 5-µm pulled tip packed with 15 cm 4-µm *Jupiter C18 resin* (Phenomenex, Torrance, CA, USA) was attached to the filter union and the entire split-column (desalting column–filter

union–analytical column) was placed inline with an Agilent 1100 quaternary HPLC (Palo Alto, CA) and analyzed using a modified 5-step separation described previously (Washburn et al., 2001). The buffer solutions used were 5% acetonitrile/0.1% formic acid (buffer A), 80% acetonitrile/0.1% formic acid (buffer B), and 500 mM ammonium acetate/5% acetonitrile/0.1% formic acid (buffer C). Step 1 consisted of a 75 min gradient from 0-100% buffer B. Steps 2-5 had a similar profile except 3 min of 100% buffer A, 5 min of X% buffer C, a 10 min gradient from 0-15% buffer B, and a 105 min gradient from 10-55% buffer B (except for step 5 which %B was increased from 10% to 100%). The 5 min buffer C percentages (X) were 10, 40, 60, 100% respectively for the 5-step analysis. As peptides eluted from the microcapillary column, they were electrosprayed directly into an LTQ mass spectrometer (ThermoFinnigan, Palo Alto, CA).

For LTQ analysis (Rat GluA2, GluK2 and normal IgG): As peptides eluted from the microcapillary column, they were electrosprayed directly into an LTQ 2-dimensional ion trap mass spectrometer (ThermoFinnigan, Palo Alto, CA) with the application of a distal 2.4 kV spray voltage. A cycle of one full-scan mass spectrum (400-1400 m/z) followed by 7 data-dependent MS/MS spectra at a 35% normalized collision energy was repeated continuously throughout each step of the multidimensional separation. Application of mass spectrometer scan functions and HPLC solvent gradients were controlled by the Xcalibur

datasystem.

For LTQ velos Orbitrap analysis (Human GluA2): A seven step MudPIT was employed (10, 30, 50, 70, 90, 100% buffer C). A cycle of one full-scan mass spectrum (400-1800 m/z) at a resolution of 60,000 followed by 20 data dependent MS/MS spectra at a 35% normalized collision energy was repeated continuously throughout each step of the multidimensional separation. Maximum ion accumulation times were set to 500ms for survey MS scans and to 100ms for MS2 scans. Charge state rejection was set to omit singly charged ion species and ions for which a charge state could not be determined for MS/MS. Minimal signal for fragmentation was set to 1000. Dynamic exclusion was enabled with a repeat count:1, duration:20.00S, list size:300, exclusion duration 30.00S, exclusion mass with high/low: 1.5m/z. Application of mass spectrometer scan functions and HPLC solvent gradients were controlled by the Xcaliber data system.

Analysis of Tandem Mass Spectra

Protein identification and quantification analysis were done with Integrated Proteomics Pipeline (IP2, Integrated Proteomics Applications, Inc. San Diego, CA) using ProLuCID, DTASelect2 and Census. Tandem mass spectra were extracted into ms1 and ms2 files (McDonald et al., 2004) from raw files using RawExtract 1.9.9 (http://fields.scripps.edu/downloads.php) and were searched

against IPI rat protein database (For Rat searches:version 3.0, released on 06-28-2007; For Shisa, SynDIG1, and Neto1 identifications from Rat purifications: concatenated human-mouse-rat version 3.71, released_03-24-2010; For Human GluR searches version 3.57, released 01-01-2009)) plus sequences of known contaminants such as keratin and porcine trypsin concatenated to a decoy database in which the sequence for each entry in the original database was reversed (Peng et al., 2003) using ProLuCID/Sequest (Eng J, 1994). LTQ data was searched with 3000.0 milli-amu precursor tolerance, for LTQ velos Orbitrap data we used 50.0ppm tolerance for precursor ions and the fragment ions for both searches were restricted to a 600.0ppm tolerance.

All searches were parallelized (Sadygov et al., 2002) and performed on The Scripps Research Institute's garibaldi 64-bit LINUX cluster with 2848 cores. Search space included all fully- and half-tryptic peptide candidates with no missed cleavages restrictions. Carbamidomethylation (+57.02146) of cysteine was considered as a static modification, we require 2 peptides per protein and at least one trypitic terminus for each peptide identification. The ProLuCID search results were assembled and filtered using the DTASelect program (version 2.0) (Cociorva et al., 2007; Tabb et al., 2002) with false discovery rate (FDR) of 0.05, under such filtering conditions, the estimated false discovery rate was below 1% at the protein level in all analysis.

The RAW files and parameter files will be publically available at http://fields.scripps.edu/published/iGluR upon publication.

Plasmid DNA Construction

Rat GSG1L cDNA was synthesized (Genscript) based on genbank entry XP_574558.2. An HA tag in the N-terminus (ntHA) or C-terminus (ctHA) was introduced using PCR. These fragment were subcloned between EcoRI and SalI sites of pTREt vector (Clontech). To generate pBOSS-GSG1LctHA-IRES-mCherry, EcoRI-SalI fragment was first cloned into pIRES-mCherry vector (Clontech), then the EcoRI-NotI fragment containing GSG1L was subcloned into modified pBOSS vector (Shanks et al., 2010). pBOSS vector drives the expression of a gene of interest using an elongation factor promoter. For the surface labeling experiments, a GSG1L construct was created that has an HA tag in the extracellualr loop1 (AAPVAA*SPAGAPY, where HA tag was inserted at the asterisk). All DNA fragments created by PCR were sequence verified.

Co-immunoprecipitation of GSG1L-HA proteins with iGluRs in HEK cells

Co-immunoprecipitation of iGluRs with GSG1L (Figure 1D1 and 2). TetON HEK cells (Clontech) were used to create stable cell lines. TetON-GluA2flipFLAG#4 (a stable TetON HEK cell line that DOX dependently express GluA2flip-FLAG) and TetON-GluK2#16 cells (a stable HEK cell line

that DOX dependently express GluK2-FLAG) were transfected with pTREt-GSG1LctHA, pTREtB-HA-Neto2 or pTREtB-EGFP constructs using calcium phosphate methods and grown for 12 hours with 30μM NBQX and 1mM kynurenic acid. Protein expression was then induced with 7.5μg/ml DOX and 1mM Na-butyrate. After 24 hours cells were washed with cold D-PBS twice and resuspended in 900ul of buffer containing 50mM Na-HEPES, 85mM NaCl, 15mM KCl and protease inhibitors (1 mM PMSF, 10 μg/ml aprotinin, 10 μg/ml leupetin, 1 μg/ml pepstatin, and 500 μM benzamidine). Membranes were lysed with 0.25% DDM (Anatrace, SOL-grade) in the above buffer for 1.5 hours at 4 ^{o}C, ultracentrifuged at 35 krpm (Beckman, TLA-55) for 15 minutes at 4 ^{o}C. The supernatant was incubated with HA antibody (HA.11 Covance) for about 15 hours. 30 μl of protein A sepharose beads were incubated for 3 hours. After washing the beads 3 times in buffer, protein was eluted off the beads by boiling with SDS-PAGE loading buffer containing 100 mM DTT. Western blotting was done using anti-GluA2CT, anti-GluK2CT and anti-HA antibody (HA.11, Covance).

Co-immunoprecipitation of GSG1L with iGluR subunits (Figure 1E1 and 2).

TetON HEK cells were used instead of receptor stable cell lines. The following combinations were transfected: pTREt-GluA2flipFLAG/pTREt-GSG1LctHA, pTREt-GluA2flipFLAG/pTREtBa-EGFP, pTREt-GluK2/pTREt-GSG1LctHA, pTREt-GluK2/pTREtBa-EGFP and 2 plates of pTREtBa-EGFP/pTREt-

GSG1LctHA. Immunoprecipications were conducted as above except anti-GluA2CT or anti-GluK2CT were used as IP antibodies.

Co-immunoprecipitation of GSG1L with GluA1 subunit (Figure 1G). TetON HEK cells were used. The following plasmids were transfected: pTREt-GSG1LctHA, pTREt-Venus-HA, pTREt-GluA1-FLAG, and pTREt-GluA2flipFLAG. The FLAG tag is located at the very C-terminal of GluA1 and 2.

Surface labeling of GluA2 in HEK cells

TetON HEK cells (Clontech) were plated on poly-L-lysine coated glass coverslips. Two days later, cells were co-transfected with pTREt-GluA2flop-FLAG and one of pTREt-GSG1LctHA, pTREt-GSG1LntHA, pTREtBa-EGFP or pTREt-Stargazin and cultured in the presence of 1mM kynurenic acid and 30μM NBQX to block the cell toxicity. The next day, transgenes were induced by the application of 7.5μg/ml DOX and 1mM sodium butyrate. Sodium butyrate is used to relax the chromatin structure and enhance protein expression of the protein of interest from DOX inducible promoter. 24 hours later, surface GluA2 were live labeled using anti-GluA2-NTD antibody (1:100, Chemicon MAB397) for 15 min in 5%CO_2 incubator at 37^{o}C. After washing, cells were fixed with 4% formaldehyde in 0.1M phosphate buffer (pH7.4) for 7min. Goat anti-mouse IgG conjugated with Alexa568 (Invitrogen, Molecular

Probes) was used to visualize the labeled GluA2. Images of each condition were recorded using a CCD camera (Hamamatsu photonics, ORCA) mounted on an epifluorescent microscope (Olympus, 10x objective lens) using the identical settings throughout the experiment.

Generation of stable TetON HEK cell line that DOX dependently expresses GluA2 and constitutively expresses GSG1L

To generate the cell line, we took the same approach as previously described (Shanks et al., 2010), but we co-transfected pBOSS-GSG1LntHA-IRES mCherry with Zeocin resistance gene encoding plasmid (pCMVZeo, Invitrogen) into TetON-GluA2flipFLAG#4 cell line.

Generation of stable TetON HEK cell line that DOX dependently expresses GluA2 and GSG1L

GSG1LntHA and GluA2-FLAG were subcloned into dual expression plasmid modified from pTREt (Clontech) described previously (Farina et al., 2011). This plasmid was co-transfected with hygromycin resistance gene encoding plasmid into TetON HEK cell (Clontech).

Cell death assay using stable cell lines

Stable cell lines, TetON-GluA2flipFLAG#4, TetON-GluA2flipFLAG-pBOSS-stargazin-IRESmCherry#7, TetON-GluA2flipFLAG-pBOSS-GSG1LntHA-

IRESmCherry#25 were replated in the culture media without NBQX at sparse density in 3 wells. Two days after the plating, 2 wells were induced with 7.5 µg/ml DOX and 1mM Na butyrate, one of them was supplemented with 30µM NBQX and 1 well was left as control without drug (no-drug). Approximately 0, 24, 48 and 72 hours after the induction, DIC images of cells were taken.

Time course experiment

TetON-GluA2flipFLAG#4,TetON-GluA2flipFLAG-pBOSS-GSG1LntHA-IRESmCherry#25 cells were plated on 6 well plates at the density of 1.5x10^6 cells / well. The next day, 4 wells of cells were induced with 7.5µg/ml DOX and 1mM Na butyrate. 6, 12, 18 and 24 hours later, 1 well of each line was washed using 1ml PBS once, harvested in 1ml PBS, spin down at 4^{o}C, supernatant removed, and flash frozen in liquid N2. At 24 hours time point, non-induced cells were also harvested. Frozen pellets were resuspended in 400µl of PBS and 200ul of 4xDTT SDS-PAGE sample buffer was added. Samples were loaded on western blotting using GluA2CT and anti-HA antibody (Covance).

Neuron transfection and surface labeling

Embryonic day 18 cortical culture and surface labeling were conducted as previously described (Shanks et al., 2010, Sala et al., 2003) with slight modifications. Briefly, the cortex without the hippocampus was dissected and culture media was supplemented with 1.5%FCS. 16DIV cortical neurons were

transfected with pTREt-GSG1L-surface HA tag and pTetON-Advanced plasmids (at a 9:1 ratio) using calcium phosphate methods. At 18 DIV, cells were induced with 5μg/ml DOX for 24~48 hours. Cells were labeled using anti-HA monoclonal antibody (1:1000, Covance) or anti-HA polyclonal (1:50, Santa Cruz) followed by rabbit GluA2CT (1:200), anti-GluA1CT (1:50) (Nakagawa et al., 2005) or anti-PSD-95 monoclonal antibody (1:200, clone K28/43) with secondary antibodies: anti-rabbit IgG conjugated with Alexa488 or anti-mouse IgG conjugated with Alexa568 (1:200, Clontech). Images were recorded using CCD camera (Hamamatsu photonics, ORCA) mounted on a spinning disk confocal fluorescent microscope (Olympus, 60x objective lens).

Electrophysiology

Voltage clamp recordings were performed on outside-out patches from HEK293T cells as described previously (Rossmann et al., 2011). Briefly, cells were transfected with GluA2-Q (flip) and GSG1L plasmids (DNA ratio 1:2) or GluA2-Q (flip) alone. Current responses of outside-out patches (voltage-clamped at -60 mV) were elicited by fast application of 10 mM L-glutamate via a Θ-tube and recorded using Axopatch-1D amplifier, Digidata1322 interface and pClamp p.2 software (Molecular Devices). The rate of receptor desensitization was measured by fitting the current decay during a 100 ms application of L-glutamate with a double-exponential function. Recovery from desensitization was assessed using a two-pulse protocol where a 100 ms

agonist application is followed by a 10 ms application in increasing intervals. The relative peaks of the response to the second pulse were then plotted against time elapsed from the first pulse and fitted with a single-exponential function.

Immunohistochemistry

Six week old rat (male) was anesthetized and perfusion fixation was conducted using 4% paraformaldehyde in normal rat Ringer solution. Brain was dissected into small pieces containing the region of interest and further cryo-protected by immersing into a sequence of 0.1 M phosphate buffer pH 7.4 containing ascending concentration of sucrose (ranging from 4, 10, 15 and 20%). The tissues were quick frozen using liquid ethane and sectioned using cryostat (Leica CM1850). Sections (40 μm) were mounted on slide glass, blocked using 0.1M phosphate buffer pH 7.4, 4% BSA, and stained using the primary antibody (anti-GSG1L, Lp1 and anti-PSD95, clone K28/43) at 10μg/ml in 0.1M phosphate buffer pH 7.4, 0.2% TritonX-100, 0.2% BSA (at 4^{o}C, overnight). Preimmune serum was used such that the IgG concentration will be equivalent to the anti-GSG1L. Alexa488 and 568 conjugated anti-rabbit IgG (Invitrogen) was used as secondary antibody (for 1 hr at room temperature). Images were recorded using Olympus FV1000 confocal microscopy (objective lens 20x and 60x).

References

Arai, A., and Lynch, G. (1998). AMPA receptor desensitization modulates synaptic responses induced by repetitive afferent stimulation in hippocampal slices. Brain Res *799*, 235-242.

Becanovic, K., Pouladi, M.A., Lim, R.S., Kuhn, A., Pavlidis, P., Luthi-Carter, R., Hayden, M.R., and Leavitt, B.R. (2010). Transcriptional changes in Huntington disease identified using genome-wide expression profiling and cross-platform analysis. Hum Mol Genet *19*, 1438-1452.

Bruses, J.L. (2010). Identification of gene transcripts expressed by postsynaptic neurons during synapse formation encoding cell surface proteins with presumptive synaptogenic activity. Synapse *64*, 47-60.

Chen, L., Chetkovich, D.M., Petralia, R.S., Sweeney, N.T., Kawasaki, Y., Wenthold, R.J., Bredt, D.S., and Nicoll, R.A. (2000). Stargazin regulates synaptic targeting of AMPA receptors by two distinct mechanisms. Nature *408*, 936-943.

Collingridge, G.L., Olsen, R.W., Peters, J., and Spedding, M. (2009). A nomenclature for ligand-gated ion channels. Neuropharmacology *56*, 2-5.

de Wit, J., Sylwestrak, E., O'Sullivan, M.L., Otto, S., Tiglio, K., Savas, J.N., Yates, J.R., 3rd, Comoletti, D., Taylor, P., and Ghosh, A. (2009). LRRTM2 interacts with Neurexin1 and regulates excitatory synapse formation. Neuron *64*, 799-806.

Farina, A.N., Blain, K.Y., Maruo, T., Kwiatkowski, W., Choe, S., and Nakagawa, T. (2011). Separation of Domain Contacts Is Required for Heterotetrameric Assembly of Functional NMDA Receptors. J Neurosci *31*, 3565-3579.

Farrant, M., and Cull-Candy, S.G. (2010). Neuroscience. AMPA receptors--another twist? Science *327*, 1463-1465.

Jackson, A.C., and Nicoll, R.A. (2011). The expanding social network of ionotropic glutamate receptors: TARPs and other transmembrane auxiliary subunits. Neuron *70*, 178-199.

Kalashnikova, E., Lorca, R.A., Kaur, I., Barisone, G.A., Li, B., Ishimaru, T., Trimmer, J.S., Mohapatra, D.P., and Diaz, E. (2010). SynDIG1: an activity-

regulated, AMPA- receptor-interacting transmembrane protein that regulates excitatory synapse development. Neuron *65*, 80-93.

Kato, A.S., Gill, M.B., Ho, M.T., Yu, H., Tu, Y., Siuda, E.R., Wang, H., Qian, Y.W., Nisenbaum, E.S., Tomita, S., and Bredt, D.S. (2010). Hippocampal AMPA receptor gating controlled by both TARP and cornichon proteins. Neuron *68*, 1082-1096.

Kessels, H.W., Kopec, C.D., Klein, M.E., and Malinow, R. (2009). Roles of stargazin and phosphorylation in the control of AMPA receptor subcellular distribution. Nat Neurosci *12*, 888-896.

Kim, E., and Sheng, M. (2004). PDZ domain proteins of synapses. Nat Rev Neurosci *5*, 771-781.

Lai, H.C., Klisch, T.J., Roberts, R., Zoghbi, H.Y., and Johnson, J.E. (2011). In vivo neuronal subtype-specific targets of Atoh1 (Math1) in dorsal spinal cord. J Neurosci *31*, 10859-10871.

Lein, E.S., Hawrylycz, M.J., Ao, N., Ayres, M., Bensinger, A., Bernard, A., Boe, A.F., Boguski, M.S., Brockway, K.S., Byrnes, E.J.*, et al.* (2007). Genome-wide atlas of gene expression in the adult mouse brain. Nature *445*, 168-176.

Menuz, K., O'Brien, J.L., Karmizadegan, S., Bredt, D.S., and Nicoll, R.A. (2008). TARP redundancy is critical for maintaining AMPA receptor function. J Neurosci *28*, 8740-8746.

Nakagawa, T., Cheng, Y., Ramm, E., Sheng, M., and Walz, T. (2005). Structure and different conformational states of native AMPA receptor complexes. Nature *433*, 545-549.

Pei, J., and Grishin, N.V. (2012). Unexpected diversity in Shisa-like proteins suggests the importance of their roles as transmembrane adaptors. Cell Signal *24*, 758-769.

Priel, A., Kolleker, A., Ayalon, G., Gillor, M., Osten, P., and Stern-Bach, Y. (2005). Stargazin reduces desensitization and slows deactivation of the AMPA-type glutamate receptors. J Neurosci *25*, 2682-2686.
Rossmann, M., Sukumaran, M., Penn, A.C., Veprintsev, D.B., Babu, M.M., and Greger, I.H. (2011). Subunit-selective N-terminal domain associations organize the formation of AMPA receptor heteromers. Embo J *30*, 959-971.

Sans, N., Prybylowski, K., Petralia, R.S., Chang, K., Wang, Y.X., Racca, C., Vicini, S., and Wenthold, R.J. (2003). NMDA receptor trafficking through an

interaction between PDZ proteins and the exocyst complex. Nat Cell Biol *5*, 520-530.

Savas, J.N., Stein, B.D., Wu, C.C., and Yates, J.R., 3rd (2011). Mass spectrometry accelerates membrane protein analysis. Trends Biochem Sci *36*, 388-396.

Schwenk, J., Harmel, N., Zolles, G., Bildl, W., Kulik, A., Heimrich, B., Chisaka, O., Jonas, P., Schulte, U., Fakler, B., and Klocker, N. (2009). Functional proteomics identify cornichon proteins as auxiliary subunits of AMPA receptors. Science *323*, 1313-1319.

Shanks, N.F., Maruo, T., Farina, A.N., Ellisman, M.H., and Nakagawa, T. (2010). Contribution of the global subunit structure and stargazin on the maturation of AMPA receptors. J Neurosci *30*, 2728-2740.

Shepherd, J.D., and Huganir, R.L. (2007). The cell biology of synaptic plasticity: AMPA receptor trafficking. Annu Rev Cell Dev Biol *23*, 613-643.

Tanaka, H., Yoshimura, Y., Nishina, Y., Nozaki, M., Nojima, H., and Nishimune, Y. (1994). Isolation and characterization of cDNA clones specifically expressed in testicular germ cells. FEBS Lett *355*, 4-10.

Tomita, S., Adesnik, H., Sekiguchi, M., Zhang, W., Wada, K., Howe, J.R., Nicoll, R.A., and Bredt, D.S. (2005). Stargazin modulates AMPA receptor gating and trafficking by distinct domains. Nature *435*, 1052-1058.

Tomita, S., Chen, L., Kawasaki, Y., Petralia, R.S., Wenthold, R.J., Nicoll, R.A., and Bredt, D.S. (2003). Functional studies and distribution define a family of transmembrane AMPA receptor regulatory proteins. J Cell Biol *161*, 805-816.

Traynelis, S.F., Wollmuth, L.P., McBain, C.J., Menniti, F.S., Vance, K.M., Ogden, K.K., Hansen, K.B., Yuan, H., Myers, S.J., Dingledine, R., and Sibley, D. (2010). Glutamate receptor ion channels: structure, regulation, and function. Pharmacol Rev *62*, 405-496.

von Engelhardt, J., Mack, V., Sprengel, R., Kavenstock, N., Li, K.W., Stern-Bach, Y., Smit, A.B., Seeburg, P.H., and Monyer, H. (2010). CKAMP44: a brain-specific protein attenuating short-term synaptic plasticity in the dentate gyrus. Science *327*, 1518-1522.

Wang, R., Walker, C.S., Brockie, P.J., Francis, M.M., Mellem, J.E., Madsen, D.M., and Maricq, A.V. (2008). Evolutionary conserved role for TARPs in the gating of glutamate receptors and tuning of synaptic function. Neuron *59*, 997-1008.

Washburn, M.P., Wolters, D., and Yates, J.R., 3rd (2001). Large-scale analysis of the yeast proteome by multidimensional protein identification technology. Nat Biotechnol *19*, 242-247.

Zhang, W., St-Gelais, F., Grabner, C.P., Trinidad, J.C., Sumioka, A., Morimoto-Tomita, M., Kim, K.S., Straub, C., Burlingame, A.L., Howe, J.R., and Tomita, S. (2009). A transmembrane accessory subunit that modulates kainate-type glutamate receptors. Neuron *61*, 385-396.

Zheng, Y., Mellem, J.E., Brockie, P.J., Madsen, D.M., and Maricq, A.V. (2004). SOL-1 is a CUB-domain protein required for GLR-1 glutamate receptor function in C. elegans. Nature *427*, 451-457.

Supplemental References

Bats, C., Groc, L., and Choquet, D. (2007). The interaction between Stargazin and PSD-95 regulates AMPA receptor surface trafficking. Neuron *53*, 719-734.

Cociorva, D., D, L.T., and Yates, J.R. (2007). Validation of tandem mass spectrometry database search results using DTASelect. Curr Protoc Bioinformatics *Chapter 13*, Unit 13 14.

de Wit, J., Sylwestrak, E., O'Sullivan, M.L., Otto, S., Tiglio, K., Savas, J.N., Yates, J.R., 3rd, Comoletti, D., Taylor, P., and Ghosh, A. (2009). LRRTM2 interacts with Neurexin1 and regulates excitatory synapse formation. Neuron *64*, 799-806.

Dong, H., O'Brien, R.J., Fung, E.T., Lanahan, A.A., Worley, P.F., and Huganir, R.L. (1997). GRIP: a synaptic PDZ domain-containing protein that interacts with AMPA receptors. Nature *386*, 279-284.

Dunah, A.W., Hueske, E., Wyszynski, M., Hoogenraad, C.C., Jaworski, J., Pak, D.T., Simonetta, A., Liu, G., and Sheng, M. (2005). LAR receptor protein tyrosine phosphatases in the development and maintenance of excitatory synapses. Nat Neurosci *8*, 458-467.

Eng J, M.A., Yates JR., 3rd (1994). J Am Soc Mass Spectrom. J Am Soc Mass Spectrom *5*, 976-989.

Ethell, I.M., Irie, F., Kalo, M.S., Couchman, J.R., Pasquale, E.B., and Yamaguchi, Y. (2001). EphB/syndecan-2 signaling in dendritic spine morphogenesis. Neuron *31*, 1001-1013.

Farina, A.N., Blain, K.Y., Maruo, T., Kwiatkowski, W., Choe, S., and Nakagawa, T. (2011). Separation of Domain Contacts Is Required for Heterotetrameric Assembly of Functional NMDA Receptors. J Neurosci *31*, 3565-3579.

Foth, B.J., Goedecke, M.C., and Soldati, D. (2006). New insights into myosin evolution and classification. Proc Natl Acad Sci U S A *103*, 3681-3686.

Garcia, E.P., Mehta, S., Blair, L.A., Wells, D.G., Shang, J., Fukushima, T., Fallon, J.R., Garner, C.C., and Marshall, J. (1998). SAP90 binds and clusters kainate receptors causing incomplete desensitization. Neuron *21*, 727-739.

Irie, M., Hata, Y., Takeuchi, M., Ichtchenko, K., Toyoda, A., Hirao, K., Takai, Y., Rosahl, T.W., and Sudhof, T.C. (1997). Binding of neuroligins to PSD-95. Science *277*, 1511-1515.

Jackson, A.C., and Nicoll, R.A. (2011). The expanding social network of ionotropic glutamate receptors: TARPs and other transmembrane auxiliary subunits. Neuron *70*, 178-199.

Kim, E., and Sheng, M. (2004). PDZ domain proteins of synapses. Nat Rev Neurosci *5*, 771-781.

Lee, S.H., Liu, L., Wang, Y.T., and Sheng, M. (2002). Clathrin adaptor AP2 and NSF interact with overlapping sites of GluR2 and play distinct roles in AMPA receptor trafficking and hippocampal LTD. Neuron *36*, 661-674.

Marshall, J., Blair, L.A., and Singer, J.D. (2011). BTB-Kelch proteins and ubiquitination of kainate receptors. Adv Exp Med Biol *717*, 115-125.

McDonald, W.H., Tabb, D.L., Sadygov, R.G., MacCoss, M.J., Venable, J., Graumann, J., Johnson, J.R., Cociorva, D., and Yates, J.R., 3rd (2004). MS1, MS2, and SQT-three unified, compact, and easily parsed file formats for the storage of shotgun proteomic spectra and identifications. Rapid Commun Mass Spectrom *18*, 2162-2168.

Nakagawa, T., Cheng, Y., Ramm, E., Sheng, M., and Walz, T. (2005). Structure and different conformational states of native AMPA receptor complexes. Nature *433*, 545-549.

O'Brien, R.J., Xu, D., Petralia, R.S., Steward, O., Huganir, R.L., and Worley, P. (1999). Synaptic clustering of AMPA receptors by the extracellular immediate-early gene product Narp. Neuron *23*, 309-323.

O'Sullivan, M.L., de Wit, J., Savas, J.N., Comoletti, D., Otto-Hitt, S., Yates, J.R., 3rd, and Ghosh, A. (2012). FLRT Proteins Are Endogenous Latrophilin Ligands and Regulate Excitatory Synapse Development. Neuron *73*, 903-910.
Pei, J., and Grishin, N.V. (2012). Unexpected diversity in Shisa-like proteins suggests the importance of their roles as transmembrane adaptors. Cell Signal *24*, 758-769.

Peng, J., Elias, J.E., Thoreen, C.C., Licklider, L.J., and Gygi, S.P. (2003). Evaluation of multidimensional chromatography coupled with tandem mass spectrometry (LC/LC-MS/MS) for large-scale protein analysis: the yeast proteome. J Proteome Res *2*, 43-50.

Rossmann, M., Sukumaran, M., Penn, A.C., Veprintsev, D.B., Babu, M.M., and Greger, I.H. (2011). Subunit-selective N-terminal domain associations organize the formation of AMPA receptor heteromers. Embo J *30*, 959-971.

Sadygov, R.G., Eng, J., Durr, E., Saraf, A., McDonald, H., MacCoss, M.J., and Yates, J.R., 3rd (2002). Code developments to improve the efficiency of automated MS/MS spectra interpretation. J Proteome Res *1*, 211-215.

Salinas, G.D., Blair, L.A., Needleman, L.A., Gonzales, J.D., Chen, Y., Li, M., Singer, J.D., and Marshall, J. (2006). Actinfilin is a Cul3 substrate adaptor, linking GluR6 kainate receptor subunits to the ubiquitin-proteasome pathway. J Biol Chem *281*, 40164-40173.

Schnell, E., Sizemore, M., Karimzadegan, S., Chen, L., Bredt, D.S., and Nicoll, R.A. (2002). Direct interactions between PSD-95 and stargazin control synaptic AMPA receptor number. Proc Natl Acad Sci U S A *99*, 13902-13907.

Shanks, N.F., Maruo, T., Farina, A.N., Ellisman, M.H., and Nakagawa, T. (2010). Contribution of the global subunit structure and stargazin on the maturation of AMPA receptors. J Neurosci *30*, 2728-2740.

Shen, L., Liang, F., Walensky, L.D., and Huganir, R.L. (2000). Regulation of AMPA receptor GluR1 subunit surface expression by a 4. 1N-linked actin cytoskeletal association. J Neurosci *20*, 7932-7940.

Sia, G.M., Beique, J.C., Rumbaugh, G., Cho, R., Worley, P.F., and Huganir, R.L. (2007). Interaction of the N-terminal domain of the AMPA receptor GluR4 subunit with the neuronal pentraxin NP1 mediates GluR4 synaptic recruitment. Neuron *55*, 87-102.

Tabb, D.L., McDonald, W.H., and Yates, J.R., 3rd (2002). DTASelect and Contrast: tools for assembling and comparing protein identifications from shotgun proteomics. J Proteome Res *1*, 21-26.

Thomas, G.M., Hayashi, T., Chiu, S.L., Chen, C.M., and Huganir, R.L. (2012). Palmitoylation by DHHC5/8 targets GRIP1 to dendritic endosomes to regulate AMPA-R trafficking. Neuron *73*, 482-496.

von Engelhardt, J., Mack, V., Sprengel, R., Kavenstock, N., Li, K.W., Stern-Bach, Y., Smit, A.B., Seeburg, P.H., and Monyer, H. (2010). CKAMP44: a brain-specific protein attenuating short-term synaptic plasticity in the dentate gyrus. Science *327*, 1518-1522.

Washburn, M.P., Wolters, D., and Yates, J.R., 3rd (2001). Large-scale analysis of the yeast proteome by multidimensional protein identification technology. Nat Biotechnol *19*, 242-247.

Woo, J., Kwon, S.K., Choi, S., Kim, S., Lee, J.R., Dunah, A.W., Sheng, M., and Kim, E. (2009). Trans-synaptic adhesion between NGL-3 and LAR regulates the formation of excitatory synapses. Nat Neurosci *12*, 428-437.

Wyszynski, M., Kim, E., Dunah, A.W., Passafaro, M., Valtschanoff, J.G., Serra-Pages, C., Streuli, M., Weinberg, R.J., and Sheng, M. (2002).

Interaction between GRIP and Liprin-alpha/SYD2 Is Required for AMPA Receptor Targeting. Neuron *34*, 39-52.

Yoshida, T., Yasumura, M., Uemura, T., Lee, S.J., Ra, M., Taguchi, R., Iwakura, Y., and Mishina, M. (2011). IL-1 receptor accessory protein-like 1 associated with mental retardation and autism mediates synapse formation by trans-synaptic interaction with protein tyrosine phosphatase delta. J Neurosci *31*, 13485-13499.

Zhang, W., St-Gelais, F., Grabner, C.P., Trinidad, J.C., Sumioka, A., Morimoto-Tomita, M., Kim, K.S., Straub, C., Burlingame, A.L., Howe, J.R., and Tomita, S. (2009). A transmembrane accessory subunit that modulates kainate-type glutamate receptors. Neuron *61*, 385-396.

Tables

Table 3_1: Comparison of AMPA-R and KA-R Interactomes by Mass Spectrometry
Known primary interactors (this page) as well as candidate interactors (next page) are listed by common name and IPI number. The spectrum count (spec), peptide count (pep) and % coverage (%AA) identified by LC-MS/MS as well as the normalized (norm) abundance of the protein relative to the IPed target protein are listed for proteins in both the GluA2 (A2) and GluK2 (K2) preparations. The current annotated rat protein database does not provide complete representation of the proteins in the rat genome. Thus, to identify Shisa-6, 9, and Neto-1 (shown in italics) we searched against a concatenated database consisting of the human-mouse-rat protein databases. References of known and candidate interactors are provided in the supplementary material. Black dots represent proteins which were also found in a smaller scale duplication experiment.

known primary interactors

IPI	GluA2 spec,pep (%AA)	GluA2 norm	GluK2 spec,pep (%AA)	GluK2 norm	Common Name
IPI00780113.1	2526, 193 (71.3)●	1.0000	17, 11 (17.2) ●	0.0215	GluA2
IPI00324555.2	876, 129 (60.4)●	0.3468	6, 3 (5.1)	0.0076	GluA1
IPI00231095.1	873, 121 (56.5)●	0.3456	6, 4 (4.8)	0.0076	GluA3
IPI00195445.1	585, 91 (48.7)●	0.2316	3, 2 (2.4)	0.0038	GluA4
IPI00207460.1	212, 26 (34.0)●	0.0839	0, 0 (0.0)	0.0000	TARP gamma-3
IPI00201313.4	193, 28 (39.6)●	0.0764	0, 0 (0.0)	0.0000	TARP gamma-2
IPI00207426.1	162, 28 (36.8)●	0.0641	5, 2 (8.3)	0.0063	TARP gamma-8
IPI00207431.1	78, 13 (32.4)●	0.0309	0, 0 (0.0)	0.0000	TARP gamma-4
IPI00214444.1	11, 4 (23.30 ●	0.0044	0, 0 (0.0)	0.0000	TARP gamma-7
IPI00207430.1	3, 2 (6.9)	0.0012	0, 0 (0.0)	0.0000	TARP gamma-5
IPI00366152.2	18, 6 (13.1)●	0.0071	0, 0 (0.0)	0.0000	CNIH-2
IPI00358957.3	11, 4 (9.0)	0.0044	0, 0 (0.0)	0.0000	CNIH-3
IPI00956073.1	*147, 13 (26.2)*	*0.0582*	*0, 0 (0.0)*	*0.0000*	*Shisa-9/CKAMP-44*
IPI00566635.2	255, 61 (65.1)●	0.1010	28, 10 (16.0) ●	0.0354	PSD-95
IPI00777470.1	80, 31 (40.7) ●	0.0317	208, 62 (62.7) ●	0.2633	SAP-97
IPI00650099.1	53, 21 (27.9)●	0.0210	140, 48 (42.4) ●	0.1772	PSD-93
IPI00568474.1	28, 14 (19.6) ●	0.0111	27, 11 (10.0)	0.0342	SAP-102
IPI00208830.1	2, 2 (3.0)	0.0008	0, 0 (0.0)	0.0000	Grip1
IPI00409970.1	0, 0 (0.0)	0.0000	2, 2 (6.3)	0.0025	Grip2
IPI00204506.1	5, 5 (6.7)●	0.0020	42, 20 (22.8) ●	0.0532	protein4.1
IPI00210635.2	16, 13 (19.5)●	0.0063	32, 20 (36.0) ●	0.0405	NSF
IPI00471901.3	11, 6 (8.4)●	0.0044	10, 6 (10.2) ●	0.0127	AP-2 alpha2
IPI00389753.1	6, 6 (9.3)●	0.0024	10, 6 (7.6)	0.0127	AP-2 beta
IPI00203346.4	5, 4 (6.3)●	0.0020	8, 6 (10.1) ●	0.0101	AP-2 alpha1
IPI00196530.1	4, 3 (5.7)	0.0016	5, 4 (11.5) ●	0.0063	AP-2 mu
IPI00198371.1	2, 2 (14.1)	0.0008	4, 3 (24.6)	0.0051	AP-2 sigma
IPI00324708.1	0, 0 (0.0)	0.0000	790, 88 (47.8) ●	1.0000	GluK2
IPI00207006.1	0, 0 (0.0)	0.0000	190, 52 (48.0) ●	0.2405	GluK5
IPI00231400.2	0, 0 (0.0)	0.0000	187, 36 (29.1) ●	0.2367	GluK1
IPI00231277.4	2, 2 (2.2) ●	0.0008	686, 77 (45.4) ●	0.8684	GluK3
IPI00326553.1	0, 0 (0.0)	0.0000	105, 32 (34.5) ●	0.1329	GluK4
IPI00359373.3	0, 0 (0.0)	0.0000	125, 37 (59.7) ●	0.1582	Neto-2
IPI00367046.2	*0, 0 (0.0)*	*0.0000*	*37, 14 (38.3)*	*0.0468*	*Neto-1*
IPI00370061.1	0, 0 (0.0)	0.0000	19, 14 (22.8) ●	0.0241	Kelch

Table 1 (continued)

secondary, tertiary and candidate interactors

IPI	GluA2 spec,pep (%AA)	GluA2 norm	GluK2 spec,pep (%AA)	GluK2 norm	Common Name
IPI00763858.2	0, 0 (0.0)	0.0000	9, 5 (13.3) ●	0.0114	MAGUK p55
IPI00365736.3	14, 11 (12.0) ●	0.0055	5, 5 (6.1)	0.0063	Liprin alpha 3
IPI00392157.3	0, 0 (0.0)	0.0000	14, 13 (13.9) ●	0.0177	Liprin alpha 4
IPI00388795.3	11, 8 (12.6)	0.0044	94, 32 (36.6)	0.1190	CASK
IPI00214300.1	0, 0 (0.0)	0.0000	37, 12 (42.6)	0.0342	Lin 7
IPI00367477.1	56, 21 (29.8) ●	0.0222	0, 0 (0.0)	0.0000	NGL-3 (LRRC 4b)
IPI00207958.1	11, 7 (11.4) ●	0.0044	0, 0 (0.0)	0.0000	NGL-1 (LRRC 4c)
IPI00360822.3	4, 3 (5.1)	0.0016	0, 0 (0.0)	0.0000	LRRTM3
IPI00454354.1	3, 3 (4.3)	0.0012	8, 6 (5.3) ●	0.0101	LRRC 7
IPI00206020.1	3, 3 (19.2)	0.0012	5, 3 (11.1)	0.0063	LRRC 59
IPI00372074.1	2, 2 (4.0)	0.0008	0, 0 (0.0)	0.0000	LRRC 8
IPI00359172.2	0, 0 (0.0)	0.0000	3, 2 (5.9)	0.0038	LRRC 47
IPI00367715.3	2, 2 (3.9)	0.0008	0, 0 (0.0)	0.0000	FLRT-2
IPI00829463.1	10, 8 (7.8) ●	0.0040	10, 7 (6.5) ●	0.0127	Nrxn-1
IPI00195792.3	10, 7 (6.8) ●	0.0004	6, 6 (7.8) ●	0.0076	Nrxn-2
IPI00829491.1	5, 4 (6.1)	0.0020	4, 2 (2.7) ●	0.0051	Nrxn-3
IPI00325649.1	3, 2 (4.9)	0.0012	0, 0 (0.0)	0.0000	Nlgn-2
IPI00325804.1	0, 0 (0.0)	0.0000	5, 2 (3.3) ●	0.0063	Nlgn-3
IPI00764645.1	30, 15 (23.2) ●	0.0119	0, 0 (0.0)	0.0000	EphB2
IPI00189428.1	4, 3 (5.5)	0.0016	0, 0 (0.0)	0.0000	EphB1
IPI00569433.1	3, 3 (6.7) ●	0.0012	0, 0 (0.0)	0.0000	EphA4
IPI00230960.1	2, 2 (4.8) ●	0.0008	0, 0 (0.0)	0.0000	EphA5
IPI00365395.2	2, 2 (13.4)	0.0008	0, 0 (0.0)	0.0000	EphrinB2
IPI00411236.1	10, 7 (8.1) ●	0.0040	13, 8 (9.3) ●	0.0165	Latrophilin 1
IPI00561212.4	9, 8 (9.2) ●	0.0036	0, 0 (0.0)	0.0000	Latrophilin 3
IPI00568123.2	4, 3 (4.3)	0.0016	0, 0 (0.0)	0.0000	Latrophilin 2
IPI00568245.2	0, 0 (0.0)	0.0000	480, 136 ●	0.6076	myosin 18
IPI00193933.3	3, 3 (6.0)	0.0012	0, 0 (0.0)	0.0000	DHHC5
IPI00357941.4	7, 7 (5.8)	0.0028	0, 0 (0.0)	0.0000	RPTP delta
IPI00231945.4	3, 2 (3.3)	0.0012	0, 0 (0.0)	0.0000	RPTP
IPI00565098.2	30, 13 (25.8) ●	0.0119	0, 0 (0.0)	0.0000	GSG1L
IPI00939232.1	*2, 2 (5.1)*	*0.0008*	*0, 0 (0.0)*	*0.0000*	*Shisa-6*
IPI00214724.3	4,20 (12.1) ●	0.0016	0, 0 (0.0)	0.0000	PPRT 1
IPI00366048.3	38, 10 (38.1)	0.0150	0, 0 (0.0)	0.0000	PPRT 2
IPI00207495.3	0, 0 (0.0)	0.0000	32, 13 (24.5) ●	0.0405	pentraxin-2 (Narp)
IPI00192125.1	0, 0 (0.0)	0.0000	58, 19 (29.9) ●	0.0734	pentraxin-1
IPI00212317.1	0, 0 (0.0)	0.0000	69, 16 (36.6) ●	0.0873	pentraxin receptor
IPI00206558.4	19, 9 (15.1) ●	0.0075	0, 0 (0.0)	0.0000	Olfm-1
IPI00337161.1	5, 3 (8.7)	0.0020	0, 0 (0.0)	0.0000	Olfm-3

Figures

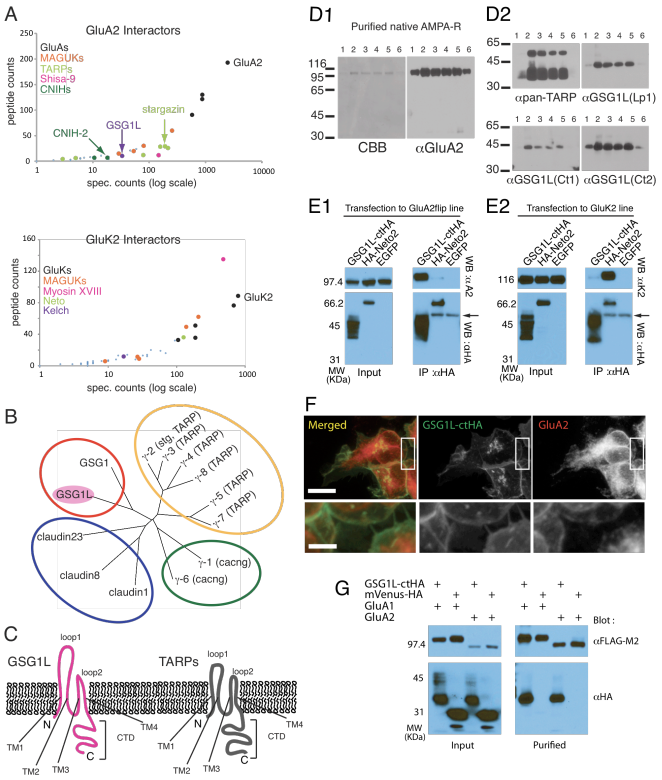

Figure 3_1. Comparative interactomes of native AMPA-R and KA-R identify GSG1L as AMPA-R interacting protein.

A. Graphical representation of proteins identified as interacting with GluA2 (top) and GluK2 (bottom). Each dot represents a protein identified by mass spec. The y-axis is the number of peptides (log scale), the x-axis is the number of spectra in which the identified proteins were found. Black dots are the bait protein receptor subunits. Other known interactor protein families are different color dots (see legend). Larger dots indicate known interactors, smaller dots indicate potential candidates. Note the location of GSG1L between data points for stg and CNIH-2. (B) Phylogenic tree of representative proteins in claudin family constructed using neighbor-joining algorithm in CLUSTALW. The red, yellow, green, and blue circles represent families of GSG, stg/TARPs, gamma subunit of calcium channels, and conventional claudins. (C) Topology of GSG1L (magenta) and TARPs (gray) relative to the membrane. TM1-4 = transmembrane domain 1-4, loop1-2 = extracellular loop 1-2, CTD = C-terminal domain. (D1) Left: CBB staining of purified native AMPA-Rs. Fractions 1-6 are consecutive elutions from the antibody column using antigen peptide. Right: Western blots of same fractions probed with anti-GluA2CT (A2). Molecular weight markers are on left (kDa). (D2) Duplicate membranes resolving fractions in D1 probed with anti-pan-TARP and anti-GSG1L (three different antibodies). (E1) Western blots of the input and IP. Stable HEK cell line expressing GluA2flip was transfected with indicated plasmid. Cellular lysates were IPed using anti-HA antibody. The arrow indicates the IgG derived from the antibody used for IP. (E2) Similar to E1 but using stable HEK cell line expressing GluK2. (F) Confocal images of HEK cells cotransfected with GSG1LctHA and GluA2. Scale bar = 10μm (upper) and 2.5 μm (lower). (G) HEK cells were transfected with plasmids expressing the proteins indicated at the top of each lane. FLAG tagged GluA1 and 2 subunits were affinity purified using FLAG beads. mVenus variant of EYFP was used as a negative control.

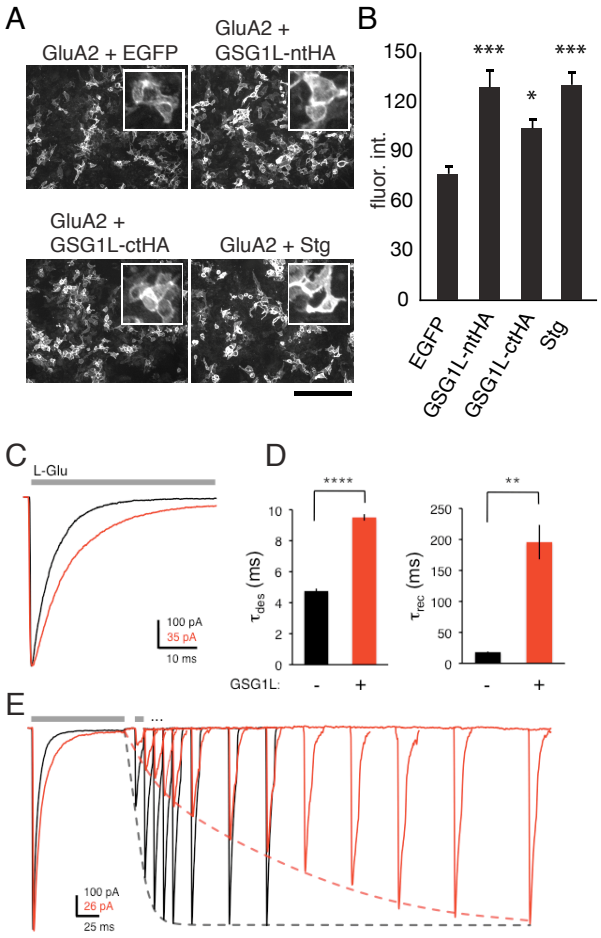

Figure 3_2. Functional modulation of AMPA-R by GSG1L
(A) Cell surface staining of GluA2 in HEK cells co-transfected with plasmids expressing the proteins indicated above each image. Scale bar = 200µm. Insets are representative enlarged views. (B) Histogram summarizing quantification obtained from C. *** and * indicate, respectively, $p < 0.0003$ and $p < 0.0166$ against control experiments using EGFP according to Bonferroni's corrected student t-test. The vertical axis represents arbitrary units of fluorescence intensity. (C) Example current responses of outside-out patches from HEK293T cells expressing GluA2 without (black) or with (red) GSG1L to a 100 ms application of 10 mM L-Glu (holding potential -60 mV). Data were fitted with two exponentials. The weighted τ_{des} of the traces presented here is 5.55 ms and 10.70 ms in the absence and presence of GSG1L, respectively. (D) Summary histogram for the time constants of desensitization (left) and recovery from desensitization (right). Data are presented as mean ± SEM. ****$p < 0.0001$ (t-test); **$p < 0.005$ (Mann-Whitney U test) (E) Representative current traces of outside-out patches from HEK293T cells expressing GluA2 demonstrating recovery from desensitization in the presence (red) or absence (black) of GSG1L. The paired-pulse protocol consisted of a 100 ms pulse of 10 mM L-Glu followed by a 10 ms pulse in an interval increasing by 10 ms (only selected sweeps are shown). Traces are peak-scaled to the amplitude of the first pulse. Dashed lines indicate the single-exponential fits of the recovery (τ_{rec} = 15 ms and 140 ms for GluA2-Q(flip) without and with GSG1L, respectively; summarized in D).

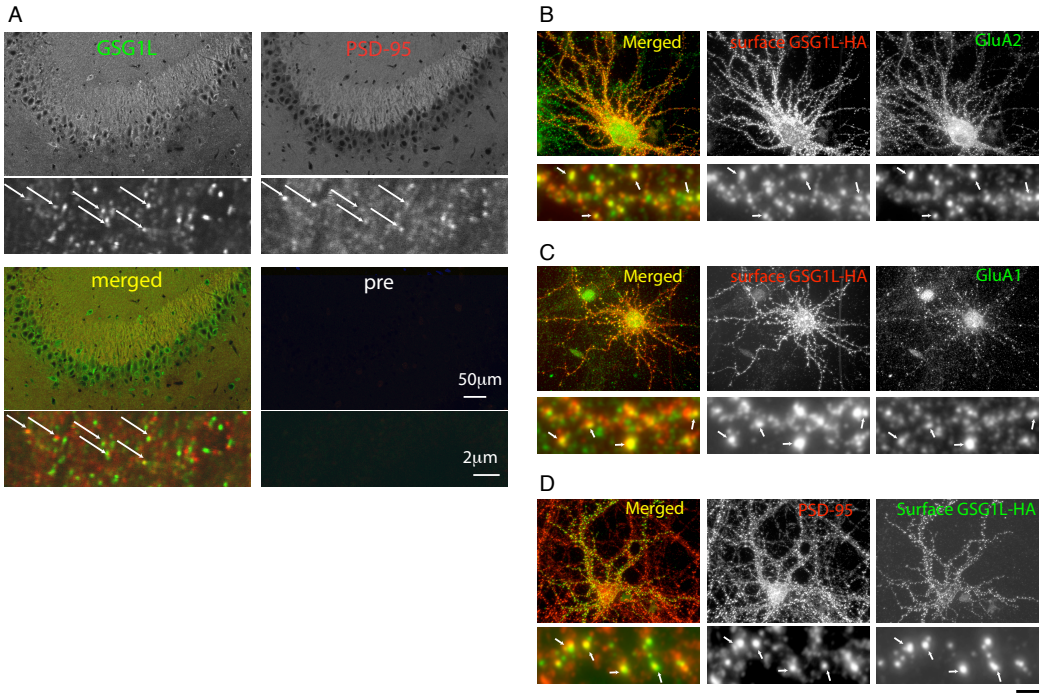

Figure 3_3. Localization of GSG1L in neurons
(A) Confocal images of sections of rat hippocampus stained with anti-GSG1L antibody Lp1 and preimmune serum control (pre). Sections were double stained with PSD-95, Scale bar = 50 μm (upper) and 2 μm (lower). Arrows indicate co-localizing puncta. (B) Confocal images of dissociated cortical neurons overexpressing HA tagged GSG1L. The HA tag is in the extracellular loop enabling surface labeling. GSG1L expressed at the cell surface (red) and colocalizes with GluA2 (green). Upper panels; low magnification. Lower panels; enlarged view of the dendrite. The single scale bar corresponds to 20 μm for the upper and 2 μm for the lower panels. Arrows indicate co-localizing puncta. (C) A similar experiment as B was conducted using anti-GluA1 antibody. GSG1L (red) expressed at the cell surface co-localizes with GluA1 (green). (D) A similar experiment as B was conducted using anti-PSD-95 antibody. GSG1L (green) expressed at the cell surface partially co-localizes with PSD-95 (red).

Supplemental Figures

A

Accession	Spec. Count	Pep. Count	% AA	Description
IPI00030882	1262	110	63.3	GRIA2 Isoform Flop of Glutamate receptor 2
IPI00152159	3	3	11.2	GSG1L Isoform 1 of Germ cell-specific gene 1-like protein
IPI00892819	3	3	13.9	GSG1L Isoform 2 of Germ cell-specific gene 1-like protein

B

Sequence	Spec. Count	Confidence (%)	Scan	Charge	Xcorr	DeltCN	ppm
R.NFHTGIWYSCEEELSGLGEK.C	1	100	13673	2	5.5248	0.5601	-2
R.NFHTGIWYSCEEELSGLGEK.C	1	100	13683	3	5.1518	0.4791	-0.4
K.VFEQGYREEPTFIDPEAIK.Y	1	98.6	9509	3	2.3175	0.2096	1.2

C

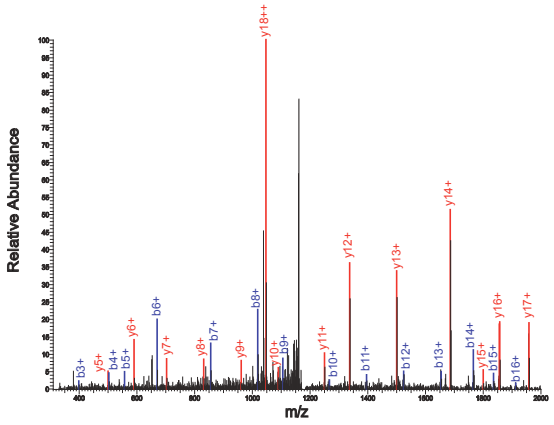

D

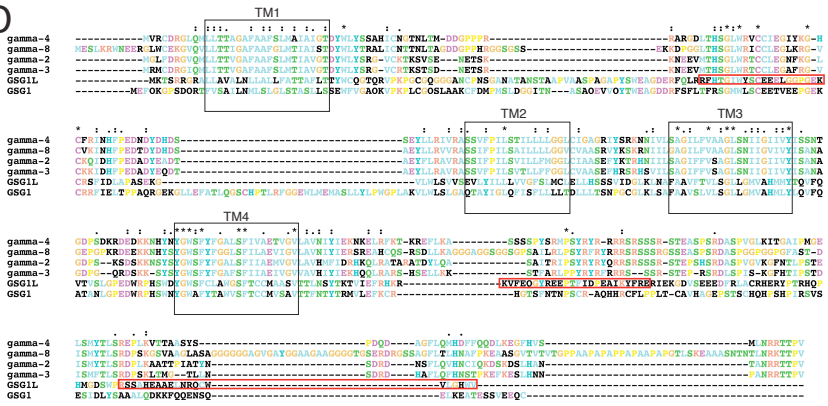

Figure 3_S1. Claudin homologue GSG1L is a candidate auxiliary subunit of human AMPA-Rs

(A) LC-MS/MS analysis identified GSG1L protein from human GluA2 purification. Shown are protein identification summaries for GluA2 and GSG1. Note, two human GSG1L isoforms were identified by the same peptides thus either isoforms, or both could be present. **(**B) Detailed peptide statistics for GSG1L protein identification. Three fully tryptic peptides were identified with confident Xcorr, DeltaCN, and precursor ppm scores as indicated. **(**C) MS/MS spectrum for the human GSG1L peptide R.NFHTGIWYSCEEELSGLGEK.C (+2 charge). **(**D) Multiple sequence alignment of rat GSG1L, GSG1, and TARPs (gamma-2, 3, 4, and 8) by CLUSTALW. The predicted location of the transmembrane domains are boxed and indicated as TM1-4. The antigen peptides used to generate anti-GSG1L antibodies are indicated by red boxes. Residues with similar chemical properties are color-coded.

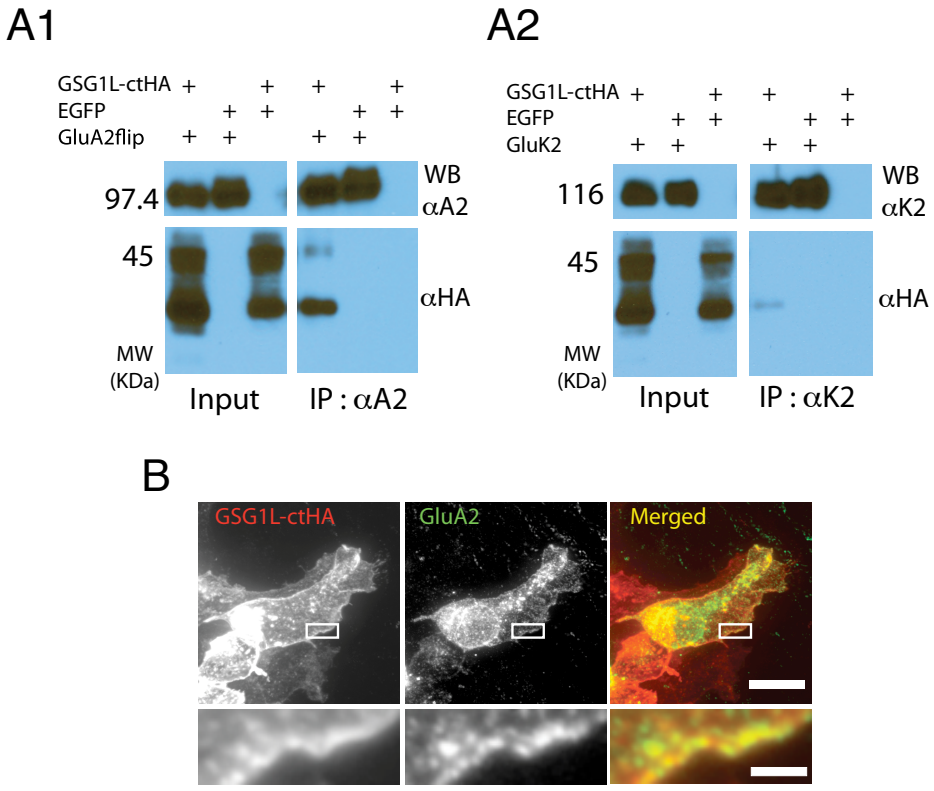

Figure 3_S2. GSG1L interacts with AMPA-R subunits
(A1) HEK cells were transfected with plasmids that express the proteins indicated at the top of each lane. Immunoprecipitation was conducted using anti-GluA2CT (A2) antibody. Western blots of the input and IP are shown. Membranes were probed with antibodies indicated in the right. EGFP was used as negative control. (A2) same as in A1, but IP was conducted using anti-GluK2CT antibody. Molecular weight markers in this figure are indicated on the left (kDa). (B) Colocalization of GSG1L and GluA2 in HEK cells. Confocal images HEK cells transiently cotransfected with plasmids driving the expression of GSG1L (ctHA indicates an HA tag at the C-terminal) and GluA2. Scale bar = 10μm (upper panels) and 0.5 μm (lower panels). The two proteins co-localize at the cell surface. The strong perinuclear staining of GSG1L is observed when transient transfection of plasmids is used but is absent when expressed moderately using DOX inducible expression system in combination with stable cell lines (Data shown in the main Figure 2C).

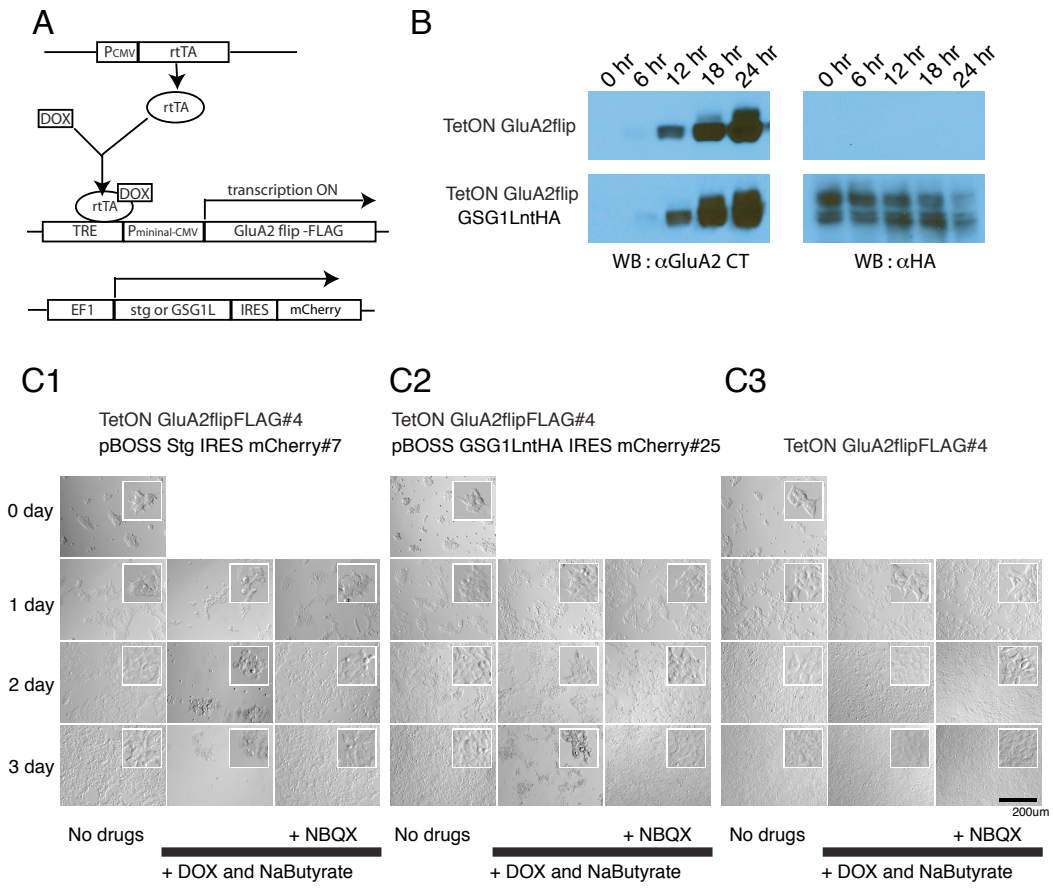

Figure 3_S3. Functional modulation of AMPA-R by GSG1L
(A) Cartoon depicting the DOX inducible expression of GluA2 and constitutive expression of stargazin (stg) or GSG1L. Specifically, these cells constitutively express (stg or GSG1L)-IRES-mCherry module under the control of constitutive elongation factor promoter, and a reverse Tet transcriptional element (rTet). The latter enhances transcription of the GluA2*flip*-FLAG transgene from the minimal CMV promoter when the drug doxycycline (DOX) is present in the cell media. Na butyrate was also added together with DOX to enhance protein induction. (B) Western blot showing the time course of GluA2 expression after DOX induction in the indicated stable cell lines. Top: TetON GluA2flipFLAG#4 cell line that DOX dependently express GluA2. Bottom: TetON GluA2flipFLAG pBOSS-GSG1LntHA#25 cell line that DOX dependently express GluA2 and constitutively express HA tagged GSG1L. Membranes were probed with antibodies indicated at the bottom. We also observed that GSG1L accelerates glycosylation of GluA2 (Fig S3B). This effect was not observed in the case of stargazin (Shanks et al., 2010) and is specific to GSG1L. (C) Trajectory of the cytotoxicity after inducing GluA2 expression is shown by the DIC images of the cells taken on different days in pBOSS-stg-IRIS-mCherry#7 (C1), TetON GluA2flipFLAG pBOSS-GSG1LntHA#25 (C2), and TetON GluA2flipFLAG (C3) cell lines. The cells on the left column were untreated (No drugs), whereas the other columns were treated with DOX+Na butyrate with (+NBQX) or without 30 μM NBQX. Scale bar = 200 μm. Insets are representative enlarged views. The time course of cell death however was slower when GSG1L was present instead of stargazin (complete cell death in 2 days for stargazin vs. 3 days for GSG1L), indicating possible differences between stargazin and GSG1L in modulating AMPA-R function.

Acknowledgments

Chapter III, in full, is a reproduction of the material as it appears in Cell Reports 2012. Shanks, Natalie F.; Savas, Jeffrey N.; Maruo, Tomohiko; Cais, Ondrej; Hirao, Atsushi; Oe, Souichi; Ghosh, Anirvan; Noda, Yasuko; Greger, Ingo H.; Yates. John R. III; Nakagawa, Terunaga, Elsevier 2012. The dissertation author was among the primary investigators and authors of the manuscript. Permission has been obtained from all authors.

The content of Supplemetal Table 1 is too large to fit in this dissertation and can be found, and downloaded in full at the following url:

http://www.cell.com/cell-reports/fulltext/S2211-1247(12)00128-3#suppinfo

Chapter IV

Membrane distal N-terminal domain of AMPA-R functions in the gating modulation by cornichon

Abstract

Cornichon homologues (CNIHs) modulate AMPA receptor (AMPA-R) function. Molecular mechanisms of modulation are unclear and investigated in this study. CNIH-3 forms a stable complex with tetrameric AMPA-Rs and contributes to the transmembrane density in the single particle EM structure. Peptide array based screening and *in vitro* mutagenesis identified two clusters of membrane proximal residues conserved among all CNIHs contributing to AMPA-R binding. Because CNIH-1 binds to AMPA-R but does not modulate gating, these residues support physical binding between AMPA-R and CNIHs. Residues in the extracellular loop of CNIH-3 absent in CNIH-1/4 are critical for both AMPA-R interaction and gating modulation. Both the membrane distal N-terminal domain (NTD) along with the ligand binding domain (LBD) of AMPA-R interact with CNIH-3. A role for the NTD as an allosteric modulator is established for NMDA receptors but unclear for AMPA-Rs. Our results support a new model in which the NTD participates in modulating AMPA-R gating through binding to the extracellular loop of CNIH-3.

Introduction

Excitatory synaptic transmission mediated by the AMPA receptor (AMPA-R) type of ligand gated ion channels is subject to modulation by a variety of structurally unrelated transmembrane proteins, such as stargazin/TARPs, cornichon homologues (CNIHs), GSG1L, CKAMP44, and synDIG1. (Chen et al., 2000; Hashimoto et al., 1999; Jackson and Nicoll, 2011; Kalashnikova et al., 2010; Nicoll et al., 2006; Schwenk et al., 2009; von Engelhardt et al., 2010). The molecular variety of AMPA-R complexes continues to grow (Kang et al., 2012; Schwenk et al., 2012; Shanks et al., 2012). However, the biochemical properties and mechanisms underlying functional modulation of AMPA-Rs are largely uncharacterized for these individual complexes.

Various neurological phenotypes and abnormal synaptic plasticity are observed in the absence of stargazin/TARPs (Jackson and Nicoll, 2011) and CKAMP44 (von Engelhardt et al., 2010), indicating that endogenous factors modulating AMPA-Rs have significant impact on normal brain function. Exogenously introduced small molecules and recombinant proteins can potentially adopt similar molecular strategies as these endogenous factors in modulating

AMPA-Rs. Precise understanding of this process may therefore contribute to developing therapeutic modulator reagents for neurological and psychiatric disorders affected by AMPA-R dysfunction.

Several unrelated types of membrane proteins interact with and modulate AMPA-R gating, yet the stability of the complex has only established for the stargazin/TARP family, distinguishing stargazin/TARPs as proper AMPA-R auxiliary subunits (Jackson and Nicoll, 2011; Nakagawa et al., 2005; Vandenberghe et al., 2005). In this study we combined single particle EM, a biochemical binding assay, in vitro mutagenesis, and electrophysiology to investigate the stability of CNIH/ AMPA-R complex and probe the molecular mechanisms of gating modulation.

Importantly, among the complex molecular associations between the two proteins, we identify interactions between both of the AMPA-R extracellular domains: the membrane distal N-terminal domain (NTD) as well as the ligand binding domain (LBD) of the GluA2 subunit and the extracellular loop of CNIH-3. The function of the LBD in modulating AMPA-R channel function is well characterized, yet a similar role for the AMPA-R NTD has only been speculated about, and is under debate (Dutta et al., 2012; Matsuda et al., 2005; Sukumaran et al., 2011). The NTD has established roles as an allosteric gating modulator for NMDA-Rs (Choi and Lipton, 1999; Hatton and

Paoletti, 2005; Perin-Dureau et al., 2002) and a protein interaction module supporting synapse maturation for GluD2 (Matsuda et al., 2010), however a similar type of function for the NTD of AMPA-Rs was unknown. Our results support a new unexpected hypothesis in which the CNIH-NTD as well as CNIH-LBD interaction contributes to gating modulation of AMPA-Rs.

Results

Specificity of interaction between cornichons and AMPA-Rs

The CNIH family consists of four family members (CNIH-1, 2, 3, and 4) sharing 56% homology and 23% identity, yet only CNIH-2 and 3 interact with AMPA-Rs in rat brain (Schwenk et al., 2009; Shanks et al., 2012). The basic topology of all the CNIH homologues is preserved, however CNIH-2 and 3 contain unique sequences within the extracellular loop that are absent in CNIH-1 and 4 (Fig 1A). Interestingly, when overexpressed in HEK cells, rat AMPA-R subunit GluA2 co-immunoprecipitates with rat CNIH-1, 2, and 3 (Fig1B). Consistently, using mass spectrometry we found that all homologues, CNIH-1, 2, 3, and 4 co-purify with GluA2 from human brain (Fig 1D,E). This is the first evidence suggesting the possible involvement of CNIH-1 and 4 in AMPA-R function in humans. Furthermore, small amounts of HEK cell derived human CNIH-1, 3, and 4 co-purify with rat GluA2 (Fig S1B). Collectively, our results highlight species-differences in molecular composition of endogenous AMPA-R/CNIH complexes. Human and rat CNIH-1 are 99% identical, and thus interaction between rat CNIH-1 and GluA2 would share its mechanism with human homologues. In the following experiments rat clones of CNIHs, GluA2, and kainite receptor (KA-R) subunit GluK2 are used.

CNIHs interact specifically with AMPA-Rs and not with KA-Rs (Shanks et al., 2012) (Fig S1A). This specificity of interaction is reproducible in HEK cells. When we immunoprecipitated CNIH-3 from detergent extracted membranes of HEK cells co-expressing CNIH-3 and either GluA2 or GluK2, a significant amount of GluA2 co-precipitated with CNIH-3, whereas GluK2 did not (Fig1A). This result suggests that CNIH-3 recognizes the difference in amino acid sequences between AMPA and kainate receptor subunits.

CNIH-3 has minor contributions during AMPA-R biogenesis

CNIHs were suggested to play roles in AMPA-R forward trafficking, possibly by functioning as a molecular chaperone (Schwenk et al., 2009; Shi et al., 2010). It is unclear, however, if CNIHs have chaperone function assisting AMPA-R biogenesis. To address this, we created stable HEK cell lines in which all cells constitutively express HA tagged CNIH-3 and DOX dependently express GluA2 (Fig S1C). Several cell lines were established that express varying levels of CNIH-3. We then compared the time course of GluA2 expression after DOX-induction in the presence of varying levels of CNIH-3. This approach was previously utilized to study the role of the auxiliary subunit stargazin (Shanks et al., 2010). The 24 hr time course of GluA2 expression was indistinguishable in all of the cell lines, indicating that CNIH-3 does not alter expression level or the rate of synthesis of GluA2 (FigS1D and

E). The band pattern of GluA2 however looks different between CNIH-3 expressing and CNIH-3 lacking cell lines. This observation is consistent with data (Shi et al., 2010) in which they demonstrate that co-expression of CNIH-2 with AMPA-Rs in HEK cells increases the amount of mature glycosylated receptor. These data point out a role for CNIH-3 in glycosylation but not for synthesis of AMPA-Rs.

Functional interaction between CNIH-3 and GluA2 in HEK cells

CNIH-2 and 3 but not CNIH-1 are known to functionally interact with AMPA-R by slowing AMPA-R deactivation and desensitization kinetics (Coombs et al., 2012; Kato et al., 2010; Schwenk et al., 2009; Shi et al., 2010). Consistently, we see a functional interaction between GluA2 and CNIH-3 but not CNIH-1. The expression of GluA2 in the presence of the AMPA-R auxiliary subunit, stargazin in HEK cells results in cytotoxicity that can be prevented by the AMPA-R antagonist NBQX. Because both stargazin and CNIHs enhance surface trafficking of AMPA-Rs and modulate channel gating (Kato et al., 2010; Schwenk et al., 2009; Shi et al., 2010), we examined if co-expression of CNIHs and GluA2 has similar cytotoxicity in HEK cells. In fact, the addition of either CNIH-3 or stargazin, but not CNIH-1 in the DOX-inducible GluA2 expressing HEK cells significantly increased the amount of cell death that occurred 30 hours after DOX-induction (Fig S1F). The cell death was blocked

by the competitive AMPA-R antagonist NBQX. We interpret that the cell death is caused by the enhanced GluA2 ion channel activation by the glutamate present in the cell media. Despite both CNIH homologues CNIH-1 and 3 can physically interact with AMPA-Rs *in vitro* (Fig 1C), only CNIH-3 but not CNIH-1 functionally interacts with AMPA-Rs in our cell death assay. This suggests that binding of CNIH to AMPA-Rs is mechanistically dissociable from AMPA-R channel modulation.

Cornichon-GluA2 purifies as stable complex

GluA2 and CNIH-3 were co-expressed in a stable HEK cell line as described in Fig S1C. We then purified GluA2 by immunoaffinty chromatography followed by gel filtration chromotography (Fig 2A). CNIH-3 robustly co-purified with GluA2, as CNIH-3 co-eluted with GluA2 in gel filtration (fractions 17-20, Fig 2B,C). Importantly, the position of the peak of GluA2 purified from GluA2/CNIH-3 expressing cells was shifted slightly leftward when compared to the GluA2 without CNIH-3 (Fig 2A), consistent with the purification of a larger protein complex in the case of GluA2/CNIH-3 versus GluA2 alone.

Western blots done against the gel filtration fractions probed with GluA2 further confirm the leftward shift of the GluA2 peak in the presence of CNIH-3

(Fig 2C) Western blots also show that a portion of CNIH-3 “falls off” the AMPA-R complex during the chromatography and is present in much later fractions (fractions 27-29), corresponding to lower molecular weight protein complexes (Fig2C). A large subset of CNIH-3 co-purifies with AMPA-Rs in gel filtration fractions 17-20 corresponding to tetrameric AMPA-Rs, indicating stable complex formation between the two proteins.

EM structure of the GluA2/CNIH-3 complex

CNIH-2 and 3 interact with AMPA-Rs and co-migrate in blue native PAGE (Kato et al.; Schwenk et al., 2009; Shi et al., 2010). It is unknown whether this observed stability is accompanied by a structurally intact AMPA-R complex. Using negative stain EM, we compared the shapes of the GluA2 homotetrameric AMPA-R particles in the presence or absence of CNIH-3.

The ultrastructure of the GluA2 tetramer expressed and purified from HEK cells was previously characterized and demonstrated to have similar structure to native AMPA-Rs purified from rat brain (Nakagawa et al., 2005; Shanks et al., 2010). Specifically, the large globular density at the bottom of the particle corresponds to the transmembrane domain (TMD), the two smaller roundish domains directly above are the ligand binding domain (LBD), and the two larger elongated bipartite densities at the top are the two dimers of the N-

terminal domain (NTD) (Fig 3A). The domains of the GluA2 homotetramer were well defined both in the absence and presence of CNIH-3, and at this resolution, the gross conformation of the GluA2 tetramer is not significantly different in the presence vs. absence of CNIH-3.

We observed that the transmembrane region (bottom density) is larger and wider in the images of the GluA2/CNIH-3 complex when compared to GluA2 alone. The enlarged transmembrane density of the GluA2/CNIH-3 particles is clearly seen in the raw particle images (Fig 3B, top images) and in the class averages (Fig 3B, smaller bottom images). The mean transmembrane density width was 101 Å and 126 Å in the absence and presence of CNIH-3, respectively. The transmembrane density widths for each condition showed normal distributions, with the median clearly shifted towards the right (larger TMD widths) in the presence of CNIH-3 (Fig 3C).

The EM structure was further interpreted by molecular labeling. The HA epitope at the extracellular C-terminus of CNIH-3 was labeled by anti-HA Fab fragments. The Fab fragments consistently bound to AMPA-R transmembrane density on the extracellular side of the protein complex (Fig3E), consistent with CNIH-3 contributing the transmembrane density of AMPA-Rs and further validating the predicted topology of the cornichons (Fig3D). While most Fab-labeled AMPA-R particles were decorated by only one Fab fragment, a subset

seemed to have two Fabs (see leftmost particle Fig 3E). These images clearly show the presence of at least one CNIH-3 molecule contributing to the TMD of the AMPA-R complex, and suggest that more than one CNIH-3 molecule can interact with each complex. Considering that a significant portion of the CNIH-3 fall off during the purification (Fig2C), the TMD of the resulting GluA2/CNIH-3 complex is still larger than GluA2 tetramer without CNIH-3. Collectively these results imply that multiple CNIHs can associate with a single GluA2 tetramer to form a stable complex.

In vitro reconstitution of the CNIH-3 and GluA2 complex

The formation of complexes between membrane proteins may require a cellular environment such as the lipid bilayer. To test if the AMPA-R/CNIH-3 complex can be reconstituted *in vitro* in the presence of detergent, we separately expressed CNIH-3 and the AMPA-R subunit GluA2 in HEK cells, and mixed the two cellular detergent extracts. Interestingly, the interaction between the two proteins was established *in vitro* as determined by a co-immunoprecipitation assay (Fig 4A). This indicates a robust interaction between these two proteins even in the absence of cellular membrane and forms a basis for investigating the interaction in a cell-free system.

Membrane proximal residues in CNIH-3 important for complex formation

After establishing that GluA2 and CNIH-3 form a stable complex, we were next interested in investigating the details of how this complex is formed. We sought to identify which portions of cornichon molecule are involved in the interaction. To do this, we created peptide arrays that contain dots on which peptides derived from sequences of CNIH-1 and CNIH-3 respectively were directly synthesized onto a membrane (Frank, 1995). Each peptide was 20 amino acids in length, the neighboring peptide overlapped by 17 amino acids, and the entire array spanned the full sequences of both CNIH proteins. We incubated the two peptide array membranes with freshly purified intact GluA2 homotetrameric AMPA-Rs, and then further labeled the receptors that were bound to the membrane using an anti-GluA2 antibody. The secondary antibody and detection techniques used for conventional western blotting were adopted to identify which dots on the membrane were positive for AMPA-R binding (cartoon in Fig 4B). By using this highly sensitive method, we identified short stretches within the CNIH proteins that directly interact with AMPA-Rs (Fig 4C). The data is quantified in a histogram by recording for each amino acid how many peptides containing that particular amino acid were positive in the peptide array blot (Fig 4D). Along the x-axis, residues that interacted with the peptide dots are highlighted in either blue (CNIH-3) or red (CNIH-1). This result identified regions of the extracellular and intracellular loops adjacent to the first two transmembrane segments as candidate AMPA-R binding regions

common between CNIH-1 and CNIH-3. It also implicates the portion of the extracellular loop specific to CNIH-2/3 as a possible interacting segment.

Identification of specific cornichon residues critical for AMPA-R binding

Based on the peptide array data, we created a series of CNIH-3 mutants to further identify minimal residues critical for the interaction. Within the regions of CNIH-3 that showed positive AMPA-R binding, we sequentially mutated three residues at a time to alanines. For example, DEL32AAA mutant denotes the conversion of the residues DEL to AAA, where the number in the middle represents the location of the first amino acid that was mutated. Nine out of the twelve mutants expressed in HEK cells. We co-expressed each of these mutants with GluA2 in HEK cells, and tested their ability to interact with GluA2 in co-immunoprecipitation experiments. While the nine mutants were expressed at approximately equal levels, three mutants (DEL32AAA, VPL104AAA, and LFY107AAA) showed significantly reduced interaction with GluA2 (Fig 5A, indicated by stars). Despite the region specific to CNIH-3 but not CNIH-1 in the extracellular loop appeared as candidates in the peptide array experiments, none of the three mutants in this area (RER61AAA, LRN64AAA, and IER67AAA) were critical for the interaction between CNIH-3 and GluA2. Collectively, these results identify specific residues in the CNIH-3 molecule that are located in two distinct regions, DEL sequence in the

membrane proximal extracellular loop regions and VPLLFY sequence in the membrane proximal cytoplasmic region in the CNIH-3 protein critical for AMPA-R binding (Fig 4D and E). Importantly these residues are highly conserved in CNIH-1.

Parallel reduction in functional and physical interaction in CNIH-3 mutants

In order to verify that the change in AMPA-R binding ability of these mutants was not due to a problem with protein folding or processing, we looked at the subcellular distribution of CNIH-3 and the CNIH-3 mutants in HEK cells. The subcellular distribution of wild-type and mutant CNIH-3 were all similar and exhibited a mixture of punctate and reticular patterns within the HEK cells, a distribution consistent with the ER/endomembrane system (Fig S5B). Additionally, CNIH-3 wild-type and the CNIH-3 mutants traffic to the HEK cell surface, demonstrated by the HA surface staining (Fig S5B) None of the mutants appeared to be aggregating or are mislocalized in the cell, indicating that their decreased interaction with GluA2 is due to obstruction of the binding site and not secondary effects due to artifacts of misfolding or mislocalization.

We tested the ability of these CNIH-3 mutants to modulate AMPA-R ion channel kinetics. CNIH-3 slows AMPA-R desensitization (Coombs et al., 2012; Kato et al., 2010; Schwenk et al., 2009; Shi et al., 2010). We compared CNIH-3 and the CNIH-3 mutants identified to have reduced physical interaction in their ability to modulate AMPA-R desensitization. To examine their function, we co-expressed the CNIH-3 constructs with GluA2 in HEK cells. AMPA-R channel kinetics were recorded with glutamate application from outside out patches. Consistent with previous reports, the addition of wild-type (WT) CNIH-3, significantly slows receptor desensitization as compared to its absence (Fig5C). The three CNIH mutants that showed reduced physical interaction with GluA2, (DEL32AAA, VPL104AAA, and LFY107AAA), showed a reduced ability to modulate the desensitization kinetics compared to WT CNIH-3, resulting in τ_{des} values intermediate between WT CNIH-3 and no CNIH-3 at all (Fig 5C). Compared to wildtype mean τ_{des}=64.54ms, the values were 28.23, 36.88, and 44.48ms for DEL32AAA, VPL104AAA, and LFY107AAA mutants respectively. Similarly, using the cell death assay in which co-expression of AMPA-Rs and CNIH-3 is toxic to HEK cells (FigS1F) we confirmed that the CNIH-3 mutants could not functionally modulate AMPA-R function. The co-expression of WT CNIH-3 with GluA2 resulted in significant cell death 30 hour after the induction of GluA2. In contrast, in the cells co-expressing GluA2 and any of the three CNIH-3 mutants that showed reduced interaction with AMPA-Rs, the cells continued to grow and divide in a healthy

manner (Fig S5C). Collectively, these experiments indicate that the functional interaction with AMPA-Rs was significantly reduced by the CNIH-3 mutations that reduced the physical interaction with GluA2. We have therefore determined two distinct regions in the membrane proximal regions of the both the intra- (residues DEL) and extracellular (residues VPLLFY) loops of CNIH-3 that are important for the physical and functional interaction with AMPA-Rs, defining the residues critical for interaction down to 9 residues.

CNIH2/3 specific extracellular loop residues contribute to interaction and gating

The peptide array experiments suggested interaction between the extracellular loop region specific to CNIH-2/3 and AMPA-Rs, however making small alanine mutations failed to confirm this result. Because AMPA-R modulation is specific to CNIH-2/3 and not to CNIH-1/4, the extracellular loop sequence specific to the modulating isoforms is of particular interest. Therefore, we designed a series of constructs with more extensive deletions within CNIH-2/3 specific portion. Specifically, this segment was completely deleted in CNIH-3del and partially deleted in CNIH-3del2 and del3 (Fig5E). While all three mutants reduced interaction with GluA2 (Fig5D) in co-immunoprecipitation (CoIP) experiments in HEK cells, constructs lacking the residues RNIERICF resulted in a more drastic reduction in interaction with

AMPA-Rs. Consistent with the reduced physical interaction compared to CNIH-3, the CNIH-3del mutants showed a parallel reduction in modulating AMPA-R desensitization kinetics (Fig5F), the mean values of τ_{des} being 26.44ms for the full deletion mutant, compared to 46.51 for del2, and 32.03ms for del3, compared to 64.54ms for wildtype CNIH-3. The peptide array results, and mutant analysis suggest that a total of 3 regions of the CNIH-3 molecule that are important for the interaction with AMPA-Rs: Two clusters of membrane proximal residues conserved among all CNIHs, as well as the sequence in the extracellular loop of CNIH-3 absent in CNIH-1/4 (depicted in Fig 5G).

Domains of GluA2 contributing to complex formation

We next investigated which domain of AMPA-R interacts with CNIH-3 specific loop utilizing the peptide array method. For this experiment, the arrays contained peptides representing the CNIH-1 and CNIH-3 extracellular loop and adjacent transmembrane regions in overlapping 15 amino acid length sequences. We separately purified the isolated GluA2 LBD (S1S2) (Armstrong and Gouaux, 2000) and the NTD (Jin et al., 2009; Rossmann et al., 2011) (Fig S6A, B) and applied these directly to two separate but identical peptide arrays (Fig 6A, D). After probing with an anti His antibody to recognize which peptides the isolated AMPA-R LBD or NTD bound to (Fig 6B,D), the data was

quantified using methods in Fig 4D and the results are shown in (Fig 6C, E) Residues that interacted with the peptide dots are highlighted in either blue (CNIH-3) or red (CNIH-1). These results demonstrate that both the GluA2 LBD and NTD interact with the CNIH-3 extracellular loop. Furthermore, we designed two versions of the NTD, V1 and V2, one of which completely lacks the NTD-LBD linker region (Fig S6D), and both version show the same interaction with the CNIH-3 extracellular loop on the peptide array results (Fig S6E). The GluA2 NTD interacts primarily with the most membrane distal portion of the loop, while the LBD shows interaction with more membrane proximal regions. This is consistent with the topology of the AMPA-R domains relative to the membrane.

The peptide array results described above demonstrated that both the AMPA-R NTD and LBD interact with the CNIH-3 extracellular loop, primarily in regions specific to CNIH-2/3 and absent in CNIH-1/4. In order to further understand these interactions we made targeted CNIH-3 deletion mutants in which we deleted the key residues that showed positive hits in the peptide array experiments, CNIH-3delNTD (delete residues HARERL) and CNIH-3delLBD (delete residues ERICFLL) (Fig 6G). In CoIP experiments, these mutants show reduced physical interaction with GluA2 compared to WT CNIH-3, although this effect is much more drastic in the case of the CNIH-3delLBD mutant than the CNIH-3delNTD mutant (Fig 6H). Consistently, both mutants

showed a reduced ability to modulate AMPA-R desensitization kinetics compared to CNIH-3WT (Fig 6F), with the CNIH-3delLBD mutant showing a greater deficit (mean τ_{des}=19.99ms for the CNIH-3delLBD mutant, 35.91ms for the CNIH-3delNTD mutant, compared to 64.54ms for CNIH-3WT). Taken together, these experiments confirm that the AMPA-R LBD and NTD are both important for the physical and functional interaction with CNIH-3. Given the greater number of positive spots in the peptide array, the LBD likely plays a more significant role in this interaction than the NTD.

Discussion

The molecular mechanisms of AMPA-R modulation by the auxiliary subunits are only partially understood for the extensively studied TARPs (Chen et al., 2000; Menuz et al., 2007; Tomita et al., 2005; Turetsky et al., 2005). The mechanism is unclear for other auxiliary subunits, such as cornichons. In this study, by combining a variety of techniques including biochemistry, single particle EM, proteomics, cell biology, electrophysiology, and high-throughput peptide arrays, we investigate the AMPA-R/CNIH interaction and determine how specific CNIH amino acid residues interact physically and functionally with the AMPA-R extracellular domains.

It has been hypothesized that TARPs amplify the conformational changes of the LBD of AMPA-Rs (Menuz et al., 2007). The functional interaction between TARPs and AMPA-Rs requires the first extracellular loop and the C-terminal portions of the TARP molecule (Tomita et al., 2005). However it is unclear whether or how these regions physically interact with the AMPA-R itself. Specifically, they could be critical for transducing allosteric modulation without physically interacting with the extracellular portion of the AMPA-R, with the actual binding ocurring elsewhere in the molecule. Currently, there was not yet direct evidence for physical interaction between

the extracellular domain of AMPA-Rs and extracellular loops of any of the known auxiliary subunits.

To address these questions, we focused on cornichons, as they are suitable for extensive structure-function correlation studies due to their low molecular weight. We identified, at a precision of several amino acids, two loci within the extracellular loop of CNIH-3 that mediates physical interaction with GluA2 (Fig 5G). An additional locus that mediates binding exists in the transmembrane region and adjacent intracellular loop (Fig 5G). Furthermore, both of the AMPA-R extracellular domains, the LBD and NTD physically interact with the CNIH-3 extracellular loop, pointing out a novel role for the NTD in auxiliary subunit induced allosteric modulation of ion channel function. In this view, our data advances our understanding of the molecular mechanisms of auxiliary subunit modulation of AMPA-Rs.

Screening by peptide array based sensitive binding assays followed by site directed mutagenesis identified segments within CNIH responsible for interacting with AMPA-R at an amino acid precision. We found negatively charged residues DE, and the non polar residue L in the region of the first extracellular loop just proximal to the first transmembrane region, as well as a stretch of primarily non-polar residues in the second transmembrane region

and membrane proximal region of the intracellular loop significantly decreased the ability of CNIH-3 to physically interact with AMPA-Rs.

CNIH-2/3 bind to AMPA-Rs and modulate gating, while CNIH-1 cannot modulate gating but is capable of binding. This suggests a dissociation in the molecular mechanisms for physical interaction and AMPA-R modulation. Consistent with this idea, two regions well-conserved among the CNIHs that are near the transmebrane segments were necessary for the physical interaction (Fig 5G, green stars). In contrast, the extracellular loop segment specific to CNIH-2/3 is involved in the physical interaction but also for modulation of AMPA-Rs (Fig 5G, red segment).

Although only CNIH-2/3 interact with AMPA-R in rat brain lysates, we detected interaction between CNIH-1 and AMPA-R subunits in vitro. We also demonstrate the existence of CNIH-1 in the human AMPA-R interactome, supporting the physiological relevance of our in vitro observation. In addition, AMPA-Rs overexpressed in HEK cells interact with other CNIH homologues endogenously present in HEK cells. Transcript levels of CNIH-1, 2, and 3 were all upregulated in the dorsolateral prefrontal cortex of brains from schizophrenic patients (Drummond et al., 2012), further consistent with the idea that there may be functional significance of CNIH-1 in human brain.

The amino acid sequences for CNIHs are identical between rats and humans. Similarly, primary structures of AMPA-R subunits are also nearly identical between rat and human, collectively suggesting that our observed interaction differences between species cannot be accounted for by sequence differences alone. There be species specific differences in AMPA-R regulation by cornichons. C. elegans has a CNIH (Accession CAB01516), however it lacks the mammalian CNIH-2/3 specific region of the extracellular loop, making it more similar to mammalian CNIH-1 than CNIH-2/3. It is possible that, analogous to humans, C. elegans may utilize a rat CNIH-1 like isoform as a glutamate receptor binding protein. Accordingly, we predict that their function would be very different from what is known for rat CNIH-2/3. Further studies will be required to clarify the precise regulatory roles of all of the CNIHs in different species.

The extracellular loops of auxiliary subunits are positioned appropriately to modulate AMPA-R ion channel function given the physical proximity to the extracellular domains of the AMPA-Rs. We provide the first direct evidence for physical interaction between the CNIH-3 extracellular loop and both the LBD and NTD of AMPA-Rs. Such interactions likely apply to other auxiliary subunits like stargazin/TARPs. Consistent with this idea, it was previously

demonstrated that glutamate binding induces a conformational change in the AMPA-R complex in which the NTD approaches the membrane in the single particle EM structures of brain derived AMPA-R complexes that contain auxiliary subunits (Nakagawa et al., 2005). Spatial proximity of the NTD with the extracellular loop of auxiliary subunits may facilitate their physical interaction during the later phases of modulation. We speculate that the gross conformational changes of the NTDs relative to the rest of the receptor complex reflect a movement that occurs during gating and may allow the NTD to interact with the extracellular loop of the auxiliary subunit.

The size of the transmembrane density of the AMAP-R particle significantly increased when CNIH-3 was present. Further Fab labeling experiments confirmed that this increase is due to the presence of CNIH-3 in that location. Although this method cannot be used quantitatively, as the Fab fragment binding affinity does not always allow stoichiometric binding, the data clearly suggest that two CNIH molecules can simultaneously bind to a single GluA2 tetramer. At the resolution of ~20 Å we did not observe and changes in the overall organization and shape of the extracellular domains of GluA2 tetramers CNIH-3 was present, indicating that the addition of CNIH-3 alone does not grossly alter the conformation of the receptor.

Glutamate receptor NTDs homologous to soluble bacterial periplasmic amino acid binding proteins such as leucine/isoleucine/valine binding protein, as well as type-C G protein coupled receptors including metabotropic glutamate receptors, mGluR1-8 (O'Hara et al., 1993; Paas, 1998; Trakhanov et al., 2005). Consistently, a role for the NTD in ligand binding has been demonstrated for NMDA-Rs, with the binding of divalent cations such as zinc and negative allosteric modulators such as ifenprodil altering NMDA-R channel activity (Hatton and Paoletti, 2005; Karakas et al., 2009; Perin-Dureau et al., 2002). The proposed mechanism involves a bidirectional allosteric pathway in which the opening and closing of the NTD clamshell is transmitted through the NTD-LBD linker, to the LBD dimer interface down the channel gate (Gielen et al., 2008; Gielen et al., 2009). Structural studies suggest a mechanism for this allostery in which the lower lobes of the NTD are separated, and therefore able to move upon ligand binding (Farina et al., 2011; Karakas et al., 2009, 2011). In contrast, the NTD dimers of other glutamate receptor subtypes are in closer proximity to one another, which could thus restrict motions of the lobes (Clayton et al., 2009; Jin et al., 2009).

Binding sites for extracellular proteins within the NTD have been suggested for many glutamate receptor types including neuronal pentraxins (O'Brien et al., 1999; Sia et al., 2007) and N-cadherin (Passafaro et al., 2003;

Saglietti et al., 2007) for AMPA-Rs, Cbln1 for delta-2 receptors (Matsuda et al., 2010), and ephrin receptors for NMDA-Rs (Dalva et al., 2000). For AMPA-Rs in particular, the NTD has been shown to play an important role in the regulation of receptor assembly, by acting as a gate-keeper to ensure iGluR subtype specific assembly (Ayalon et al., 2005; Ayalon and Stern-Bach, 2001; Leuschner and Hoch, 1999). However, recent structural data and computation modeling suggest that NTDs of AMPA-Rs are flexible enough to accommodate inter protomer rotation which could potentially be transduced to the downstream receptor components that mediate gating (Dutta et al., 2012; Sukumaran et al., 2011). This is in line with our idea that the AMPA-R NTDs are targets of modulation mediated by auxiliary subunits.

In conclusion, our detailed analysis of the interaction provides greater insight about the complexity of AMPA-R modulation by auxiliary subunits. We mapped out the interactions between the AMPA-R and CNIH-3, confirming previous speculations about interactions between extracellular loops of auxiliary subunits with the AMPA-R LBD. More importantly, we also determined that the AMPA-R NTD is important in this interaction. This is a novel function for the AMPA-R NTD as an allosteric modulator of channel function, a function similar to one previously only realized for the NMDA-R NTDs. However, in contrast to binding soluble extracellular factors, the AMPA-

R NTD is seemingly allosterically modulated by interactions with auxiliary subunits, other membrane proteins that form part of the greater AMPA-R complex. Such knowledge will be useful in conducting further higher resolution structural studies of AMPA-R complexes, which may pave paths towards developing new therapeutic agents targeting AMPA-Rs.

Methods

Recombinant DNA

GluA2 construct: The rat GluA2 *flip* splice variant was used for all experiments. The flag tag was inserted at the C-terminal domain (FAT**DYKDDDDK**EGYNVYGIESVKI, where bold case indicates FLAG epitope) and placement preserves the original anti-GluA2CT epitope.

GluA2 S1S2 extended linker construct: pETQG was created according to (Chen et al., 1998). The S1S2 Flop extended linker construct is made with S1 boundaries being SGNDTSGLEN and ending with with the sequence SIMIKK, the linker is GT, and the boundaries of S2 are PIESAE extending into pre-M4, ending with the sequence GGGDSKEKTS.

GluA2 NTD constuct

The entire GluA2 NTD up to the sequence CTAACTGAGCTCCCCATCAGGA (V1) or GACACGTCTGGGCTTGAAAACAAG (V2) was subcloned into a PIRESmcherry 5Glycine Thrombin His8 vector.

NMDA-R subunit constructs: Rat GluN1-1a splice variant was subcloned into the NotI site of pTRE-A vector as (Farina et al., 2011). pTRE-B-GluN2B3xFLAG: Rat GluN2B cDNA bearing 3xFLAG tag at the C-terminal domain (...PRAFNG **DYKDHDGDYKDHDIDYKDDDDK** SSNGHVYEKLSSIESDVstop, where bold case indicates 3xFLAG epitope) was cloned into pTRE-B vector between restriction enzyme sites EcoRI and

EcoRV. pTRE-A-GluN1 and pTRE-B-GluN2B3xFLAG#1 vectors were then combined to a single dual expression vector as described previously (Farina et al., 2011).

CNIH-1,2,3 constructs: Mouse CNIH cDNA clones were obtained from OpenBiosystems. The HA tag was inserted at the very C-terminus of CNIH-3: The CNIH-3-HA mcherry cassette was subcloned into pBOSS vector (a gift from Shigekazu Nagata and Hideki Sakahira) downstream of the elongation factor promoter. To create CNIH-3 point mutants, 3 residues at a time were mutated to alanines using in vitro mutagenesis Quick change protocol (Stratagene). In the CNIH-3 deletion mutant, the sequences indicated in figures within the extracellular loop was removed by PCR.

Generation of stable HEK cell lines that expresses GluA2-FLAG by DOX induction (TetONGluA2 *flip* stable HEK cells)

A previously described method was adopted (Shanks et al., 2010). In brief, a neomycin (G418) resistant TetON-HEK cell line (Clontech) has in its genome the expression module to produce rtTA (see Fig 2A). TetON-HEK cells were co-transfected with a plasmid that expresses a hygromycin resistant gene and a FLAG tagged GluA2 *flip* construct in pTREtight described above. Transfection was done by calcium phosphate and selection of clones was done over two weeks in the presence of 120 µg/ml hygromycin. Colonies of HEK cells that survived selection were plated and grown up. We detected the

expression of GluA2 using western blotting after inducing the isolated clones with 5 μg/ml DOX for 24 hours.

Generation of stable HEK cell lines that expresses GluA2-FLAG by DOX induction and constitutively expresses CNIH-2HAIRESmcherry (TetONGluA2/CNIH-3 stable HEK cells).

The cell line described above that inducibly expresses GluA2 was co-transfected with a pBOSS-CNIH-3HA-IRES-mCherry and pCMVZeocin (Invitrogen) were co-transfected at a ration of 25:1 into the TetONGluA2 *flip* stable HEK cells. Selection of clones was done over two weeks in the presence of 120 μg/ml zeocin, 120 μg/ml hygromycin, 120 μg/ml G418, and 1mM kynurenic acid. Colonies positive for mcherry were identified, isolated, and cultured separately. The presence of CNIH-3HA as well as DOX inducible GluA2 was confirmed in the mCherry positive clones by Western blotting using an HA (HA.11, Covance) and GluA2CT (Nakagawa et al., 2005) antibody, respectively.

Generation of stable HEK cell lines that express GluN1 and GluN2B

The DOX inducible GluN1/GluN2B3xFLAG#1 dual expressing cell line was generated as following; pTRE-GluN1/GluN2B3xFLAG#1 dual expressing vector was linearized by digesting with ScaI, of which target site is located outside of expression units, and was purified. The DNA was co-transfected

with a plasmid that expresses a hygromycin resistant gene into HEK TetON cells. Selection of clones was done over two weeks in DMEM (Mediatech) containing 10%FCS, Peni/strep(Invitrogen), 120µg/ml G418, 120µg/ml hygromycin, 1mM kynurenic acid, 10mM MgSO4 and 2.5µM (+)MK801(Ascent). Colonies of HEK cells that survived selection were plated and grown up. A portion of each clone was cultured in 96 well format and induced in the absence of (+)MK801. Cell death exhibiting clones were further expanded as candidate clones. As the final check, expression of GluN1 and GluN2B3xFLAG#1 in the same cells was examined by western blotting and immunocytochemistry using antibodies against GluN1 C1 exon (rabbit polyclonal) (Sheng et al., 1994) and FLAG epitope(M2 mouse monoclonal, Sigma).

Purification of recombinant GluA2 or GluA2/CNIH-3 from HEK cells

Cell pellet is obtained from 20 x 20cm plates of TetOn GluA2 cells, after a 24 hour induction with DOX. About 6ml of HEK cell pellet was resuspended in 50 ml of buffer containing 50 mM Na-HEPES pH7.4, 85 mM NaCl, 15mM KCl, 30µm NBQX and, protease inhibitors (1 mM PMSF, 10 mg/ml leupeptin, atropinin, benzamidine, and pepstatin A). Extraction was accomplished with, DDM (0.25%) at 4 oC for three hours. The lysate was ultracentrifuged (Beckman 45 Ti rotor) at 45,000 rpm for 1 hour at 4 ^{o}C, and the supernatant passed through a column made of protein A sepharose beads (GE

Amersham) cross-linked using DMP (Pierce) to anti-FLAG M2 monoclonal antibody (Sigma) at a concentration of 2 mg/ml. After three washes, bound proteins were eluted using 0.5 mg/ml of FLAG epitope peptide in buffer. The peak elution sample was further separated by size using Superdex 200 gel filtration column (GE Amersham) in 50 mM Na-HEPES pH 7.4, 85 mM NaCl, 15mM KCl, and 0.1% DDM.

Purification of recombinant GluN1/GluN2B Purification from HEK cells

Cell pellet is obtained from 40 x 20 cm plates of GluN1wtGluN2B cells. The purification procedure is same as above but the buffer is 50mM NaHEPES pH 7.4, 300mM NaCl, 1umM kynurenic acid, 10mM MgSO4 and 100um ifenprodil throughout.

Purification of GluA2 S1S2 Extended linker (LBD)

The GluA2 S1S2 extended linker construct was produced and purified as described in (Chen et al., 1998) for the HS1S2I construct.

Purification of GluA2 NTD

400 mLs of Optimem (Gibco) culture supernatant from GluA2NTD-8His expressing HEK cell line was spun down at 3500 rpm for 10 minutes. The supernatant was adjusted such that the final solution contained 50mM sodium phosphate buffer and 25mM immidazole, pH 7.5. The media was gravity

loaded onto a chelating sepharose column charged with Ni2+ that was pre-equilibrated with Optimem containing sodium phosphate buffer and immidazole, pH 7.5 (50 and 25mM, respectively). After the medium passed through, and the column was washed with 10 column volumes of wash buffer (50mM sodium phosphate buffer, 30mM immidazole pH7.5), the bound protein was eluted from the column with 20mM Tris-HCl pH 7.5, 250mM immidazole, and 150 mM NaCl. This was spun down at 35,000 rpm for 15 minutes, and loaded for gel filtration.

Purification of receptor complexes from rat and human brain

These procedures are described in (Shanks et al., 2012). Human brain (cortex) was obtained through the National Disease Research Interchange (NDRI), Researcher: Yates (code YAJ2), TSRI: IRB-11-5719

Mass Spectrometry

Sample preparation**:** Bound proteins were eluted from the beads by incubation with Pierce elution buffer and TCA precipitated over night. The precipitate was resuspended in 8 M Urea with ProteasMAX (Promega, Madison, WI, USA) per the manufacture's instruction. The samples were subsequently reduced by 20 minute incubation with 5mM TCEP (*tris*(2 carboxyethyl)phosphine) at room temperature and alkylated in the dark by treatment with 10mM iodoacetamide for 20 additional minutes. The proteins were digested over-night at 37

degrees with Sequencing Grade Modified Trypsin (Promega, Madison, WI, USA) and the reaction was stopped by acidification.

Multidimensional Protein Identification Technology (MudPIT): The protein digest was pressure-loaded onto a 250--µm i.d capillary packed with 2.5cm of 10-µm Jupiter C18 resin (Phenomenex, Torrance, CA, USA) followed by an additional 2.5cm of 5-µm Partisphere strong cation exchanger (Whatman, Clifton, NJ). The column was washed with buffer containing 95% water, 5% acetonitrile, and 0.1% formic acid. After washing, a 100--µm i.d capillary with a 5-µm pulled tip packed with 15 cm 4-µm Jupiter C18 resin (Phenomenex, Torrance, CA, USA) was attached to the filter union and the entire split-column (desalting column–filter union–analytical column) was placed inline with an Agilent 1100 quaternary HPLC (Palo Alto, CA) and analyzed using a modified 5-step separation described previously (Washburn et al., 2001). The buffer solutions used were 5% acetonitrile/0.1% formic acid (buffer A), 80% acetonitrile/0.1% formic acid (buffer B), and 500 mM ammonium acetate/5% acetonitrile/0.1% formic acid (buffer C). Step 1 consisted of a 75 min gradient from 0-100% buffer B. Steps 2-5 had a similar profile except 3 min of 100% buffer A, 5 min of X% buffer C, a 10 min gradient from 0-15% buffer B, and a 105 min gradient from 10-55% buffer B (except for step 5 which %B was increased from 10% to 100%). The 5 min buffer C percentages (X) were 10, 40, 60, 100% respectively for the 5-step analysis. As peptides eluted from the

microcapillary column, they were electrosprayed directly into an LTQ mass spectrometer (ThermoFinnigan, Palo Alto, CA) with the application of a distal 2.4 kV spray voltage. A cycle of one full-scan mass spectrum (400-2000 m/z) followed by 6 data-dependent MS/MS spectra at a 35% normalized collision energy was repeated continuously throughout each step of the multidimensional separation. Application of mass spectrometer scan functions and HPLC solvent gradients were controlled by the Xcaliber datasystem.

FOR LTQ: As peptides eluted from the microcapillary column, they were electrosprayed directly into an LTQ 2-dimensional ion trap mass spectrometer (ThermoFinnigan, Palo Alto, CA) with the application of a distal 2.4 kV spray voltage. A cycle of one full-scan mass spectrum (400-1400 m/z) followed by 8 data-dependent MS/MS spectra at a 35% normalized collision energy was repeated continuously throughout each step of the multidimensional separation. Application of mass spectrometer scan functions and HPLC solvent gradients were controlled by the Xcalibur datasystem.

Analysis of Tandem Mass Spectra: MS/MS spectra were analyzed using the following software analysis protocol. Poor quality spectra were removed from the dataset using an automated spectral quality assessment algorithm (Bern et al., 2004). MS/MS spectra remaining after filtering were searched with the ProLuCID algorithm against the EBI-IPI_Human_3_30_06-28-2007

concatenated to a decoy database in which the sequence for each entry in the original database was reversed (Peng et al., 2003). All searches were parallelized and performed on a Beowulf computer cluster consisting of 100 1.2 GHz Athlon CPUs (Sadygov et al., 2002). Only peptides with at least 1 tryptic termini were considered. Searches were performed with Cystein carbamidomethylation as a fixed modification.

ProLuCID (Eng et al.,1994) results were assembled and filtered using the DTASelect (version 2.0) program (Tabb et al., 2002). DTASelect 2.0 uses a linear discriminant analysis to dynamically set XCorr and DeltaCN thresholds for the entire dataset to achieve a user-specified false positive rate (5% in this analysis). The false positive rates are estimated by the program from the number and quality of spectral matches to the decoy database. Confidence for modifications was estimated from overlapping modified peptides as described previously (MacCoss et al., 2002).

Immunoprecipitation of CNIH-HA proteins in HEK cells

TetONGluA2 *flip* cells were plated on 0.2% gelatin at a density of $0.5x10^6$ cells/ml. 20 hours later, cells were transfected with wildtype and mutant CNIH3-HA constructs using calcium phosphate method. 24 hours after transfection cells were washed with cold PBS twice, and resuspended in 750µl of buffer containing 50mM Na-HEPES pH7.4, 85mM NaCl, 15mM KCl, 30 µM

NBQX and protease inhibitors (1 mM PMSF, 10 µg/ml leupeptin, atropinin, benzamidine, and pepstatin A). Cells were lysed with 0.25% DDM for 1.5 hours at 4 degrees, ultracentrifuged at 35krpm in a Beckman TLA-55 rotor for 15 minutes. The supernatant was incubated with HA antibody (HA.11 Covance) at a concentration 1:300 for about 15 hours. 30 µl of protein A sepharose beads were added, and incubated with the lysate for 3 hours. After washing the beads twice, protein was eluted from the beads by boiling with DTT/ SDS loading buffer. Western blotting was done using anti -R2CT at 1:300 (Nakagawa et al., 2005)and anti-HA antibody at 1:1000 (HA.11 Covance)

Negative staining of purified proteins and EM

400 mesh copper grids were coated with carbon to create a substrate for proteins to bind. 4 µl of protein solution was applied to a glow discharged grid and left for 30 sec to 5 min to allow the proteins to bind. The excess water was blotted on filter paper and the grid was washed twice in water droplets to remove excess detergents. Purified proteins were negatively stained with 0.75% (w/v) uranyl formate as described (Ohi et al., 2004). Images were recorded using a FEI Sphera electron microscope equipped with a LaB_6 filament operated at an acceleration voltage of 200 keV. Images were taken at a magnification of 50,000 X and defocus value = -1.5 mm. All images were recorded using SO-163 film and developed with a Kodak D-19 developer at full

strength for 12 min at 20 °C. Particle images were taken at room temperature and under low dose conditions (20 e/Å^2) to minimize radiation damage.

Fab labeling

The immunopure IgG1 F(ab') and the F(ab')2 Fab purification kit (Pierce) was used to digest anti-HA monoclonal antibody (HA.11, Covance). Fab fragment was further purified by gel filtration on a Superdex 200 column (Pharmacia). The labeling of particles was performed by incubating the AMPA-R/ CNIH-3 particles with the Fab fragments at a molar ratio of 1:2 to 1:4 overnight at at 4oC in 50 mM HEPES, pH 7.4, 100 mM NaCl, 0.1% DDM.

Image processing

Electron micrographs were digitized with a CoolScan 9000 (Nikon) using a step size of 6.35 mm and the pixels were binned by a factor of 3 such that the specimen level pixel size used was 3.81 Å. Projection averages were calculated from windowed small images of 100 x 100 pixels over 10 cycles of K-means classification and multi-reference alignment specifying 100 classes. A total of 9,300 particles for GluA2 and 8,951 particles for GluA2/CNIH-3 were interactively selected using WEB display program for SPIDER. (Frank et al., 1996).

Transmembrane domain width calculation and comparison

The width of the transmembrane domain was measured at its widest point in Image J for each class average. Class averages in which the transmembrane domain was not clear enough to be accurately measured were eliminated from calculations. This measurement was recorded in pixels and calculated back into angstroms. The measurement for each class average was attributed to the number of particles contained in that class average.

Timecourse of GluA2 expression in TetONGluA2/CNIH-3HA cell lines.

Various clones of TetONGluA2-CNIH-3HA cell lines and the parental TetONGluA2 cell were plated at a density of 0.6 x 10^6 cells/well on 6 well plates. 24 hours later, cells were induced with 2.5-7.5µg/mL of DOX in the presence of 1mM kynureic acid, 30µM NBQX and 1mM Na-butyrate. At time points: 0, 6, 12, 18 and 24 hours(after induction, cells were washed with PBS and harvested in 1ml PBS. After spin-down and aspiration of supernatant, cells were flash frozen in liquid N_2. SDS PAGE samples were prepared with 400µl PBS and 200µl 4xDTT and boiled 15min. Western blotting was done using anti-HA (HA.11 Covance) and anti-GluA2CT polyclonal antibodies (Nakagawa et al., 2005). Western blots films were scanned and analyzed using image J software. Background-subtracted total signal at each time point was normalized to the signal at 24hr after induction. 3 sets of experiments were conducted, and the bands of each time point of each cell line were averaged and plotted as a line graph.

Immunocytochemistry in HEK cells

TetONGluA2-CNIH-3-HA-IRES-mCherry or TetONGluA2*flip* cells grown on PLL coated glass coverslips were washed once with PBS, and fixed with 4% formaldehyde in 0.1 M phosphate buffer pH 7.4 for 9 minutes around 24hr after DOX induction. Cells were then incubated in primary antibodies: Dilution rate of antibodies are: Anti-GluA2CT at 1:300 or 1:200 M2Flag (Sigma) at 1;200, pan-TARP antibody (Nakagawa et al., 2005) at 1;200 and anti-HA at 1:1000 (HA.11, Covance). Alexa 568 and Alexa 488 conjugated secondary antibodies were used at a dilution of 1:200 (Invitrogen). Images of the cells were recorded using an Epi-fluoresencent microscope (Olympus) and recorded on a cooled CCD camera (Hamamatsu Orca). Under the imaging condition used, the mCherry signal was negligible compared to the signal derived from Alexa 568.

Surface labeling of HEK cells

Expression of GluA2 was induced with 7.5 µg/ml DOX. 24 hr after induction cells were live labeled using an anti-GluA2 (MAB397 Chemicon @1:200) monoclonal antibody for 15 min placed in plain DMEM media. Cells were washed with warm DMEM and fixed with 4% formaldehyde in 0.1M phosphate buffer pH 7.4. Alexa 488 conjugated anti-mouse IgG secondary antibody (Invitrogen) was used for detection.

Cell death assay experiments

Each stable cell line was plated at a density of approximately $0.2x10^6$ cell/ml in a 12 wells plate. 24 hours after plating, DIC images were taken of cells at 10x magnification. Cells were then induced with 7.5µg/mL DOX and 1mM Na-butyrate. AMPA-R antagonist, NBQX (30µM) was used to inhibit cell death. 30 hours after induction, DIC images were taken of induced cells in both the +/- NBQX conditions.

Peptide Array Experiments

The peptide arrays were synthesized using SPOT synthesis (Frank, 1995). Two arrays were synthesized separately, one for CNIH-1 and one for CNIH-3. Each dot on the array corresponds to 20 amino acids of the protein. Each subsequent dot contains another 20 amino acids, each time shifted by 3 amino acids along the protein moving from the N to the C-terminus. In the first peptide array experiments (Fig 4) probed with the full length GluA2, the entire CNIH-3 and CNIH-1 sequences are represented. In the second set of peptide array experiment (Fig 6) probed with the GluA2 S1S2 and NTD protein, the sequence begins at the N-terminus of CNIH-3 and extends partway through the second transmembrane domain, primarily highlighting the first transmembrane domain and the first extracellular loop. In these arrays, each dot on the array corresponds to 15 amino acids of the protein. Each

subsequent dot contains another 15 amino acids, each time shifted by 2 amino acids along the protein. In in all cases, membranes were washed sequentially with methanol, water, protein purification buffer, and blocking buffer (purification buffer with 5% BSA) for 10 minutes. Then the peak fractions of protein from gel filtration of full length GluA2 purified from HEK cells or S1S2 extended linker protein or GluA2 NTD (as described above) were added to the blocking buffer and incubated on the membranes at 4 ^{o}C for 4 hours. After washing the with purification buffer, using the procedures analogous to conventional Western blotting, the membrane was probed using anti-GluA2CT antibody (Nakagawa et al., 2005) as primary probe and HRP conjugated anti-rabbit IgG as secondary probe to detect full lenth GluA2 positive dots or the penta-His HRP conjugate antibody (Qiagen) to detect GluA2 S1S2 or NTD positive dots. The signal was detected using chemiluminescent method and recorded on film.

Analysis of peptide array results

The dots on the film were visually identified as either positive or negative for GluA2 interaction. The amino acid sequences corresponding to each dot were checked. A histogram was created such that the appropriate sequences of CNIH-1 and CNIH-3 form the horizontal axis. Each point of the horizontal axis corresponds to a single residue of each protein and the number of positive dots containing each residue was recorded in the vertical axis. Amino acids

with more positive dots would have stronger interaction with GluA2. Stretches of amino acids with positive scores were identified. These amino acid clusters were interpreted as positive for a GluA2 interaction. These positive residues were altered in the series of CNIH-3 alanine substitution mutants.

Electrophysiology

Voltage clamp recordings were performed on outside-out patches from HEK293T cells as described previously (Rossmann et al., 2011). Cells were transfected with GluA2-Q (flip) and CNIH-3 plasmids or GluA2-Q (flip) alone. Current responses of outside-out patches (voltage-clamped at -60 mV) were elicited by fast application of 10 mM L-glutamate via a Θ-tube and recorded using Axopatch-1D amplifier, Digidata1322 interface and pClamp p.2 software (Molecular Devices). The rate of receptor desensitization was measured by fitting the current decay during a 100 ms application of L-glutamate with a double-exponential function.

References

Armstrong, N., and Gouaux, E. (2000). Mechanisms for activation and antagonism of an AMPA-sensitive glutamate receptor: crystal structures of the GluR2 ligand binding core. Neuron *28*, 165-181.

Ayalon, G., Segev, E., Elgavish, S., and Stern-Bach, Y. (2005). Two regions in the N-terminal domain of ionotropic glutamate receptor 3 form the subunit oligomerization interfaces that control subtype-specific receptor assembly. J Biol Chem *280*, 15053-15060.

Ayalon, G., and Stern-Bach, Y. (2001). Functional assembly of AMPA and kainate receptors is mediated by several discrete protein-protein interactions. Neuron *31*, 103-113.

Chen, G.Q., Sun, Y., Jin, R., and Gouaux, E. (1998). Probing the ligand binding domain of the GluR2 receptor by proteolysis and deletion mutagenesis defines domain boundaries and yields a crystallizable construct. Protein Sci *7*, 2623-2630.

Chen, L., Chetkovich, D.M., Petralia, R.S., Sweeney, N.T., Kawasaki, Y., Wenthold, R.J., Bredt, D.S., and Nicoll, R.A. (2000). Stargazin regulates synaptic targeting of AMPA receptors by two distinct mechanisms. Nature *408*, 936-943.

Choi, Y.B., and Lipton, S.A. (1999). Identification and mechanism of action of two histidine residues underlying high-affinity Zn2+ inhibition of the NMDA receptor. Neuron *23*, 171-180.

Clayton, A., Siebold, C., Gilbert, R.J., Sutton, G.C., Harlos, K., McIlhinney, R.A., Jones, E.Y., and Aricescu, A.R. (2009). Crystal structure of the GluR2 amino-terminal domain provides insights into the architecture and assembly of ionotropic glutamate receptors. J Mol Biol *392*, 1125-1132.

Coombs, I.D., Soto, D., Zonouzi, M., Renzi, M., Shelley, C., Farrant, M., and Cull-Candy, S.G. (2012). Cornichons modify channel properties of recombinant and glial AMPA receptors. J Neurosci *32*, 9796-9804.

Dalva, M.B., Takasu, M.A., Lin, M.Z., Shamah, S.M., Hu, L., Gale, N.W., and Greenberg, M.E. (2000). EphB receptors interact with NMDA receptors and regulate excitatory synapse formation. Cell *103*, 945-956.

Drummond, J.B., Simmons, M., Haroutunian, V., and Meador-Woodruff, J.H. (2012). Upregulation of cornichon transcripts in the dorsolateral prefrontal cortex in schizophrenia. Neuroreport *23*, 1031-1034.

Dutta, A., Shrivastava, I.H., Sukumaran, M., Greger, I.H., and Bahar, I. (2012). Comparative dynamics of NMDA- and AMPA-glutamate receptor N-terminal domains. Structure *20*, 1838-1849.

Farina, A.N., Blain, K.Y., Maruo, T., Kwiatkowski, W., Choe, S., and Nakagawa, T. (2011). Separation of domain contacts is required for heterotetrameric assembly of functional NMDA receptors Journal of Neuroscience.

Frank, R. (1995). Simultaneous and combinatorial chemical synthesis techniques for the generation and screening of molecular diversity. J Biotechnol *41*, 259-272.

Gielen, M., Le Goff, A., Stroebel, D., Johnson, J.W., Neyton, J., and Paoletti, P. (2008). Structural rearrangements of NR1/NR2A NMDA receptors during allosteric inhibition. Neuron *57*, 80-93.

Gielen, M., Siegler Retchless, B., Mony, L., Johnson, J.W., and Paoletti, P. (2009). Mechanism of differential control of NMDA receptor activity by NR2 subunits. Nature *459*, 703-707.

Hashimoto, K., Fukaya, M., Qiao, X., Sakimura, K., Watanabe, M., and Kano, M. (1999). Impairment of AMPA receptor function in cerebellar granule cells of ataxic mutant mouse stargazer. J Neurosci *19*, 6027-6036.

Hatton, C.J., and Paoletti, P. (2005). Modulation of triheteromeric NMDA receptors by N-terminal domain ligands. Neuron *46*, 261-274.

Jackson, A.C., and Nicoll, R.A. (2011). The expanding social network of ionotropic glutamate receptors: TARPs and other transmembrane auxiliary subunits. Neuron *70*, 178-199.

Jin, R., Singh, S.K., Gu, S., Furukawa, H., Sobolevsky, A.I., Zhou, J., Jin, Y., and Gouaux, E. (2009). Crystal structure and association behaviour of the GluR2 amino-terminal domain. EMBO J *28*, 1812-1823.

Kalashnikova, E., Lorca, R.A., Kaur, I., Barisone, G.A., Li, B., Ishimaru, T., Trimmer, J.S., Mohapatra, D.P., and Diaz, E. (2010). SynDIG1: an activity-regulated, AMPA- receptor-interacting transmembrane protein that regulates excitatory synapse development. Neuron *65*, 80-93.

Kang, M.G., Nuriya, M., Guo, Y., Martindale, K.D., Lee, D.Z., and Huganir, R.L. (2012). Proteomic analysis of AMPA receptor complexes. J Biol Chem.

Karakas, E., Simorowski, N., and Furukawa, H. (2009). Structure of the zinc-bound amino-terminal domain of the NMDA receptor NR2B subunit. EMBO J *28*, 3910-3920.

Karakas, E., Simorowski, N., and Furukawa, H. (2011). Subunit arrangement and phenylethanolamine binding in GluN1/GluN2B NMDA receptors. Nature *475*, 249-253.

Kato, A.S., Gill, M.B., Ho, M.T., Yu, H., Tu, Y., Siuda, E.R., Wang, H., Qian, Y.W., Nisenbaum, E.S., Tomita, S., and Bredt, D.S. Hippocampal AMPA Receptor Gating Controlled by Both TARP and Cornichon Proteins. Neuron *68*, 1082-1096.

Kato, A.S., Gill, M.B., Ho, M.T., Yu, H., Tu, Y., Siuda, E.R., Wang, H., Qian, Y.W., Nisenbaum, E.S., Tomita, S., and Bredt, D.S. (2010). Hippocampal AMPA Receptor Gating Controlled by Both TARP and Cornichon Proteins. Neuron *68*, 1082-1096.

Leuschner, W.D., and Hoch, W. (1999). Subtype-specific assembly of alpha-amino-3-hydroxy-5-methyl-4-isoxazole propionic acid receptor subunits is mediated by their n-terminal domains. J Biol Chem *274*, 16907-16916.

Matsuda, K., Miura, E., Miyazaki, T., Kakegawa, W., Emi, K., Narumi, S., Fukazawa, Y., Ito-Ishida, A., Kondo, T., Shigemoto, R.*, et al.* (2010). Cbln1 is a ligand for an orphan glutamate receptor delta2, a bidirectional synapse organizer. Science *328*, 363-368.

Matsuda, S., Kamiya, Y., and Yuzaki, M. (2005). Roles of the N-terminal domain on the function and quaternary structure of the ionotropic glutamate receptor. J Biol Chem *280*, 20021-20029.

Menuz, K., Stroud, R.M., Nicoll, R.A., and Hays, F.A. (2007). TARP auxiliary subunits switch AMPA receptor antagonists into partial agonists. Science *318*, 815-817.

Nakagawa, T., Cheng, Y., Ramm, E., Sheng, M., and Walz, T. (2005). Structure and different conformational states of native AMPA receptor complexes. Nature *433*, 545-549.

Nicoll, R.A., Tomita, S., and Bredt, D.S. (2006). Auxiliary subunits assist AMPA-type glutamate receptors. Science *311*, 1253-1256.

O'Brien, R.J., Xu, D., Petralia, R.S., Steward, O., Huganir, R.L., and Worley, P. (1999). Synaptic clustering of AMPA receptors by the extracellular immediate-early gene product Narp. Neuron *23*, 309-323.

O'Hara, P.J., Sheppard, P.O., Thogersen, H., Venezia, D., Haldeman, B.A., McGrane, V., Houamed, K.M., Thomsen, C., Gilbert, T.L., and Mulvihill, E.R. (1993). The ligand-binding domain in metabotropic glutamate receptors is related to bacterial periplasmic binding proteins. Neuron *11*, 41-52.

Paas, Y. (1998). The macro- and microarchitectures of the ligand-binding domain of glutamate receptors. Trends Neurosci *21*, 117-125.

Passafaro, M., Nakagawa, T., Sala, C., and Sheng, M. (2003). Induction of dendritic spines by an extracellular domain of AMPA receptor subunit GluR2. Nature *424*, 677-681.

Perin-Dureau, F., Rachline, J., Neyton, J., and Paoletti, P. (2002). Mapping the binding site of the neuroprotectant ifenprodil on NMDA receptors. J Neurosci *22*, 5955-5965.

Rossmann, M., Sukumaran, M., Penn, A.C., Veprintsev, D.B., Babu, M.M., and Greger, I.H. (2011). Subunit-selective N-terminal domain associations organize the formation of AMPA receptor heteromers. Embo J *30*, 959-971.

Saglietti, L., Dequidt, C., Kamieniarz, K., Rousset, M.C., Valnegri, P., Thoumine, O., Beretta, F., Fagni, L., Choquet, D., Sala, C.*, et al.* (2007). Extracellular interactions between GluR2 and N-cadherin in spine regulation. Neuron *54*, 461-477.

Schwenk, J., Harmel, N., Brechet, A., Zolles, G., Berkefeld, H., Muller, C.S., Bildl, W., Baehrens, D., Huber, B., Kulik, A.*, et al.* (2012). High-resolution proteomics unravel architecture and molecular diversity of native AMPA receptor complexes. Neuron *74*, 621-633.

Schwenk, J., Harmel, N., Zolles, G., Bildl, W., Kulik, A., Heimrich, B., Chisaka, O., Jonas, P., Schulte, U., Fakler, B., and Klocker, N. (2009). Functional proteomics identify cornichon proteins as auxiliary subunits of AMPA receptors. Science *323*, 1313-1319.

Shanks, N.F., Maruo, T., Farina, A.N., Ellisman, M.H., and Nakagawa, T. (2010). Contribution of the global subunit structure and stargazin on the maturation of AMPA receptors. J Neurosci *30*, 2728-2740.

Shanks, N.F., Savas, J.N., Maruo, T., Cais, O., Hirao, A., Oe, S., Ghosh, A., Noda, Y., Greger, I.H., Yates, J.R., 3rd, and Nakagawa, T. (2012). Differences in AMPA and Kainate Receptor Interactomes Facilitate Identification of AMPA Receptor Auxiliary Subunit GSG1L. Cell Rep *1*, 590-598.

Shi, Y., Suh, Y.H., Milstein, A.D., Isozaki, K., Schmid, S.M., Roche, K.W., and Nicoll, R.A. (2010). Functional comparison of the effects of TARPs and cornichons on AMPA receptor trafficking and gating. Proc Natl Acad Sci U S A *107*, 16315-16319.

Sia, G.M., Beique, J.C., Rumbaugh, G., Cho, R., Worley, P.F., and Huganir, R.L. (2007). Interaction of the N-terminal domain of the AMPA receptor GluR4 subunit with the neuronal pentraxin NP1 mediates GluR4 synaptic recruitment. Neuron *55*, 87-102.

Sukumaran, M., Rossmann, M., Shrivastava, I., Dutta, A., Bahar, I., and Greger, I.H. (2011). Dynamics and allosteric potential of the AMPA receptor N-terminal domain. EMBO J *30*, 972-982.

Tomita, S., Adesnik, H., Sekiguchi, M., Zhang, W., Wada, K., Howe, J.R., Nicoll, R.A., and Bredt, D.S. (2005). Stargazin modulates AMPA receptor gating and trafficking by distinct domains. Nature *435*, 1052-1058.

Trakhanov, S., Vyas, N.K., Luecke, H., Kristensen, D.M., Ma, J., and Quiocho, F.A. (2005). Ligand-free and -bound structures of the binding protein (LivJ) of the Escherichia coli ABC leucine/isoleucine/valine transport system: trajectory and dynamics of the interdomain rotation and ligand specificity. Biochemistry *44*, 6597-6608.

Turetsky, D., Garringer, E., and Patneau, D.K. (2005). Stargazin modulates native AMPA receptor functional properties by two distinct mechanisms. J Neurosci *25*, 7438-7448.

Vandenberghe, W., Nicoll, R.A., and Bredt, D.S. (2005). Stargazin is an AMPA receptor auxiliary subunit. Proc Natl Acad Sci U S A *102*, 485-490.

von Engelhardt, J., Mack, V., Sprengel, R., Kavenstock, N., Li, K.W., Stern-Bach, Y., Smit, A.B., Seeburg, P.H., and Monyer, H. (2010). CKAMP44: a brain-specific protein attenuating short-term synaptic plasticity in the dentate gyrus. Science *327*, 1518-1522.

Figures

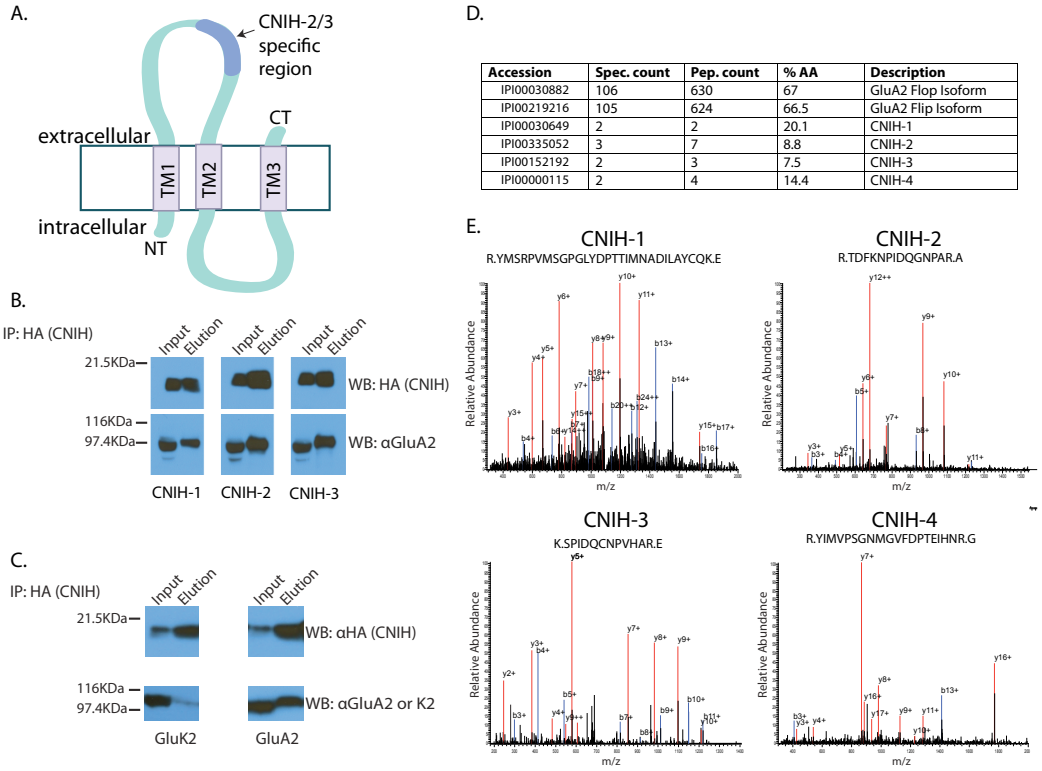

Accession	Spec. count	Pep. count	% AA	Description
IPI00030882	106	630	67	GluA2 Flop Isoform
IPI00219216	105	624	66.5	GluA2 Flip Isoform
IPI00030649	2	2	20.1	CNIH-1
IPI00335052	3	7	8.8	CNIH-2
IPI00152192	2	3	7.5	CNIH-3
IPI00000115	2	4	14.4	CNIH-4

Figure 4_1: Specificity of Interaction between AMPA-Rs and CNIHs
(A) Cartoon schematic of CNIH molecules showing the basic topolgy. They have three transmembrane domains (TM1-3), and intracellular N-terminal domain (NT), and an extracellular C-terminal domain (CT). The intracellular loop has an extra sequence present in homologues CNIH-2/3 but lacking in CNIH-1/4 (shown in blue) **(B)** HEK cell CoIPs. CNIH-1, 2, and 3HA that were co-expressed with GluA2 were pulled down with the HA antibody. Western blots were probed with HA to recognize recombinant CNIH-3 and GluA2 antibody.
(C) HEK cell CoIPs. CNIH-3HA that was co-expressed with either GluA2 or GluK2 was pulled down with an HA antibody. Western blots were probed with HA to recognize recombinant CNIH-3 and GluA2 or GluK2 antibodies. Detergent solubilized inputs and CNIH-3HA pull down elutions are depicted. **(D)** Native AMPA-Rs were purified from human cortex using a GluA2 antibody. This sample of AMPA-R interacting proteins was analyzed by mass spectrometry (LC-MS/MS on Velos Orbitrap mass spectrometers) The MS data presented here had a dataset protein false discovery rate was <5% at the protein level, required two peptides per protein, and at least one end of each peptide tryptic. The table summarizes CNIH homolgues that co-purifiied with GluA2 from this human sample. The spectrum count (Spec), peptidecount (Pep), and coverage percentage (%AA) identified by LC-MS/MS are listed for proteins**. (E)** Human GluA2 AP-MS from cortex identifies distinct peptides for CNIH-1, CNIH-2, CNIH-3, CNIH-4. Shown are representative MS/MS spectra which each CNIH isoform was successfully identified.

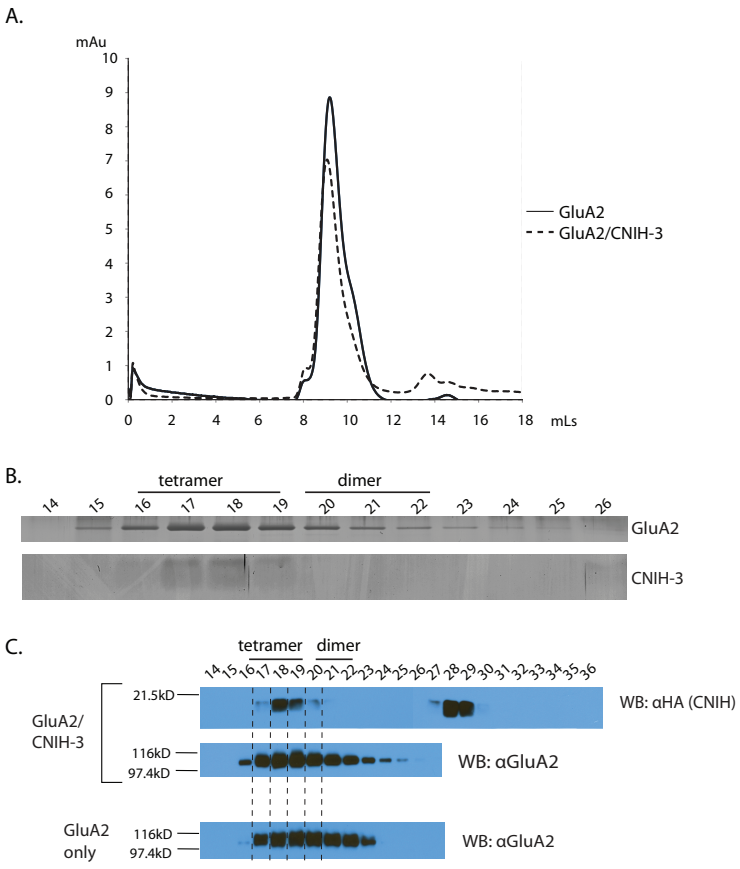

Figure 4_2: Co-purification of CNIH-3 with the GluA2 Complex
(A) Gel filtration elution profiles of both the GluA2 alone (solid line) purification and the GluA2/CNIH-3 (dotted line) purification. **(B)** Silver stain of the gel filtration fractions of the GluA2/CNIH3 purification demonstrating the presence of both GluR2 and CNIH-3. Top panel shows GluA2, and bottom shows CNIH-3. **(C)** Western blotting of the gel filtration fractions of the GluR2/CNIH-3 purification (top two panels) and GluA2 only purification (bottom), probed with either HA antibody to recognize CNIH-3 or GluA2 antibody. CNIH-3 is present in the same fractions as GluA2, demonstrating that they co-purify.

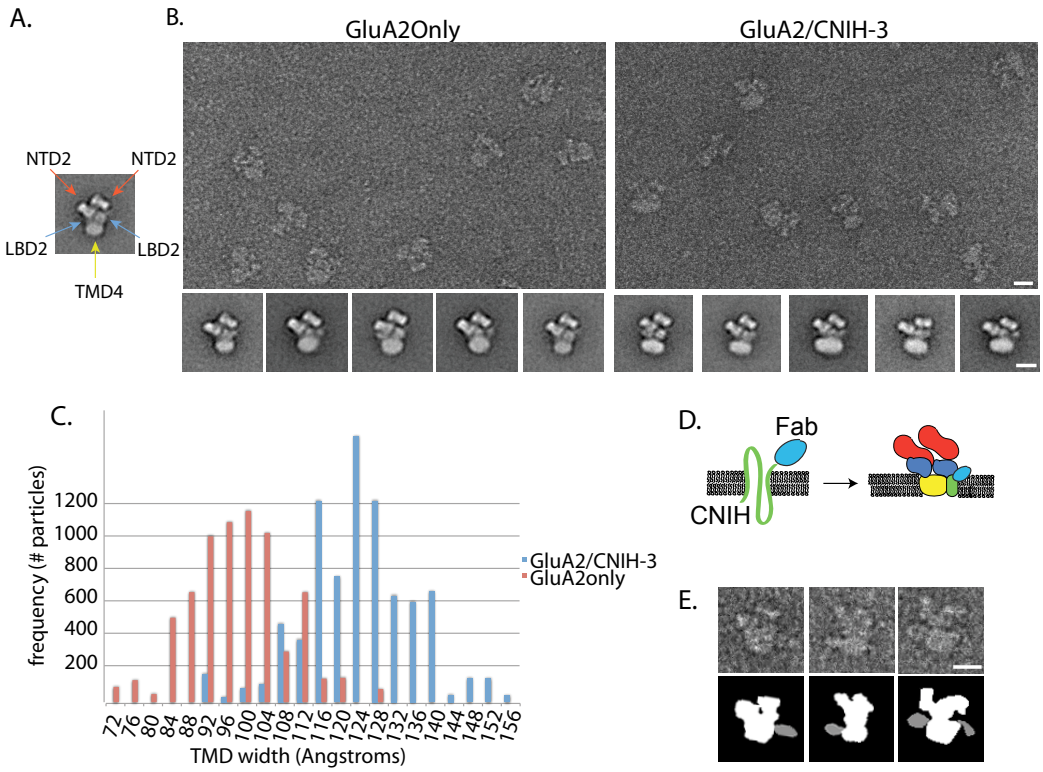

Figure 4_3: CNIH-3 contributes to the membrane density of GluA2 complex
(A) Tetrameric HEK cell-derived AMPA-R class average marked with domain assignments. NTD=N-terminal domain, LBD=ligand binding domain, and TMD=transmembrane domain. Proceeding numbers represent dimeric (2) or tetrameric (4) nature of labeled domain. **(B)** Large representative raw images (upper) and representative class averages (lower) of GluA2only (left) and GluA2/CNIH3 (right) particles purified from HEK cells. Scale bars=10nm. **(C)** Histogram of the TMD widths of the particles from GluA2 (red) and GluA2/CNIH-3 (blue) particles demonstrating a clear shift in size. **(D)** Cartoon schematic of Fab fragment labeling of the extracellular C-terminus of CNIH-3 in relation to the AMPA-R complex. **(E)** Raw images of representative Fab labeled AMPA-R particles (top) and a cartoon version of each raw image to facilitate interpretation (bottom) in which the receptor complexes are shown in white and the fab fragments in gray. Scale bar=10nm.

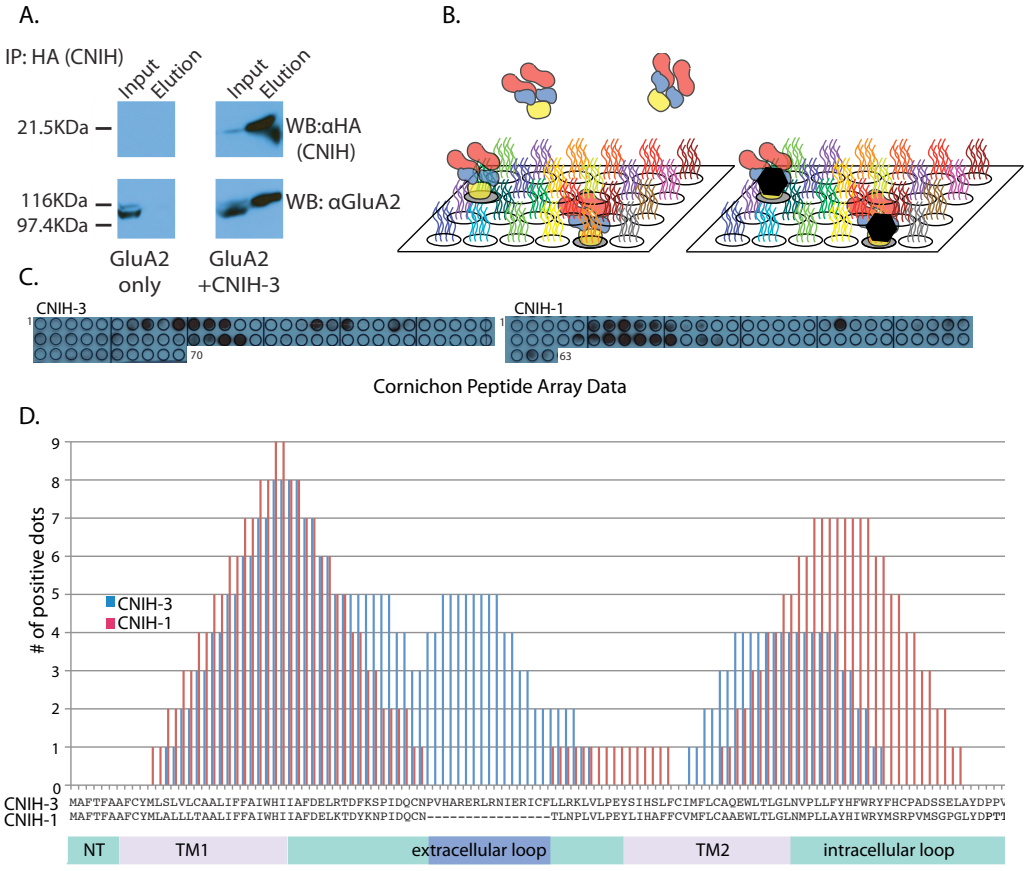

Figure 4_4: Identification of specific CNIH-3 residues critical for interaction with GluA2 **(A)** HEK cell CoIPs. CNIH-3HA and GluA2 were expressed separately, and the cell lysates mixed later. CNIH-3 was pulled down using HA antibody. Western blots were probed with HA to recognize recombinant CNIH-3 and GluA2 antibody. This demonstrates a robust interaction between the proteins in an in vitro system. **(B)** Cartoon of peptide array assay. 20 amino acid peptides spanning the entire CNIH-3 protein shifted by 3 amino acids are synthesized onto a blot. Purified AMPA-R protein is incubated on peptide arrays, and western blotting is carried out to determine which peptides AMPA-Rs are bound to. **(C)** Western blot of peptide array. The top left dot on each array represents the first 20 amino acids of the protein. Dots go from left to right to cover whole sequence. Blackened dots are positive for AMPA-R binding. **(D)** Histogram representing the number of positive dots for each amino acid in the aligned protein sequences (shown across x-axis with CNIH-3 on top and CNIH-1 on bottom) CNIH-3 is represented in blue and CNIH-1 in red. Below the amino acids on the x-axis is a schematic showing the corresponding domain assignments: NT=N-terminus, intra and extracellular loops, and CT=C-terminus (all in green) and TM1-2=transmembrane domains (in violet). The region present in CNIH-3 but lacking in CNIH-1 is shown in blue.

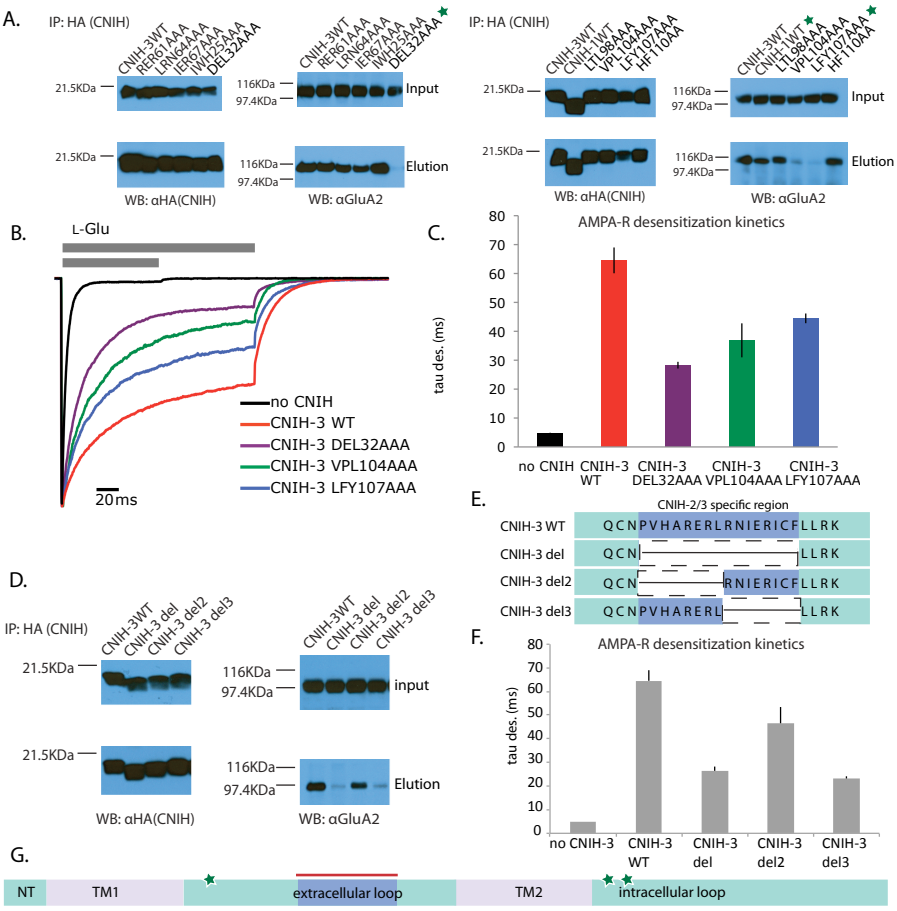

Figure 4_5: CNIH mutants show reduced interaction with GluA2
(A) We created alanine mutants spanning the regions that came up highly positive for AMPA-R binding on the peptide arrays. Western blots showing CoIPs of GluA2 and CNIH-3 mutants co-expressed in HEK cells. Pull down was through HA on CNIH-1, CNIH-3 or CNIH-3 mutants. Inputs are shown on the top and CNIH-HA elutions on bottom. CNIH-3 mutants: DEL32AAA, VPL104AAA, and LFY107AAA show reduced interaction with GluA2. The location of these mutants is noted with a green star in domain assignments schematic in 5D. **(B)** Representative recordings (normalized) from outside out patches obtained from HEK cells expressing GluA2 and various CNIH mutants. Glutamate was applied for 100ms in the absence of CNIH and for 200ms in the presence of CNIH variants using fast ligand application methods. The CNIH-3 mutants show a reduced ability to modulate AMPA-R desensitization **(C)** Summary graph of time constants of AMPA-R desensitization in the presence or absence of CNIH-3 variants. **(D)** Western blots showing CoIPs of GluA2 and CNIH-3 mutants co-expressed in HEK cells. These mutants have varying amounts of the CNIH-2/3 specific region deleted (see schematic in F for details of deletion mutants). All mutants shown have reduced interaction with GluA2. **(E)** Schematic showing the deletions made to the CNIH-2/3 specific region. **(F)** Summary of time constants of AMPA-R desensitization in the presence or absence of CNIH-3 deletion mutants. **(G)** Schematic of the CNIH-3 domain assignments. Green stars represent areas where mutation of three residues to alanine resulted in decreased interaction with GluA2, and red region is CNIH-2/3 specific region which when deleted also reduced interaction.

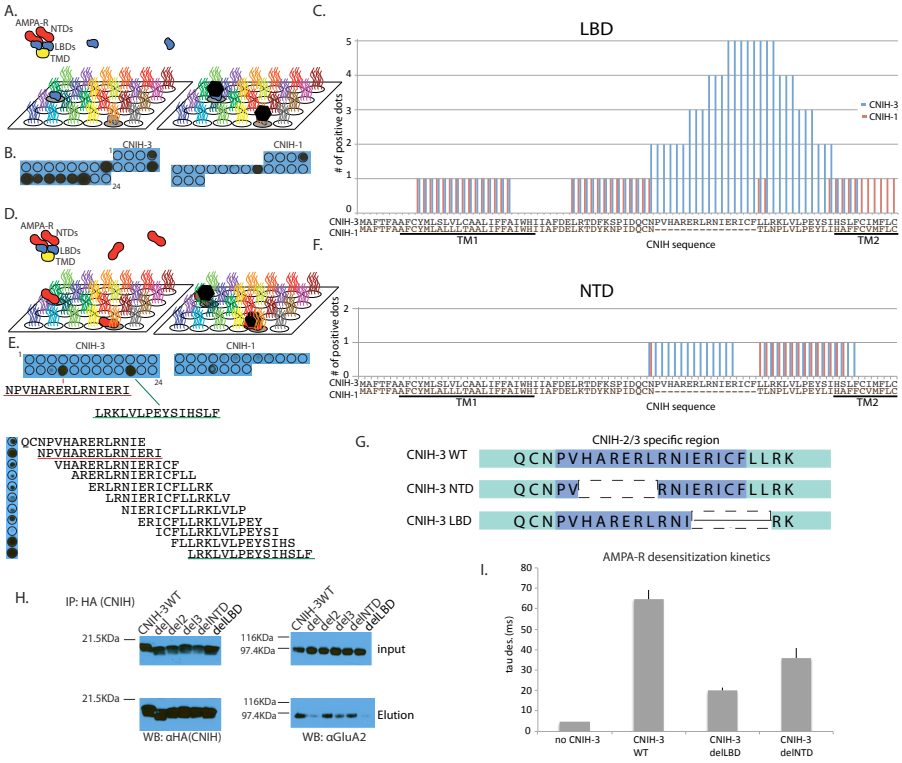

Figure 4_6: Interaction of Isolated AMPA-R Domains with CNIH-3
(A) Cartoon of peptide array assay. Instead of full length AMPA-R protein, the isolated LBD AMPA-R (GluA2 S1S2) is incubated on peptide arrays, and western blotting is carried out to determine which peptides AMPA-Rs are bound to. **(B)** Western blot of peptide array with LBD. The top left dot on each array represents the first 20 amino acids of the protein. Dots go from left to right to cover whole sequence. Blackened dots are positive for AMPA-R binding. **(C)** Histogram representing the number of positive dots for each amino acid in the aligned protein sequence for CNIH-3 and CNIH-1 when GluA2 LBD was applied**. (D)** Cartoon of peptide array assay. Instead of full length AMPA-R protein, the isolated NTD AMPA-R (GluA2 NTD) is incubated on peptide arrays, and western blotting is carried out to determine which peptides AMPA-Rs are bound to. **(E)** Top: Western blot of peptide array with NTD. The top left dot on each array represents the first 20 amino acids of the protein. Dots go from left to right to cover whole sequence overlapping by 3 amino acids each time. Blackened dots are positive for AMPA-R binding. Bottom: alternate peptide array for the NTD, in which the peptides were shifted by two amino acids not 3, but represented that same portion of the CNIH molecule. The peptide sequences underlined in re and green are identical between the top and bottom. **(F)** Histogram representing the number of positive dots for each amino acid in the aligned protein sequence for CNIH-3 and CNIH-1 when GluA2 NTD was applied. **(G)** Schematic showing the deletions made to CNIH-3. These deletions are based on the highest hit residues from the peptide array results. CNIH-3delNTD and CNIH-3delLBD are the mutants in which the hot spots identified for the NTD and LBD were deleted. **(H)** Western blots showing CoIPs of GluA2 and CNIH-3 mutants co-expressed in HEK cells. Inputs are shown on the top and CNIH-HA elutions on bottom. Both CNIH-3 NTD and LBD deletion mutants show a reduced interaction with GluA2, although this is more pronounced for the LBD mutant. **(I)** Summary of time constants of AMPA-R desensitization in the presence or absence of CNIH-3 deletion mutants.

Supplementary Figures

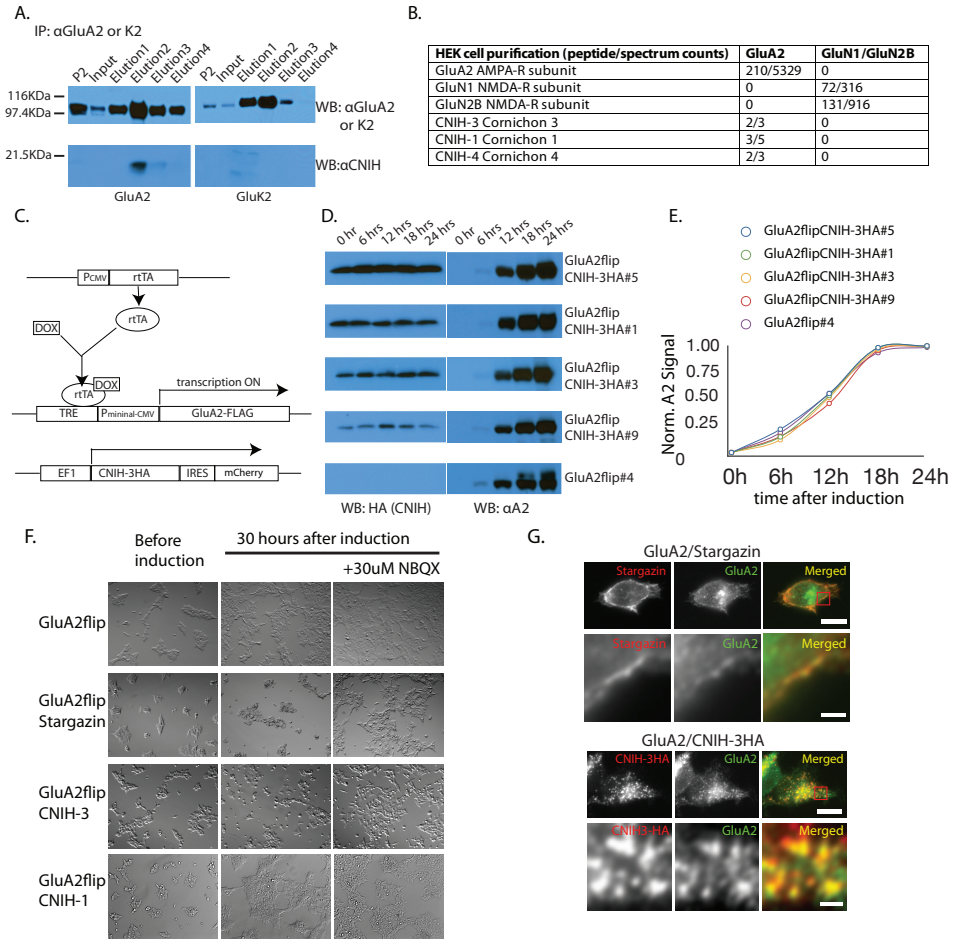

Figure 4_S1: AMPA-Rs interact physically and functionally with CNIHs
(A) Western blots of GluA2 or GluK2 IP from rat brain probed with GluA2, or GluK2 and CNIH antibody (Hoshino et al., 2007) The P2 fractions, post detergent solubilized inputs and IP four elutions are shown for each IP. **(B)** Endogenous proteins in HEK cells that interact with either GluA2 or GluN1/GluN2B identified by mass spectrometry. **(C)** Schematic of strategy to co-express GluA2 and CNIH3-HA in HEK cells: TetOn System of protein induction in which the addition of DOX to the cell media promotes GluA2Flag production in a cell line which stably expresses CNIH-3HA IRESmcherry **(D)** Western blots showing time course of protein expression after addition of DOX to the HEK cell media in GluA2 only parental cell line (bottom) and different GluA2/CNIH-3 cell lines (above). **(E)** Quantification of GluA2 expression time course after induction in different cell lines. Signal densities are normalized to 24 hour time point. **(F)** Cell death assay of GluA2 only parental cell line, GluA2/stargazin, GluA2/CNIH-3HA and GluA2/CNIH-1HA cell lines. DIC images of HEK cells are provided before DOX-induction of GluA2 and 30 hours after induction both in the absence and presence of the competitive AMPA-R antagonist NBQX. Scale bar = 50μm. **(G)** Immunofluorescent images of GluA2/CNIH-3HA cells 24hr after DOX induction. GluA2 is in green, and CNIH-3HA in red. Lower panels are enlarged images of inset in upper images. Scale bar = 10μm (upper panels) or 2μm (lower panels). GluA2 and CNIH-3 colocalize primary intracellularly.

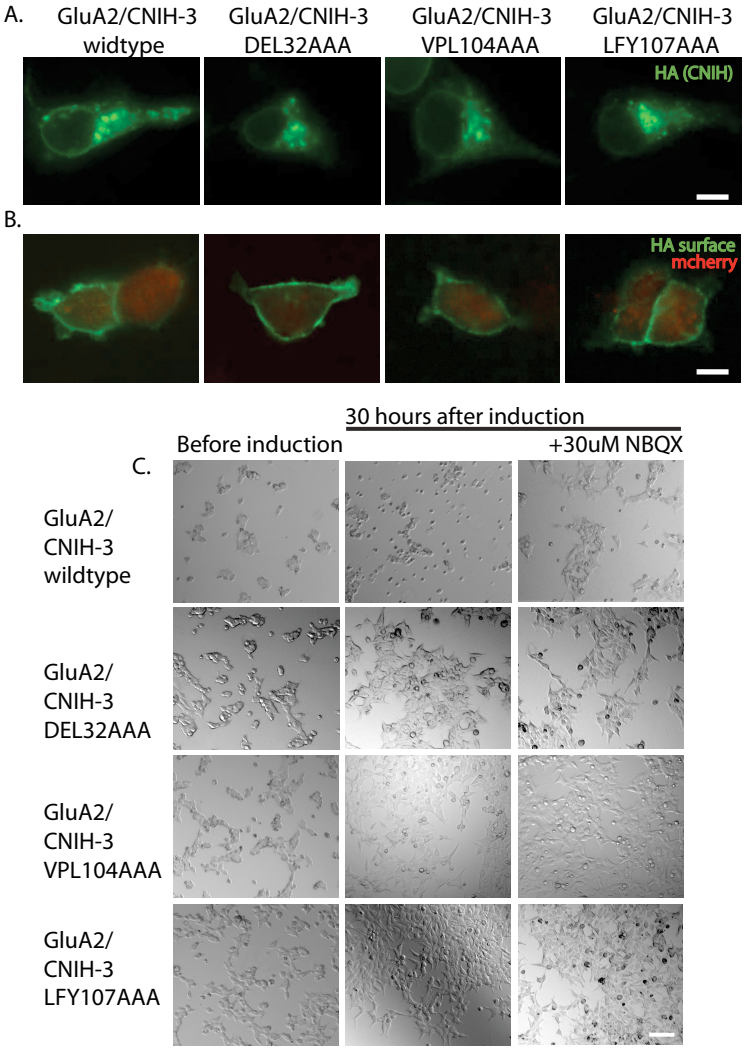

Figure 4_S5: CNIH-3 mutants reduce interaction with GluA2
(A) Subcellular distribution of CNIH-3 and CNIH-3 mutants that showed decreased interaction in HEK cells stained using anti-HA antibody (green).
Scale bar=10um. The mutants show similar distributions in the cell to CNIH-3WT.
(B) CNIH-HA surface staining (shown in green) done in HEK cells lines expressing CNIH-3 or CNIH-3 mutants and GluA2. Cells positive for CNIH-3 or CNIH-3 mutants are red due to presence of mcherry. Scale bar =10um. The mutants can all localize to the cell surface like CNIH-3WT, indicating that they are not mislocalized in the cell. **(C)** Cell death assay of GluA2/CNIH-3WT or mutant cell lines. DIC images of HEK cells are provided before DOX-induction of GluA2 and 30 hours after induction both in the absence and presence of the competitive AMPA-R antagonist NBQX. Scale bar = 50μm. The co-expression of CNIH-3WT but not the mutants leads to AMPA-R mediated cell death.

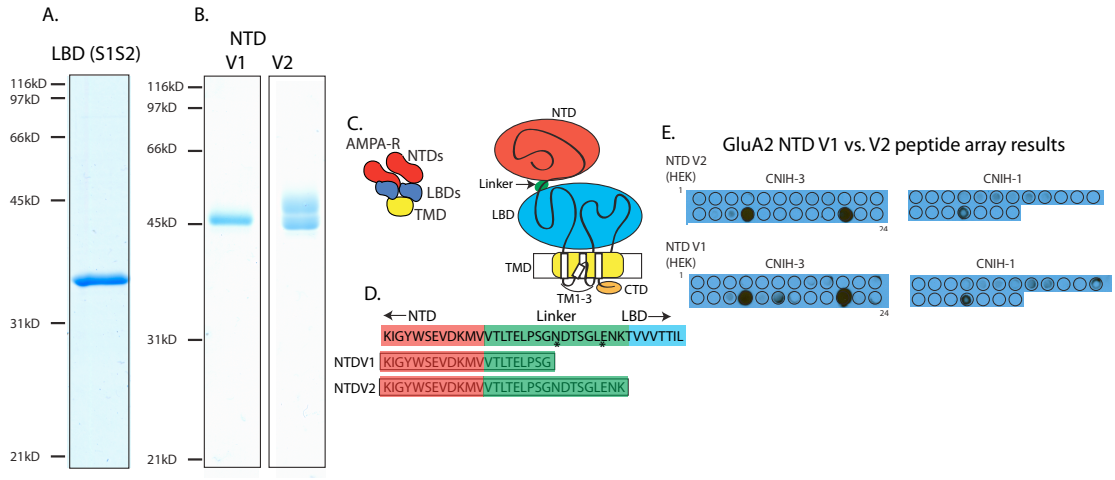

Figure 4_S6: GluA2 LBD and NTD domain purifications
(A) Purified GluA2LBD from peak gel filtration fraction run on SDS-page gel and stained with coomassie blue **(B)** Purified GluA2NTD from peak gel filtration fraction run on SDS-page gel and stained with coomassie blue. 2 version of this NTD are V1 and V2. **(C)** Schematic of tetrameric (left) and single AMPA-R subunit (right) showing the different domains including LBD (blue) and NTD (red) with the NTD-LBD linker in green. **(D)** Schematic representing the differences between the AMPA-R NTD V1 and V2. V2 contains the entire NTD-LBD linker region which includes to glycosylation sites. **(E)** Western blots of peptide arrays with NTD V2 (top) and NTD V1 (bottom). The top left dot on each array represents the first 20 amino acids of the protein. Dots go from left to right to cover whole sequence overlapping by 3 amino acids each time. Blackened dots are positive for NTD binding. Note that the results are identical for both versions.

Acknowledgements

Chapter IV, in full, is currently being prepared for submission for publication. Shanks, Natalie F.; Cais, Ondrej; Maruo, Tomohiko; Savas, Jeffrey N; Yates. John R. III; Greger, Ingo H.; Nakagawa, Terunaga. The dissertation author is the primary investigator and author of the manuscript. Permission of all authors has been obtained.

We thank Osamu Chisaka (Kyoto Univ.) for anti-CNIH antibody and C.J Allison for preparing the original peptide array. We acknowledge the use of the UCSD Cryo-Electron Microscopy Facility which was supported by NIH grants 1S10RR20016 and GM033050 to Dr. Timothy S. Baker and a gift from the Agouron Institute to UCSD. N.F.S was partially supported by the NIH Molecular Biophysics Training Grant (NIH GM08326). This work was supported by NIH grant R01HD061543 (to T.N.).

Chapter V

Conclusions and Discussion

AMPA-Rs are the primary mediators of fast excitatory transmission in the central nervous system. Decades of work has revealed that AMPA-Rs exhibit diversity in functional properties. Such diversity allows synapses to have unique properties, thus enabling different types of information transfer in the central nervous system. AMPA-Rs are assembled from different combinations of subunits that can undergo RNA editing and exist as different splice variants, leading to a range of functional properties. To further complicate that matter, we now know of multiple families of AMPA-R auxiliary subunits that associate with AMPA-Rs and can modulate AMPA-R localization and channel kinetics. Taken together, the combinatorial possibilities lead to a very diverse and complicated functional repertoire for AMPA-Rs.

Such a strategy to achieve functional diversity is not unique to the mammalian brain. Infact, genetic screens in the simple invertebrate nematode, C. elegans have led to the identification of auxiliary proteins that regulate their own AMPA-R homologue, GLR-1. As in mammals, GLR-1 appears to be a multiprotein receptor signalling complex. SOL-1, a CUB domain containing transmembrane protein is required for GLR-1 current function (Zheng et al., 2004), and regulates GLR-1 desensitization kinetics (Walker et al., 2006;

Zheng et al., 2006) This GLR-1 complex contains SOL-1 along with a C. elegans TARP homologue, STG-1 or STG-2, which have conserved roles as AMPA-R auxiliary subunits (Wang et al., 2008). There is also a cornichon homologue present in C. elegans (Accession CAB01516). Further characterization of CNIHs in C. elegans will reveal if they play similar roles as in the mamailian CNS, and also whether other emerging families of AMPA-R auxiliary subunits in mammals will have homologues in simpler organisms. The mammalian Neto proteins are similar to the SOL-1 homologue in that they are also single pass transmembrane proteins with extracellular CUB domains, however SOL-1 and the mammalian Neto proteins belong to different families of CUB domain containing proteins. Neto2 was identified as a KA-R auxiliary subunit (Zheng et al., 2004). Both Neto2 and its homologue Neto1 have been shown to slow the decay kinetics of KA-Rs (Fisher and Mott, 2012; Tomita and Castillo, 2012), and Neto1 also functionally interacts with NMDA-Rs (Ng et al., 2009). More recently, it was discovered that C. elegans SOL-2 interacts with the GLR-1 complex, and that both SOL-1 and SOL-2 can modify the channel properties of GLR-1 (Wang et al., 2012). Interestingly, SOL-2 is closely related to the mammalian Neto proteins. Given the role for Netos in mammalian KA-R but not AMPA-R function, they tested whether C. elgans SOL-2 could modify KA-R function in heterologous systems. Unlike the Neto proteins, SOL-2 could not modify KA-R channel properties (Wang et al., 2012). It is interesting that in the case of SOL/Netos, structurally related auxiliary subunits modulate

different glutamate receptor subtypes, while in the case of the TARPs, the function seems to be restricted to AMPA-Rs. C. elegans also has many different GLR types, (Brockie and Maricq, 2006), and the full investigation of their modulation by accessory proteins is still underway. What is clear is that C. elegans have a very simplistic nervous system with stereotyped neuronal connectivity, yet like mammals, they also utilize auxiliary subunits to diversify glutamatergic transmission within their neural circuitry.

AMPA-Rs are essential neuronal communication components, and uncovering their interacting partners in order to better understand their function is still an active avenue of research. Stargazin and the TARP homologues were functionally validated as AMPA-R interactors and modulators (reviewed in (Jackson and Nicoll, 2011). Only recently, over a decade later, have novel transmembrane AMPA-R interactors been identified and validated as unique AMPA-R auxiliary subunits (Schwenk et al., 2009; von Engelhardt et al., 2010). The identification of novel AMPA-R interactors and characterization of new AMPA-R auxiliary subunits greatly contributes to our knowledge of the synaptic molecular machinery that regulated glutamate receptor function in the brain.

Novel AMPA-R auxiliary subunits

The research described Chapter 3 of this dissertation describes one such proteomic endeavor to uncover novel uncovering novel AMPA-R auxiliary subunits. In this mass spectrometry study, we sought to better understand the molecular composition of two glutamate receptor subtypes at the synapse: AMPA and kainate receptors. This proteomic analyis was particularly fruitful, due to the combination of our robust purification protocols (Nakagawa et al., 2005) with liquid chromatographic separations in line with tandem mass spectrometers (LC-MS/MS). For the most comprehensive analysis, we directly analyzed the samples using multidimensional protein identification technology (MudPIT) (Washburn et al., 2001), resulting in lengthy lists of synaptic proteins present in the samples. In this manner, we identified the majority of known interacting proteins for both receptor types, validating our methodology and, more importantly, the resulting comparative interactome data is a useful resource and provides novel candidates for further studies.

By following up on candidates from the list, ultimately, this study identified a novel AMPA-R auxiliary subunit. Peptides for GSG1L appeared in our AMPA-R interactor list with relatively high abundance. While only a predicted protein at the time, the GSG1L gene was implicated to play roles in the nervous system. (Bruses, 2010; Lai et al., 2011). Both GSG1L and TARPs

are members of the tetraspanin superfamily, but GSG1L belongs to the evolutionarily distant claudin family, and while structurally similar, the actual sequences are not well conserved. Like the other known auxiliary subunits, GSG1L increases AMPA-R surface trafficking in HEK cells, and also changes AMPA-R channel gating kinetics. Similar to the TARPs and also to the CNIHs, which are structurally unrelated AMPA-R auxiliary subunits, GSG1L appears to slow the desensitization of AMPA-Rs. However, in stark contrast to the TARPs, which greatly speed recovery from the desensitized state, GSG1L infact significantly slows this parameter, a feature that the structurally unrelated Cys-knot protein CKAMP44 (von Engelhardt et al., 2010) also confers on AMPA-Rs. Therefore, the addition of GSG1L to an AMPA-R complex prolongs the channel open time by slowing the desensitization parameter, but also increases the amount of time before the channel can be reused by slowing the recovery. Desensitization and recovery from the desensitization are parameters that affect the frequency transmission (Arai and Lynch, 1998). Synaptic AMPA-Rs associated with GSG1L may be useful in the temporal summation of synaptic events upon single activation, but would not be useful in faithfully transmitting high frequency spike trains. Ultimately, the most important question remaining is how GSG1L functions to modulate AMPA-Rs in the brain.

Further work is also necessary to define the mechanisms of binding and functional modulation between GSG1L and AMPA-Rs. TARPs functionally modulate AMPA-R by two distinct domains, with the CTD required for synaptic targeting of AMPA-Rs and the first extracellular critical for the modulation of AMPA-R ion channel function (Tomita et al., 2005). Further experiments are required to ascertain whether GSG1L is even involved in AMPA-R synaptic targeting, or simply just AMPA-R surface expression. GSG1L is structurally related to TARPs, however unlike TARPs, the CTD of GSG1L does not contain a conventional PDZ binding motif sequence. Therefore, if GSG1L can interact with the MAGUK scaffolding proteins at the PSD or is involved in the synaptic targeting of AMPA-Rs, the mechanism of such actions is likely distinct from that of the TARPs. The first extracellular loop of TARPs is required for AMPA-R channel modulation (Tomita et al., 2005). This same loop of GSG1L is substantially longer than that of TARPs and, shares only 19% homology with that of stargazin (Fig 1C and S1D of Chapter 3). A cartoon representation of the known AMPA-R auxiliary subunits in mammals is also included as Figure 1 in this final chapter. There are likely mechanistic differences in how GSG1L interacts with AMPA-Rs compared to how TARPs interact. This would account for the distinct properties that GSG1L imparts on AMPA-R function. Even once we understand the exact interactions that occur between all of the known auxiliary subunits and AMPA-Rs, it remains a very large question in the

field, how exactly these interactions can modulate AMPA-R channel kinetics properties in such different ways.

The work in Chapter 3 challenges to answer this critical question, as it identified a novel AMPA-R subunit that confers a unique functional repertoire to AMPA-Rs. This interactome study and the characterization of GSG1L were published in a paper (Shanks et al, 2012) that came out on the same day as a similar and complementary study (Schwenk et al., 2009), further validating the work, and providing an additional resource on the complexity of the AMPA-R interactome. Both publications were together recommended by the Faculty of 1000 (Cull-Candy and Coombs, 2012). This sort of functional variety of AMPA-Rs provided by auxiliary subunits diversifies excitatory modulation of neural circuits.

Mechanisms of Modulation by Auxiliary Subunits

Chapter 4 of this dissertation contributes to our understanding of the specific mechanisms of interaction with and modulation by AMPA-R auxiliary subunits. The focus of the work is one particular family of auxiliary subunits, the cornichon homologues. To date, only CNIH-2 and CNIH-3 were previously shown to interact with AMPA-Rs and modulate their channel properties (Kato et al., 2010; Schwenk et al., 2009; Shi et al., 2010). Work in Chapter 4

highlights that the other CNIH homologues, CNIH-1 and CNIH-4 are likely also important in the brain. CNIH-1 and CNIH-4 can interact with AMPA-R subunits in heterologous cells, although these homologues do not modulate AMPA-R ion channel function like CNIH-2 and CNIH-3 have been shown to (Kato et al., 2010; Shi et al., 2010). Even more interestingly, CNIH-1 and CNIH-4 in addition to CNIH-2 and CNIH-3 co-purify with native AMPA-Rs purified from human brain, but we did not observe this in rat brain, nor have other groups in the past (Schwenk et al., 2012; Schwenk et al., 2009; Shanks et al., 2012). These results about the specificity of interaction between AMPA-Rs and CNIH homologues are very interesting as they suggest novel roles for CNIH-1 and CNIH-4, and possible species-specific differences in AMPA-R modulation.

Part of understanding the interactions of auxiliary subunits with AMPA-Rs involves investigating how they contribute to the structure of the AMPA-R. Like stargazin, CNIH-3 forms a stable complex with tetrameric AMPA-Rs, I report the structures of recombinant AMPA-Rs in the presence vs. absense of CNIH-3 by single particle EM. The contribution of the auxiliary subunit, CNIH-3 to the transmembrane density of the AMPA-R complex observed parallels the contribution of stargazin to the native AMPA-R complex (Nakagawa et al., 2006). Fab fragment labeling clearly suggests that more than one CNIH molecule can simultaneously bind to one tetrameric AMPA-R complex. This method cannot be used strictly quantitatively, as the Fab

fragment binding affinity does not always allow stoichiometric binding. Thus further studies will be required to determine the precise stoichiometric composition of the native AMPA-R/CNIH complex.

The mechanisms of interaction between AMPA-Rs and auxiliary are very poorly understood, even for the TARPs, which have been extensively studied for over a decade. As previously mentioned earlier in this discussion, it was initially believed that stargazin modulates AMPA-R function by two distinct domains: the first exracellular loop modulates AMPA-R channel function and the intracellular intracellular C-terminal tail modulates AMPA-R trafficking (Tomita et al., 2005) Later work demonstated some additional roles for the TARP C-terminus in AMPA-R gating as well as trafficking (Milstein and Nicoll, 2009). While TARPs and CNIHs are both multipass transmembrane proteins, they are otherwise structurally unrelated. Figure 1 in this chapter shows a cartoon schematic of the known AMPA-R auxiliary subunits in mammals. It was previously reported, that like stargazin, the first extracellular loop of CNIH-2 previously is critical for exerting modulatory effects on AMPA-Rs (Kato et al., 2010). Thus, these two unrelated families of auxiliary subunits both modulate AMPA-R channel function using their extracellular loops.

In terms of basic topology, the extracellular loops of auxiliary subunits are likely in close proximity to the LBD of the AMPA-Rs. It has been

hypothesized that the extracellular loop of auxiliary subunits could be capable of interacting with the AMPA-R LBD, and therefore have the ability to modulate channel function either by allowing an increased closure of the S1S2 clamshell or by allowing the more efficient coupling of domain closure to channel pore opening (Menuz et al., 2007; Nicoll et al., 2006). However, such an interaction had never previously been demonstrated.

The work in Chapter 4 provides the direct evidence that the AMPA-R LBD interacts with the CNIH-3 extracellular loop, and further extends this by demonstrating that the other more membrane distal AMPA-R extracellular domain, the NTD can also interact with the extracellular loop. Thus, this study experimentally proves previous hypotheses about the LBD and also suggests a completely novel role for the AMPA-R NTD in which interactions with auxiliary subunits are involved in allosteric modulation of AMPA-R channel function. Such a role for the NTD is of particular interest in the field. Glutamate receptor NTDs share homology and structural similarity to the ligand domains of other proteins, including metabotropic glutamate receptors, mGluR1-8 (O'Hara et al., 1993; Paas, 1998; Trakhanov et al., 2005), and a role for the NTD of NMDA type glutamate receptors in ligand binding and allosteric modulation of ion channel function has been well established (Hatton and Paoletti, 2005; Karakas et al., 2009; Perin-Dureau et al., 2002). No such function has previously been described for AMPA-Rs. Infact, initial

interpretation of the structures of the NTDs of NMDA vs AMPA-type glutamate receptors indicated that such a function for the AMPA-R NTD was likely not even possible due to the fact that the separation across the NTD lobes was less flexible in AMPA and kainate receptors, and could not accommodate the movement required for allosteric actions (Clayton et al., 2009; Jin et al., 2009). However, more recent structural data and computational modeling methods have suggested that AMPA-R NTDs may infact have a more open dimer interface that could allow rotational movements that could be transduced into allosteric motions ultimately affecting receptor gating (Dutta et al., 2012; Sukumaran et al., 2011).

The AMPA-R NTD's previously known roles were primarily in subunit assembly stringency (Ayalon et al., 2005; Ayalon and Stern-Bach, 2001; Leuschner and Hoch, 1999). In addition, they were shown to interact with extracellular proteins including neuronal pentraxins (O'Brien et al., 1999; Sia et al., 2007) and N-cadherin (Passafaro et al., 2003; Saglietti et al., 2007). We now know that the AMPA-R NTD can also interact with the extracellular loop of CNIH-3. This interaction could occur under all conditions or just during AMPA-R gating states. In EM structures, the gross conformation of the AMPA-R complex changes when it is bound to glutamate in favor of the separation of the NTDs in a membrane proximal movement (Nakagawa et al., 2005). Such a conformational change could provide the extracellular loops of

the auxiliary subunit better access to the NTD, and thereby extending the ability of the auxiliary subunit to modify channel gating properties. Figure 1 in in this chapter shows cartoon schematics demonstrating how the AMPA-R NTD may be interacting with the extracellular loop of CNIH-3. Determining the atomic structure of the complex will be necessary to address these ideas more directly. Such interactions may likely extend to other auxiliary subunits. Thus we put forth a model in which the binding of the extracellular loop portion of the auxiliary subunit to the NTD allosterically modulates AMPA-R ion channel function.

The crystal structure of the full length AMPA-Rs (Sobolevsky et al., 2009) brought to light the presence of gaps between the a central cavity ion channel pore and what would be the lipid environment within the transmembrane domain region. The authors speculate that transmembrane residues of auxiliary subunits may be able to occupy these gaps when in complex with AMPA-Rs, thus providing a mechanism by which they could help to modulate the ion channel properties of AMPA-Rs. Such an interpretation is consistent with the primary structural contribution of auxiliary subunits being to the transmembrane density of the AMPA-Rs as seen by EM in Chapter 4 and (Nakagawa et al., 2006). This transmembrane interaction hypothesis could explain the ability of TARPs (Soto et al., 2007) and CNIHs (Coombs et al., 2012) to modify the extent to which intracellular polyamines can block calcium permeable AMPA-Rs. However, we believe that the primary modulatory

effects on gating kinetics are likely mediated by interactions of the auxiliary subunit extracellular loops with the extracellular AMPA-R domains that are allosterically transduced to the transmembrane domain. Chapter 5 helps to elucidate the interactions between AMPA-Rs and CNIHs, which provide novel mechanistic insight into the functional modulation of AMPA-Rs by auxiliary subunits.

Future Directions

With the recent identification of many new auxiliary subunits, this brings up the question of whether there are even more auxiliary subunits left to be discovered, and exactly how complicated this story is going to get. Multiple lines of evidence point towards the idea that CNIHs and TARPs can act together on one AMPA-R complex, and that CNIHs can modulate AMPA-Rs in different manners depending on which TARP isoform is present. It thus seems as if TARPs and CNIHs can act on the AMPA-R in a synergistic manner (Gill et al., 2011; Gill et al., 2012; Kato et al., 2010). Another study suggests that the addition of CNIHs can regulate the number of TARPs associated with the AMPA-R complex, which in turn can modulate AMPA-R pharmacology and gating properties (Gill et al., 2011). The mechanisms of the interplay between TARPs and CNIHs on a single AMPA-R complex have yet to be investigated. It is still unclear whether or not TARPs and CNIHs have distinct binding sites.

Issues of competition or steric hindrance could limit the assembly of AMPA-Rs with too many auxiliary subunits types. We still have no idea whether all of the new auxiliary subunits can interact with AMPA-R complexes containing other auxiliary subunits, or how this might affect the functional parameters of the receptor. The potential interplay between different auxiliary subunits adds a whole other layer of complexity to the functional diversity of AMPA-R function in the brain. Future work will have to be carried out to understand and characterize the interactions both physically and functionally, and ultimately to help us understand how such AMPA-R regulation and modification is relevant in shaping neurotransmission. Ultimately we want to understand the roles of all of these auxiliary subunits in the brain, including during synaptic plasticity, in learning and memory, and during development and disease.

References

Arai, A., and Lynch, G. (1998). AMPA receptor desensitization modulates synaptic responses induced by repetitive afferent stimulation in hippocampal slices. Brain Res *799*, 235-242.

Ayalon, G., Segev, E., Elgavish, S., and Stern-Bach, Y. (2005). Two regions in the N-terminal domain of ionotropic glutamate receptor 3 form the subunit oligomerization interfaces that control subtype-specific receptor assembly. J Biol Chem *280*, 15053-15060.

Ayalon, G., and Stern-Bach, Y. (2001). Functional assembly of AMPA and kainate receptors is mediated by several discrete protein-protein interactions. Neuron *31*, 103-113.

Brockie, P.J., and Maricq, A.V. (2006). Ionotropic glutamate receptors: genetics, behavior and electrophysiology. WormBook, 1-16.

Bruses, J.L. (2010). Identification of gene transcripts expressed by postsynaptic neurons during synapse formation encoding cell surface proteins with presumptive synaptogenic activity. Synapse *64*, 47-60.

Clayton, A., Siebold, C., Gilbert, R.J., Sutton, G.C., Harlos, K., McIlhinney, R.A., Jones, E.Y., and Aricescu, A.R. (2009). Crystal structure of the GluR2 amino-terminal domain provides insights into the architecture and assembly of ionotropic glutamate receptors. J Mol Biol *392*, 1125-1132.

Coombs, I.D., Soto, D., Zonouzi, M., Renzi, M., Shelley, C., Farrant, M., and Cull-Candy, S.G. (2012). Cornichons modify channel properties of recombinant and glial AMPA receptors. J Neurosci *32*, 9796-9804.

Cull-Candy, S and Coombs, I: F1000Prime Recommendation of [Shanks NF et al., Cell Rep 2012, 1(6):590-8]. In F1000Prime, 07 Aug 2012; DOI: 10.3410/f.717952732.793458209. F1000Prime.com/717952732#eval793458209

Dutta, A., Shrivastava, I.H., Sukumaran, M., Greger, I.H., and Bahar, I. (2012). Comparative dynamics of NMDA- and AMPA-glutamate receptor N-terminal domains. Structure *20*, 1838-1849.

Fisher, J.L., and Mott, D.D. (2012). The auxiliary subunits Neto1 and Neto2 reduce voltage-dependent inhibition of recombinant kainate receptors. J Neurosci *32*, 12928-12933.

Gill, M.B., Kato, A.S., Roberts, M.F., Yu, H., Wang, H., Tomita, S., and Bredt, D.S. (2011). Cornichon-2 modulates AMPA receptor-transmembrane AMPA receptor regulatory protein assembly to dictate gating and pharmacology. J Neurosci *31*, 6928-6938.

Gill, M.B., Kato, A.S., Wang, H., and Bredt, D.S. (2012). AMPA receptor modulation by cornichon-2 dictated by transmembrane AMPA receptor regulatory protein isoform. Eur J Neurosci *35*, 182-194.

Hatton, C.J., and Paoletti, P. (2005). Modulation of triheteromeric NMDA receptors by N-terminal domain ligands. Neuron *46*, 261-274.

Jackson, A.C., and Nicoll, R.A. (2011). The expanding social network of ionotropic glutamate receptors: TARPs and other transmembrane auxiliary subunits. Neuron *70*, 178-199.

Jin, R., Singh, S.K., Gu, S., Furukawa, H., Sobolevsky, A.I., Zhou, J., Jin, Y., and Gouaux, E. (2009). Crystal structure and association behaviour of the GluR2 amino-terminal domain. EMBO J *28*, 1812-1823.

Karakas, E., Simorowski, N., and Furukawa, H. (2009). Structure of the zinc-bound amino-terminal domain of the NMDA receptor NR2B subunit. EMBO J *28*, 3910-3920.

Kato, A.S., Gill, M.B., Ho, M.T., Yu, H., Tu, Y., Siuda, E.R., Wang, H., Qian, Y.W., Nisenbaum, E.S., Tomita, S., and Bredt, D.S. (2010). Hippocampal AMPA Receptor Gating Controlled by Both TARP and Cornichon Proteins. Neuron *68*, 1082-1096.

Lai, H.C., Klisch, T.J., Roberts, R., Zoghbi, H.Y., and Johnson, J.E. (2011). In vivo neuronal subtype-specific targets of Atoh1 (Math1) in dorsal spinal cord. J Neurosci *31*, 10859-10871.

Leuschner, W.D., and Hoch, W. (1999). Subtype-specific assembly of alpha-amino-3-hydroxy-5-methyl-4-isoxazole propionic acid receptor subunits is mediated by their n-terminal domains. J Biol Chem *274*, 16907-16916.

Menuz, K., Stroud, R.M., Nicoll, R.A., and Hays, F.A. (2007). TARP auxiliary subunits switch AMPA receptor antagonists into partial agonists. Science *318*, 815-817.

Milstein, A.D., and Nicoll, R.A. (2009). TARP modulation of synaptic AMPA receptor trafficking and gating depends on multiple intracellular domains. Proc Natl Acad Sci U S A *106*, 11348-11351.

Nakagawa, T., Cheng, Y., Ramm, E., Sheng, M., and Walz, T. (2005). Structure and different conformational states of native AMPA receptor complexes. Nature *433*, 545-549.

Nakagawa, T., Cheng, Y., Sheng, M., and Walz, T. (2006). Three-dimensional structure of an AMPA receptor without associated stargazin/TARP proteins. Biol Chem *387*, 179-187.

Ng, D., Pitcher, G.M., Szilard, R.K., Sertie, A., Kanisek, M., Clapcote, S.J., Lipina, T., Kalia, L.V., Joo, D., McKerlie, C*., et al.* (2009). Neto1 is a novel CUB-domain NMDA receptor-interacting protein required for synaptic plasticity and learning. PLoS Biol *7*, e41.

Nicoll, R.A., Tomita, S., and Bredt, D.S. (2006). Auxiliary subunits assist AMPA-type glutamate receptors. Science *311*, 1253-1256.

O'Brien, R.J., Xu, D., Petralia, R.S., Steward, O., Huganir, R.L., and Worley, P. (1999). Synaptic clustering of AMPA receptors by the extracellular immediate-early gene product Narp. Neuron *23*, 309-323.

O'Hara, P.J., Sheppard, P.O., Thogersen, H., Venezia, D., Haldeman, B.A., McGrane, V., Houamed, K.M., Thomsen, C., Gilbert, T.L., and Mulvihill, E.R. (1993). The ligand-binding domain in metabotropic glutamate receptors is related to bacterial periplasmic binding proteins. Neuron *11*, 41-52.

Paas, Y. (1998). The macro- and microarchitectures of the ligand-binding domain of glutamate receptors. Trends Neurosci *21*, 117-125.

Passafaro, M., Nakagawa, T., Sala, C., and Sheng, M. (2003). Induction of dendritic spines by an extracellular domain of AMPA receptor subunit GluR2. Nature *424*, 677-681.

Perin-Dureau, F., Rachline, J., Neyton, J., and Paoletti, P. (2002). Mapping the binding site of the neuroprotectant ifenprodil on NMDA receptors. J Neurosci *22*, 5955-5965.

Saglietti, L., Dequidt, C., Kamieniarz, K., Rousset, M.C., Valnegri, P., Thoumine, O., Beretta, F., Fagni, L., Choquet, D., Sala, C*., et al.* (2007). Extracellular interactions between GluR2 and N-cadherin in spine regulation. Neuron *54*, 461-477.

Schwenk, J., Harmel, N., Brechet, A., Zolles, G., Berkefeld, H., Muller, C.S., Bildl, W., Baehrens, D., Huber, B., Kulik, A.*, et al.* (2012). High-resolution proteomics unravel architecture and molecular diversity of native AMPA receptor complexes. Neuron *74*, 621-633.

Schwenk, J., Harmel, N., Zolles, G., Bildl, W., Kulik, A., Heimrich, B., Chisaka, O., Jonas, P., Schulte, U., Fakler, B., and Klocker, N. (2009). Functional proteomics identify cornichon proteins as auxiliary subunits of AMPA receptors. Science *323*, 1313-1319.

Shanks, N.F., Savas, J.N., Maruo, T., Cais, O., Hirao, A., Oe, S., Ghosh, A., Noda, Y., Greger, I.H., Yates, J.R., 3rd, and Nakagawa, T. (2012). Differences in AMPA and Kainate Receptor Interactomes Facilitate Identification of AMPA Receptor Auxiliary Subunit GSG1L. Cell Rep *1*, 590-598.

Shi, Y., Suh, Y.H., Milstein, A.D., Isozaki, K., Schmid, S.M., Roche, K.W., and Nicoll, R.A. (2010). Functional comparison of the effects of TARPs and cornichons on AMPA receptor trafficking and gating. Proc Natl Acad Sci U S A *107*, 16315-16319.

Sia, G.M., Beique, J.C., Rumbaugh, G., Cho, R., Worley, P.F., and Huganir, R.L. (2007). Interaction of the N-terminal domain of the AMPA receptor GluR4 subunit with the neuronal pentraxin NP1 mediates GluR4 synaptic recruitment. Neuron *55*, 87-102.

Sobolevsky, A.I., Rosconi, M.P., and Gouaux, E. (2009). X-ray structure, symmetry and mechanism of an AMPA-subtype glutamate receptor. Nature *462*, 745-756.

Soto, D., Coombs, I.D., Kelly, L., Farrant, M., and Cull-Candy, S.G. (2007). Stargazin attenuates intracellular polyamine block of calcium-permeable AMPA receptors. Nat Neurosci *10*, 1260-1267.

Sukumaran, M., Rossmann, M., Shrivastava, I., Dutta, A., Bahar, I., and Greger, I.H. (2011). Dynamics and allosteric potential of the AMPA receptor N-terminal domain. EMBO J *30*, 972-982.

Tomita, S., Adesnik, H., Sekiguchi, M., Zhang, W., Wada, K., Howe, J.R., Nicoll, R.A., and Bredt, D.S. (2005). Stargazin modulates AMPA receptor gating and trafficking by distinct domains. Nature *435*, 1052-1058.

Tomita, S., and Castillo, P.E. (2012). Neto1 and Neto2: auxiliary subunits that determine key properties of native kainate receptors. J Physiol *590*, 2217-2223.

Trakhanov, S., Vyas, N.K., Luecke, H., Kristensen, D.M., Ma, J., and Quiocho, F.A. (2005). Ligand-free and -bound structures of the binding protein (LivJ) of the Escherichia coli ABC leucine/isoleucine/valine transport system: trajectory and dynamics of the interdomain rotation and ligand specificity. Biochemistry *44*, 6597-6608.

von Engelhardt, J., Mack, V., Sprengel, R., Kavenstock, N., Li, K.W., Stern-Bach, Y., Smit, A.B., Seeburg, P.H., and Monyer, H. (2010). CKAMP44: a brain-specific protein attenuating short-term synaptic plasticity in the dentate gyrus. Science *327*, 1518-1522.

Walker, C.S., Francis, M.M., Brockie, P.J., Madsen, D.M., Zheng, Y., and Maricq, A.V. (2006). Conserved SOL-1 proteins regulate ionotropic glutamate receptor desensitization. Proc Natl Acad Sci U S A *103*, 10787-10792.

Wang, R., Mellem, J.E., Jensen, M., Brockie, P.J., Walker, C.S., Hoerndli, F.J., Hauth, L., Madsen, D.M., and Maricq, A.V. (2012). The SOL-2/Neto auxiliary protein modulates the function of AMPA-subtype ionotropic glutamate receptors. Neuron *75*, 838-850.

Wang, R., Walker, C.S., Brockie, P.J., Francis, M.M., Mellem, J.E., Madsen, D.M., and Maricq, A.V. (2008). Evolutionary conserved role for TARPs in the gating of glutamate receptors and tuning of synaptic function. Neuron *59*, 997-1008.

Washburn, M.P., Wolters, D., and Yates, J.R., 3rd (2001). Large-scale analysis of the yeast proteome by multidimensional protein identification technology. Nat Biotechnol *19*, 242-247.

Zheng, Y., Brockie, P.J., Mellem, J.E., Madsen, D.M., Walker, C.S., Francis, M.M., and Maricq, A.V. (2006). SOL-1 is an auxiliary subunit that modulates the gating of GLR-1 glutamate receptors in Caenorhabditis elegans. Proc Natl Acad Sci U S A *103*, 1100-1105.

Zheng, Y., Mellem, J.E., Brockie, P.J., Madsen, D.M., and Maricq, A.V. (2004). SOL-1 is a CUB-domain protein required for GLR-1 glutamate receptor function in C. elegans. Nature *427*, 451-457.

Figures

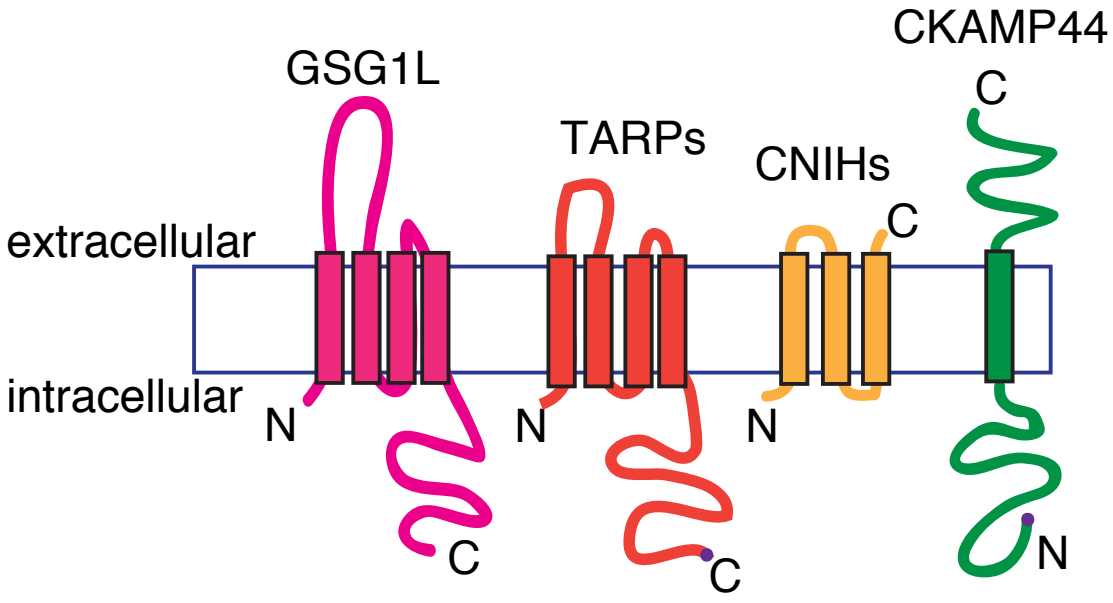

Figure 5_1: Known AMPA-R auxiliary subunits in mammals
GSG1L, TARPs, CNIHs, and CKAMP44 are represented in cartoon form. The blue blue box represents the lipid membrane on the cell surface. The N- and C-termini of each is represnted with N and C, respectively. The transmemrane domains are represented ast the black outlined rectangles spanning the blue plasma membrane. The small purple dots represent known PDZ binding motifs.

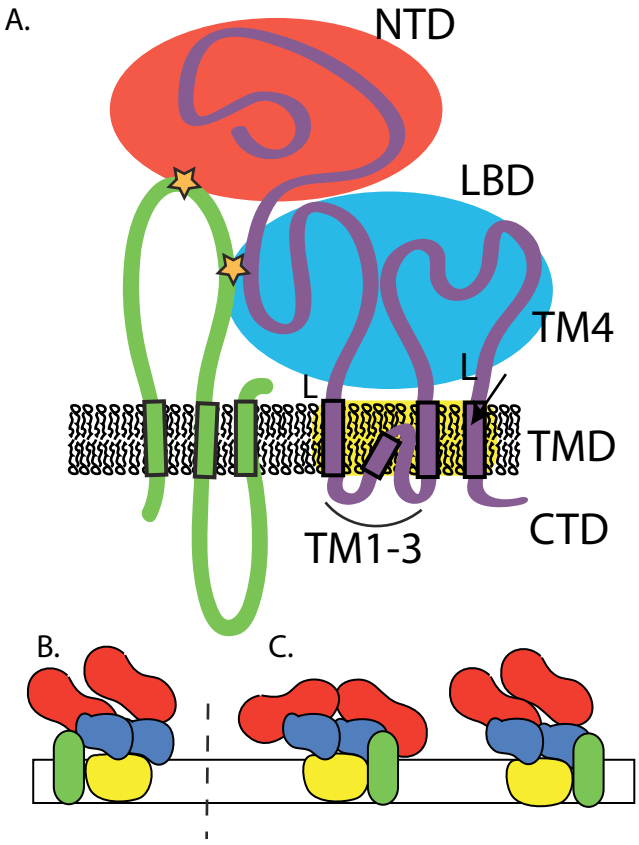

Figure 5_2: Model of auxiliary subunit Interaction with AMPA-R complex
(A) Schematic of a single AMPA-R subunit, with NTD (red), LBD (blue), and TMD (yellow) interacting with CNIH-3 (green). Interaction occurs between CNIH-3 extracellular loops and AMPA-R LBD and NTD regions. Potential interactions sites are shown by orange stars.
(B) Schematic of AMPA-R tetramers interating with CNIH-3. The colors of molecules and domains are the same as in (A). In this model, the extracellular loop of CNIH-3 can interact with both the AMPA-R LBD and NTD during the resting state conformation of the receptor.
(C) In this model, the CNIH-3 extracellular loop can interact with both the AMPA-R LBD and NTD only when the AMPA-R is in a gating conformation where the NTD domains are spread apart and move closer to the membrane as in (Nakagawa et al, 2005)(left), but during the resting conformation the CNIH-3 extracellular loop only has access to interact with the LBD (right).